molecules

MDPI

Article

Comparative Study of Lewatit S5428 and S5528 for Vanadium(V) Removal from Aqueous Solutions: Batch and Column Studies

Anna Wołowicz [1,*] and Elżbieta Zambrzycka-Szelewa [2]

[1] Department of Inorganic Chemistry, Faculty of Chemistry, Institute of Chemical Sciences, Maria Curie Sklodowska University, Maria Curie-Sklodowska Square 2, 20-031 Lublin, Poland
[2] Department of Analytical and Inorganic Chemistry, Faculty of Chemistry, University of Bialystok, K. Ciołkowskiego 1K, 15-245 Białystok, Poland; elazamb@uwb.edu.pl
* Correspondence: anna.wolowicz@umcs.pl; Tel.: +48-537-57-27

Abstract

V(V) removal using Lewatit S5428 and Lewatit S5528 was studied in batch and column experiments. V(V) adsorption was optimized by varying the adsorbent mass (0.01–0.1 g), pH (2–10), initial concentration (5–1000 mg/L), contact time (1–1440 min), and temperature (298–333 K). The adsorbents were characterized using SEM-EDS, ATR-FTIR, and XPS. Adsorption depended on all analyzed parameters, with Lewatit S5528 showing higher V(V) adsorption capacity. The maximum experimental adsorption capacities for V(V) ions were 181.2 mg/g for Lewatit S5428 and 226.3 mg/g for Lewatit S5528, respectively. Equilibrium data followed the Freundlich model, while kinetic data fitted the pseudo-second-order model best. Both intraparticle and film diffusion influenced adsorption kinetics. The equilibrium time was approximately 30–240 min for Lewatit S5428 and 15–60 min for Lewatit S5528, depending on the initial V(V) ion concentration (50–200 mg/L). The thermodynamic parameters indicated that the V(V) adsorption is spontaneous and exothermic. The loaded resins were efficiently regenerated with 1 mol/L NaOH solutions, and the main vanadium adsorption mechanism is ion exchange. The column experiments showed that Lewatit S5528 has a higher adsorption capacity than Lewatit S5428. A maximum overall V(V) removal efficiency of 98.22% was obtained for a 100-fold diluted real leachate (S1*) (C_0 = 47.74 mg/L).

Keywords: ion exchangers; vanadium; removal; spent catalyst; wastewater treatment

Academic Editor: Antonio Zuorro

Received: 25 September 2026
Revised: 9 November 2026
Accepted: 20 November 2026
Published: 25 November 2026

Copyright: © 2026 by the authors. Licensee MDPI, Basel, Switzerland. This article is an open access article distributed under the terms and conditions of the Creative Commons Attribution (CC BY) license.

1. Introduction

Due to vanadium unique properties, it is widely used in modern industrial processes—for instance, as an additive, a catalyst, or a component [1]. The role of vanadium has evolved over the years, moving beyond its initial use in strengthening steel. Today, this element plays a key role in infrastructure, catalysis, and clean energy storage technologies (vanadium redox flow batteries,–VRFB) (Figure 1) [1]. Given its extensive industrial application, economic importance, and the risk of supply chain disruptions, vanadium has been classified by the European Union as a critical raw material [2–4]. Vanadium is a redox sensitive metal that occurs in multiple oxidation states with +3, +4, and +5 being

dominant in environments. V(V), which typically presents as oxyanions, is the most mobile and toxic form. V(IV) is less harmful and precipitates under near-neutral conditions, whereas V(III) occurs frequently in strongly reducing environments [5–9].

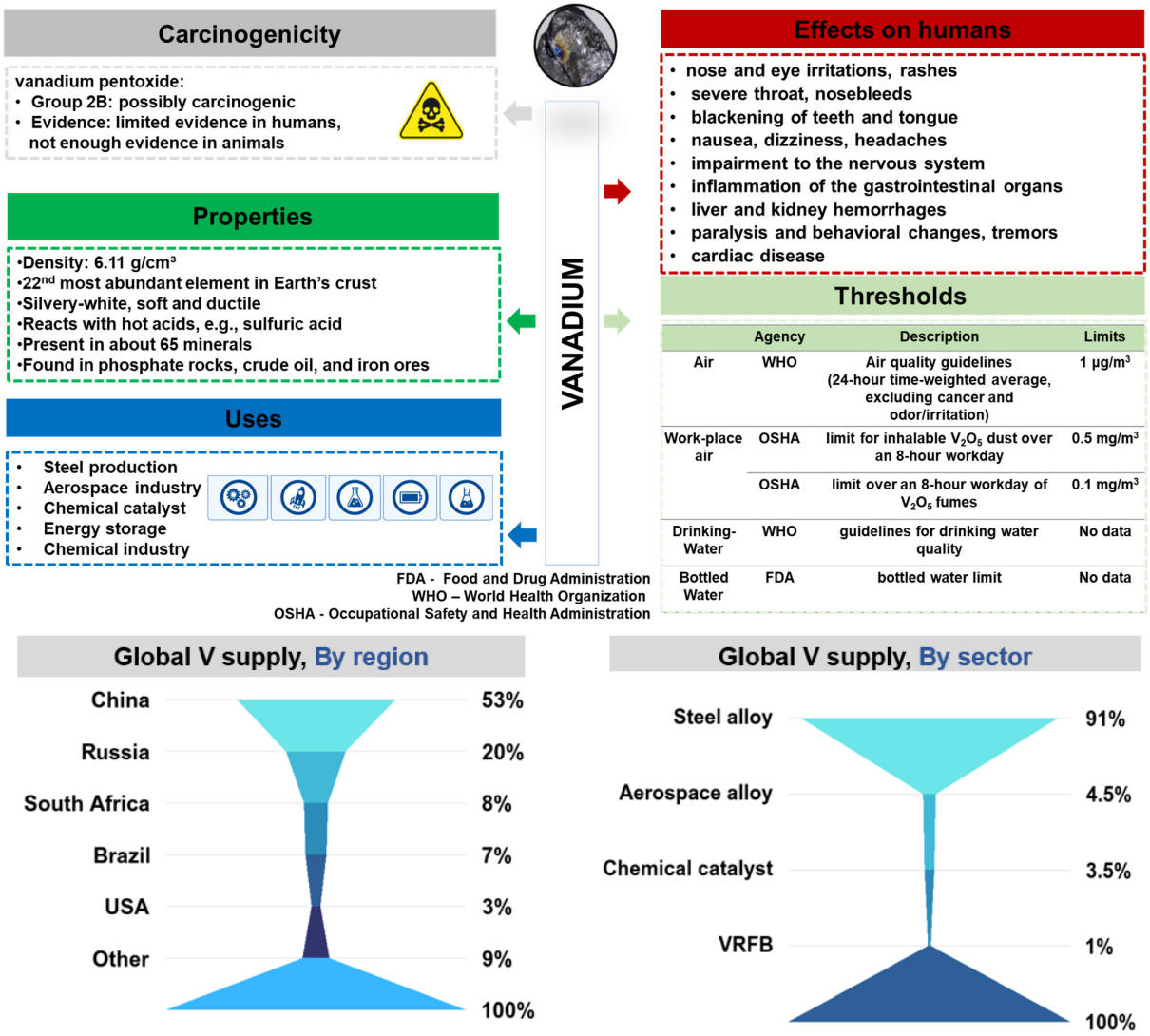


Figure 1. Vanadium properties, uses, carcinogenicity, effect on humans, and thresholds.

Expanding urbanization and rapid industrialization has led to an increase in the disposal of heavy metals, among others vanadium, into the environment to the atmosphere, hydrosphere, lithosphere, and biosphere [10,11]. The main sources of vanadium in the environment are natural sources (approximately 65,000 tons annually) such as volcanic activity, evaporation of ocean water, forest fires, continental dust, marine aerosols, rock erosion, and soil formation [7,11]. However, the greatest sources of vanadium in the environment result from anthropogenic activity (200,000 tons annually) [12]. Approximately 37,000 tons of vanadium enter the atmosphere annually from natural sources (volcanic emissions, marine aerosols, and continental dust), and more than 60,000 tons of V get into the atmosphere due to anthropogenic human activity such as smelting activities or fuel combustion [9,13]. In the hydrosphere and lithosphere, vanadium enters water and soil through natural sources such as leaching of vanadium from rocks and soils, reverie transport, and atmospheric deposition, whereas the anthropogenic sources include industrial wastewater, mining, and metallurgical waste, runoff from industrial areas (pesticide

and fertilizer application), and landfill leachate [8,9]. In the biosphere, vanadium is taken up by organisms from soil and water, and its transfer through food chains and bioaccumulation may be intensified by anthropogenic pollution [11].

Vanadium is found in the Earth's crust, where it makes up about 0.02–0.03% of the total composition, and it is also commonly found in the natural environment [14]. Vanadium has been detected in various environmental media across all continents, with reported global concentrations averaging 63.91 ± 54.95 μg/g (range: 0.1–2114 μg/g) in sediments, 9.05 ± 23.42 μg/L (range: 0.001–120 μg/L) in seawater, 0.73 ± 1.41 μg/g (range: 0.0008–17.58 μg/g) in invertebrates, and 0.37 ± 0.73 μg/g (range: 0.0001–15 μg/g) in fish [15]. The average concentration of vanadium in the Earth's crust is 97 mg/kg [12], 90 mg/kg in soils [12], 150 mg/kg in surface waters [14], 0.71 μg/L in rivers [12], 1.8 μg/L in oceans [12,14], >400 mg/kg in marine sediments [12], and 1000 ng/m^3 in the atmosphere [14]. Vanadium concentrations in surface waters typically fall within the range of 0.5–2.4 μg/L, primarily as a result of the natural weathering of rocks and minerals [16]. The weathering of vanadium-rich rocks and sediments contributes to elevated vanadium concentrations in groundwater. For instance, concentrations of 288 μg/L have been reported in El Hierro, Spain, 2470 μg/L in the Pampean region of Argentina, 201 μg/L near Mount Etna, Italy, and 58–99 μg/L near Mount Fuji, Japan [14]. Anthropogenic activities, including mining, industrial processes, fossil fuel combustion, the application of fertilizers and pesticides, and household waste recycling, have also contributed to increased vanadium(V) concentrations in soils and natural water bodies [14]. In industrial wastewater, the concentration of vanadium ranges from 30 to 199 mg/L [16], with values in China reaching between 50 and 200 mg/L [14]. The wastewater collected from the vanadium plant in Chengde, China, contained a concentration of vanadium varying from 50–200 mg/L, and 0.076–0.208 mg/L in Panzhihua, China, which was far more than the regulatory standard (50 μg/L = 0.05 mg/L) [17]. The presence of industrial wastewater containing vanadium at varying concentrations (e.g., 30–100 mg V(V)/L [18,19] and 1111 mg V(V)/L [18,20]) presents a significant environmental hazard. Vanadium concentrations in industrial leachates vary depending on the source material, ranging from approximately 1–5 mg/L in bauxite residue (red mud) leachates to as high as 200 mg/L in leachates from steelmaking slags [21]. It poses a risk of contaminating groundwater, soil, and plants, and of degrading surface water quality. This renders the water unsuitable for various uses, including food, municipal, and industrial purposes. On the one hand, vanadium may play a role in nutrient metabolism in higher organisms, although its essentiality for humans has not yet been conclusively established. On the other hand, excessive vanadium exposure can have adverse effects on living organisms [22–24]. Given the increasing amount of vanadium in water and wastewater and its potential toxicity to humans (Figure 1) (V_2O_5 is classified as possibly carcinogenic, Group 2B by the International Agency for Research on Cancer), animals and plants, its effective removal is essential to protect human health and the environment [25,26]. Consequently, appropriate treatment processes are required, and there is a need for further research into and the development of simple, highly effective methods for vanadium removal [13,18].

Common methods for removing vanadium from aqueous solutions include adsorption, microbial treatment, ion exchange, chemical precipitation, solvent extraction, electrokinetic remediation, photocatalysis, coagulation, membrane filtration, etc. [14,16,27,28]. Each technique has its own advantages and also limitations, which were presented in Supplementary Materials in Figure S1. Therefore, the selection of the most suitable method should be based on several factors, including vanadium removal efficiency, the type and amount of chemicals or adsorbents required, the initial vanadium concentration, the optimal pH of the solution, and other operating conditions [28].

In recent years, there has been growing interest in adsorption technologies as effective methods for removing vanadium ions from aqueous solutions, e.g., industrial effluents or leachates from spent vanadium-bearing catalysts used for sulfuric acid production [29–32]. Various ion exchangers, in particular chelating and anion-exchange resins, are promising adsorbents for industrial applications due to their high selectivity for vanadate anions, chemical stability, and regeneration potential [29,31–45]. The studies on vanadium removal and separation using ion-exchange resins such the cation-exchange resins (Amberlite IR–120 plus, Dowex 50W X4-100, Dowex 50W X4 [33]), the weakly basic anion exchangers (Lewatit MonoPlus TP220 [40], Purolite A830 [41], D314 [44], D453, D301FC, ZGA414 [38]), the strongly basic anion exchangers (Amberlite IRA 400 [32], Lewatit MonoPlus SR7, Purolite A400TL, Dowex PSR2, Dowex PSR3 [41], Amberlite® IRA958, Dowex® 1X2 [45], TA-62 [34], 717 [35], 201 *7 [42], D201 [43], D202, ZGA351 [38]), and the chelating ones (Lewatit MonoPlus TP220, Dowex M4195 [40], Amberlite IRA 743 [32], Amberlite® IRA 400 [29], Amberjet™ 4200 [36], Purolite S984 [41], D851 [43], DHDS, DHES, DHFS, DD1 S, DDAS, DGES and CW-1, CW-2 [37]), as well as others such as the natural ion exchanger [30], which is adsorbent without functional groups such as Lewatit AF5 [41], and modified ion exchangers such as nano-hydrous zirconium oxide-modified anion-exchange resin [31] and Amberlite IRA-904 modified with TCPP [39], which have demonstrated that their adsorption performance is strongly influenced by pH and the presence of co-existing inorganic ions [46].

Research on vanadium removal from aqueous solutions and industrial wastewater using ion-exchange materials has mainly focused on synthetic solutions and laboratory-scale batch experiments [31–45]. Although these studies have provided valuable information on adsorption capacities, kinetics, equilibrium behaviour, and the influence of operational parameters, their results are not always directly transferable to real industrial wastewater, where the presence of competing ions and other components may significantly affect vanadium adsorption. Furthermore, studies involving real industrial solutions and dynamic column experiments remain relatively limited compared with investigations based exclusively on synthetic solutions and batch systems. In particular, the evaluation of ion-exchange resins under both static and dynamic conditions, combined with regeneration studies, is important for assessing their potential applicability in practical treatment processes. Another aspect that deserves further investigation is the influence of the polymer matrix on the adsorption performance of strongly basic anion-exchange resins containing the same type of functional groups. While the adsorption properties of different ion-exchange materials have been widely investigated, comparative studies allowing the potential contribution of polymer matrix composition to be assessed under identical experimental conditions are less common. Such comparisons may provide additional insight into the relationship between resin structure, vanadium adsorption behaviour, and operational performance. In this context, the present study aims to comparatively evaluate the removal of Vanadium(V) using two commercially available strongly basic anion-exchange resins, Lewatit S5428 and Lewatit S5528, from both synthetic aqueous solutions and a real leaching solution obtained from a spent catalyst used in sulfuric acid production. Both resins contain type-I quaternary ammonium functional groups and exhibit comparable ion-exchange capacities and particle-size characteristics but differ in their polymer matrix composition. Lewatit S5428 is based on crosslinked polyacrylamide, whereas Lewatit S5528 contains a crosslinked polyacrylate matrix. This provides an opportunity to investigate the potential influence of polymer matrix composition on Vanadium(V) removal while maintaining the same type of ion-exchange functional groups.

The experimental investigation combines batch adsorption experiments, dynamic column tests, and regeneration studies. Moreover, to the best of our knowledge, neither

of these resins has previously been investigated and comparatively evaluated for Vanadium(V) removal from both synthetic and real solutions, particularly under static and dynamic conditions. The effects of adsorbent dosage, solution pH, initial vanadium concentration, contact time, and temperature were examined under static conditions, allowing kinetic, equilibrium, and thermodynamic parameters to be determined. Furthermore, regeneration efficiency was evaluated using HCl and NaOH solutions at concentrations ranging from 0.1 to 1 mol/L. Dynamic column experiments were conducted to determine the working ion-exchange capacities and bed distribution coefficients and to assess resin performance under flow conditions. The adsorption behaviour was also analysed to provide insight into the processes governing Vanadium(V) removal.

The main contribution of this study is therefore not the development of a new sorbent or the demonstration of the highest adsorption capacity among previously reported materials, but rather a comparative assessment of two commercially available anion-exchange resins differing in their polymer matrix composition, supported by batch, column, and regeneration experiments and validated using a real industrial leaching solution. By combining these approaches, the study provides additional information on the relationship between resin characteristics, operating conditions, and vanadium removal performance. The results may contribute to a more informed selection of commercially available anion-exchange resins for the treatment of vanadium-containing industrial wastewater.

2. Results and Discussion

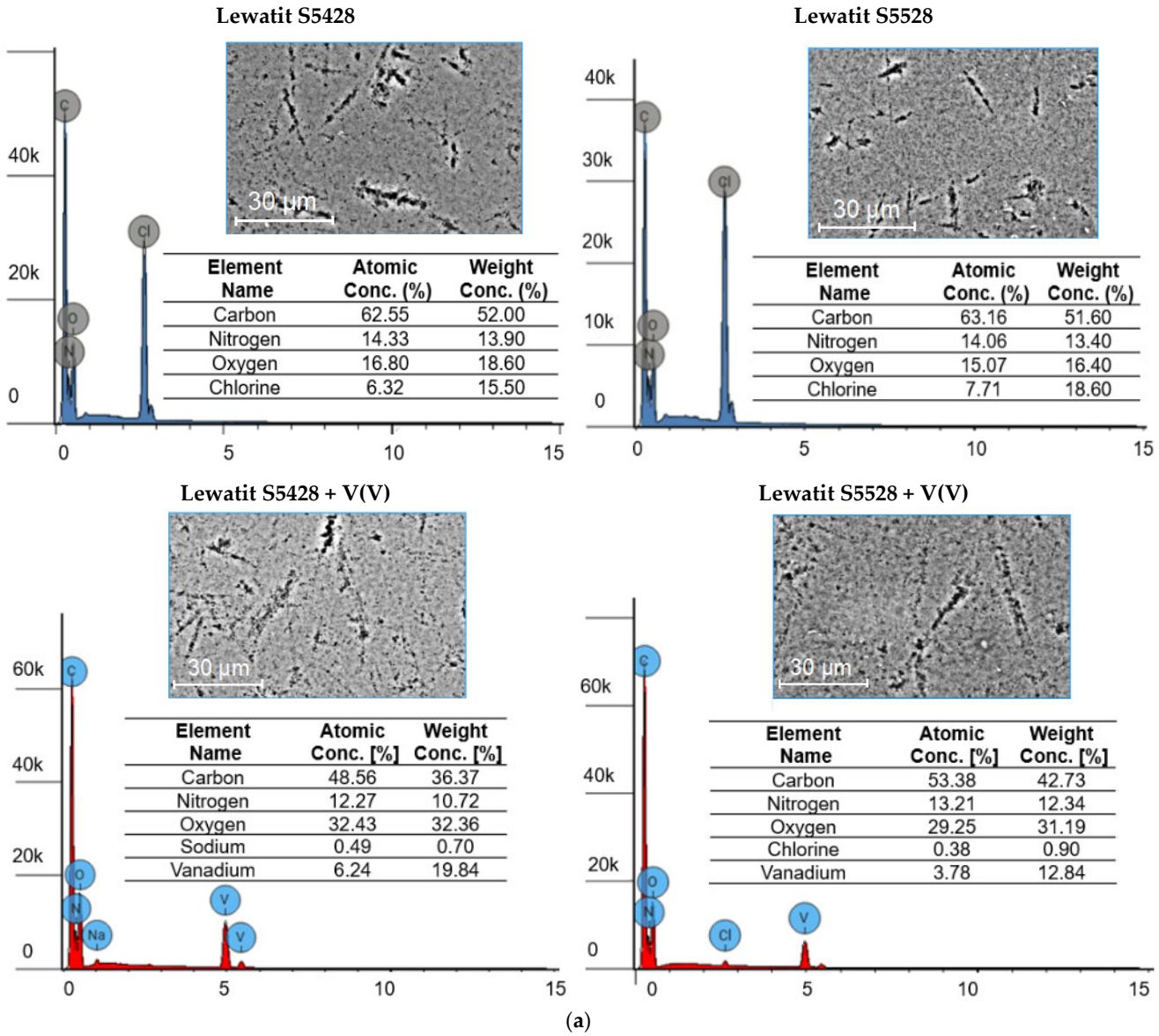
2.1. Physicochemical Characterization of Lewatit Anion Exchangers Before and After V(V) Adsorption

The CHN/CHNS elemental analysis was performed to determine the percentage abundance of carbon, nitrogen, hydrogen, and sulfur elements in the adsorbents prior to V(V) adsorption. The results are presented in Table S1. Both the Lewatit S5428 and Lewatit S5528 resins are categorized within the same group of anion-exchange resins. It should be noted that the resins differ in their chemical composition. The Lewatit S5428 resin is based on polyacrylamide, whereas the Lewatit S5528 is based on crosslinked polyacrylate. For these reasons, these resins may exhibit variations in their physicochemical and functional properties. Elemental analysis revealed that Lewatit S5528 contains a slightly higher nitrogen content (10.6%) than Lewatit S5428 (10.0%), which may indicate minor differences in the amount of nitrogen-containing functional groups within the polymer matrix. Although Lewatit S5528 is based on a cross-linked polyacrylate matrix that did not contain nitrogen, nitrogen is introduced through quaternary ammonium functional groups responsible for anion-exchange properties [47–49]. The difference in N content may be related also to variations in the degree of functionalization, polymer structure, or water content of the resins [50]. On the other hand, the surface-sensitive EDX and XPS analyses revealed a slightly higher nitrogen concentration for Lewatit S5428 compared with Lewatit S5528, whereas CHNS analysis provided the average nitrogen content of the bulk sample. This difference may result from the different sampling depths of the analytical techniques and variations between the surface and bulk composition of the resins [51–53]. The XPS and SEM-EDX techniques provide more information on surface elemental distribution; XPS give the total atomic concentration of elements to a depth of approximately 4–8 nm [52], whereas the SEM-EDX extends to depths of 0.1 to 3.0 μm [53].

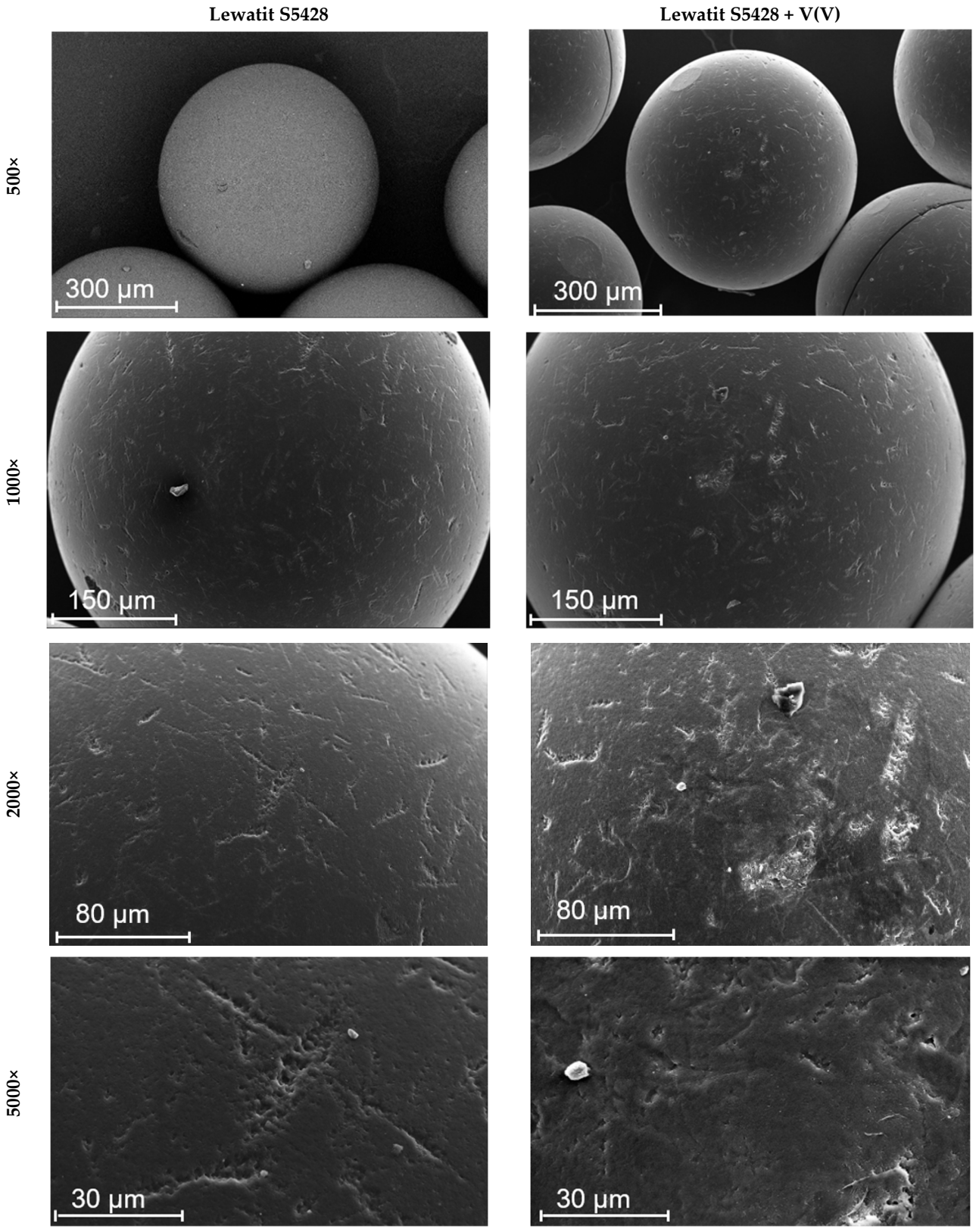
The carbon content of both ion-exchange resins is comparable, with values of 43.4% and 44.0% observed for Lewatit S5428 and Lewatit S5528, respectively. The hydrogen content of these resins is recorded as 11.0% and 11.2%, respectively. The C:H ratios in both resins are almost identical, indicating similarities in their overall organic composition. Furthermore, no sulfur was detected in either resin, suggesting the absence of sulfonic functional groups.

https://doi.org/10.3390/molecules31234308

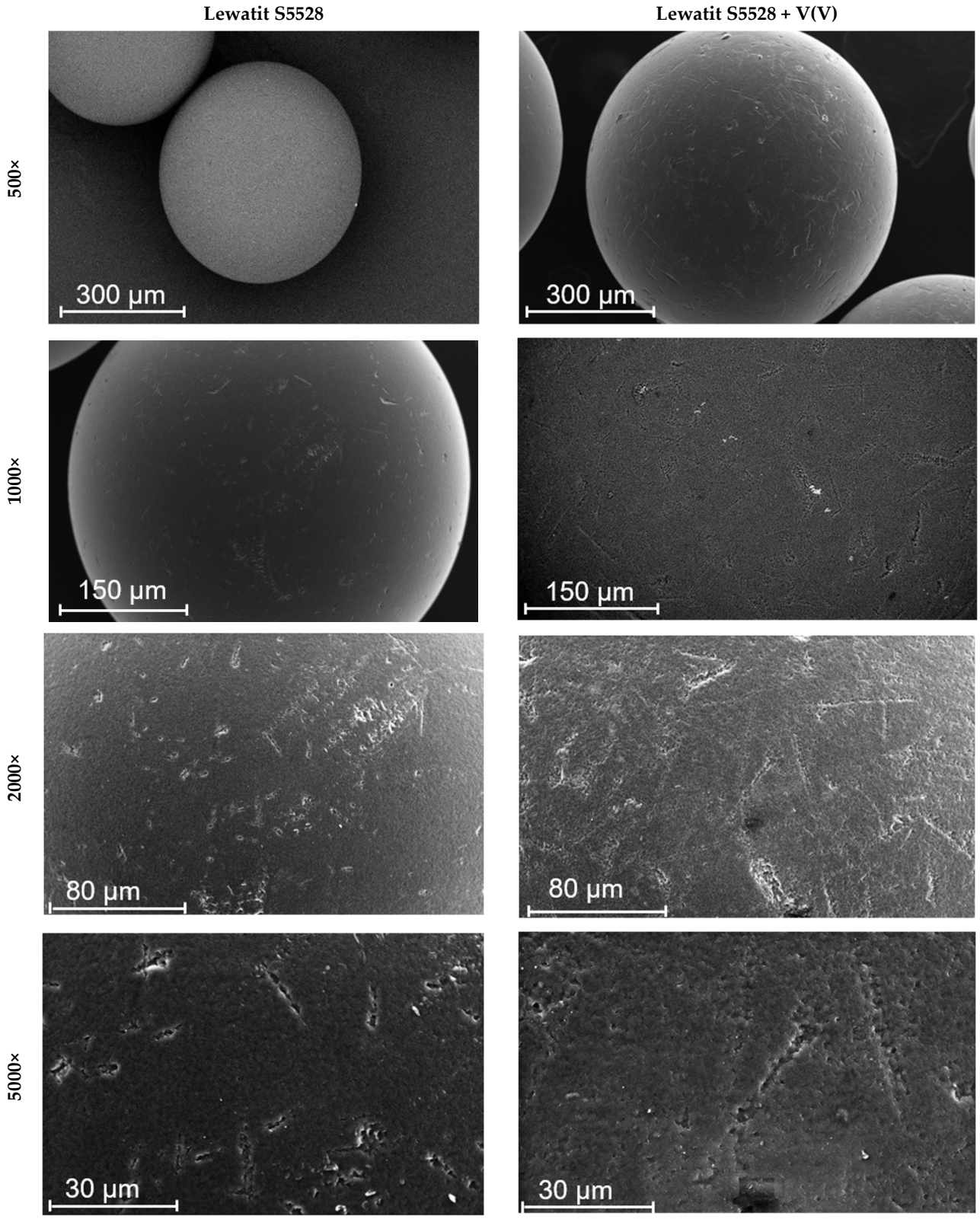
Details of the EDX analysis of the discussed anion-exchange resins are presented in Figure 2a. In addition to carbon, nitrogen, and hydrogen, which were detected in the CHNS analysis, the anion-exchange resins also contained chlorine and oxygen before adsorption with Vanadium(V). Commercially available anion-exchange resins were supplied by the manufacturer in chloride form and, after preliminary purification with distilled water, used in chloride form in the adsorption studies [48]. The chlorine content in the EDX analysis was 6.32% and 7.71% for the Lewatit S5428 and Lewatit S5528 anion-exchange resins, respectively, confirming that the anion-exchange resins used were in the chloride form (chloride counterions and exchangeable ions) [52].



(**a**)


Lewatit S5428
Lewatit S5428 + V(V)
500×
1000×
2000×
5000×
300 µm
300 µm
150 µm
150 µm
80 µm
80 µm
30 µm
30 µm

(**b**)



(**c**)

Figure 2. (**a**) EDX and (**b**,**c**) SEM micrographs of anion exchangers Lewatit S5428 and Lewatit S5528 before (Lewatit S5428 and Lewatit S5528) and after V(V) loading (Lewatit S5428 + V(V) and Lewatit S5528 + V(V)).

https://doi.org/10.3390/molecules31234308

The presence of oxygen in the ion-exchange resins can result from three sources: (1) the polymer structure, (2) the presence of oxygen-containing functional groups, and (3) adsorbed water, which EDX does not distinguish from oxygen originating from the polymer. Adsorbed water is always present, but its atomic fraction in EDS is typically much less than 15%, usually a few percent. The oxygen content for the anion exchangers considered was 16.8% and 15.7% for the Lewatit S5428 and Lewatit S5528 anion exchangers, respectively, likely as a result of their polymeric matrix and the crosslinked polyacrylamide (Lewatit S5428) or polyacrylate (Lewatit S5528) matrix [54]. SEM analysis showed that at 500× magnification, both anion exchangers appeared as well-formed, spherical beads with smooth surfaces. As magnification increased, the beads' surfaces became rougher. The structure of both Lewatit S5428 and Lewatit M5528 anion exchangers seems to be porous. SEM observations are consistent with the structural type of these anion exchangers: Lewatit S5428 and Lewatit S5528 have a macroporous structure according to the producer data sheets [48]. Macroporous ion exchangers have larger pores within the particles, which increase the active surface area, and their outer surfaces may appear smoother because the pores are located deeper within the structure. Gel ion exchangers, on the other hand, reveal larger irregularities and cracks at higher magnifications, which can make their surface appear less uniform [49]. The SEM images and energy-dispersive X-ray spectroscopy (EDS) elemental maps before and after V(V) adsorption, presented in Figure S2 indicate that the elements are uniformly distributed across the surface of the anion exchanger. No significant aggregation or localized enrichment of elements was observed, suggesting a homogeneous surface composition both prior to and following adsorption.

The surface morphology of Lewatit S5428 and Lewatit S5528 anion exchangers before and after V(V) adsorption was investigated using Atomic Force Microscopy (AFM). The corresponding 2D and 3D images are presented in Figure S3. AFM images suggest that V(V) adsorption is accompanied by changes in the surface morphology of both anion exchangers, although the nature of these changes differs. In the case of the Lewatit S5428 anion exchanger, local smoothing of the surface is visible following the adsorption process, whilst in the case of Lewatit S5528, a distinctly developed, heterogeneous topography is observed to be maintained, with a possible increase in local irregularities.

The low-temperature adsorption/desorption isotherm of nitrogen Lewatit S5428 and Lewatit S5528 before and after V(V) adsorption depicted in Figure 3 does not show a distinct hysteresis loop. The shape of the isotherms exhibits characteristics similar to those of Type III isotherms and, in combination with low BET-specific surface area values, suggests a non-porous or macroporous nature of the resins under study [55]. Lewatit S5428 has approximately three times less specific surface area compared to the Lewatit S5528 anion exchanger. The adsorption of V(V) ions causes a decrease in the S_{BET} surface area in both cases, which may be associated with changes in the surface accessibility of the anion exchangers after V(V) adsorption. S_{BET} value decreases from 0.197 m^2/g to 0.072 m^2/g, a reduction of 63% for Lewatit S5428, and from 0.605 m^2/g to 0.360 m^2/g, a reduction of 40% for Lewatit S5528. Thus, the relative decrease in the BET surface area is more pronounced for Lewatit S5428. The sharp increase in the amount of adsorbed N_2 at a relative pressure close to ($p/p_0 = 1$) may be related to adsorption on the external surface and the condensation of nitrogen in large pores or interparticle spaces.

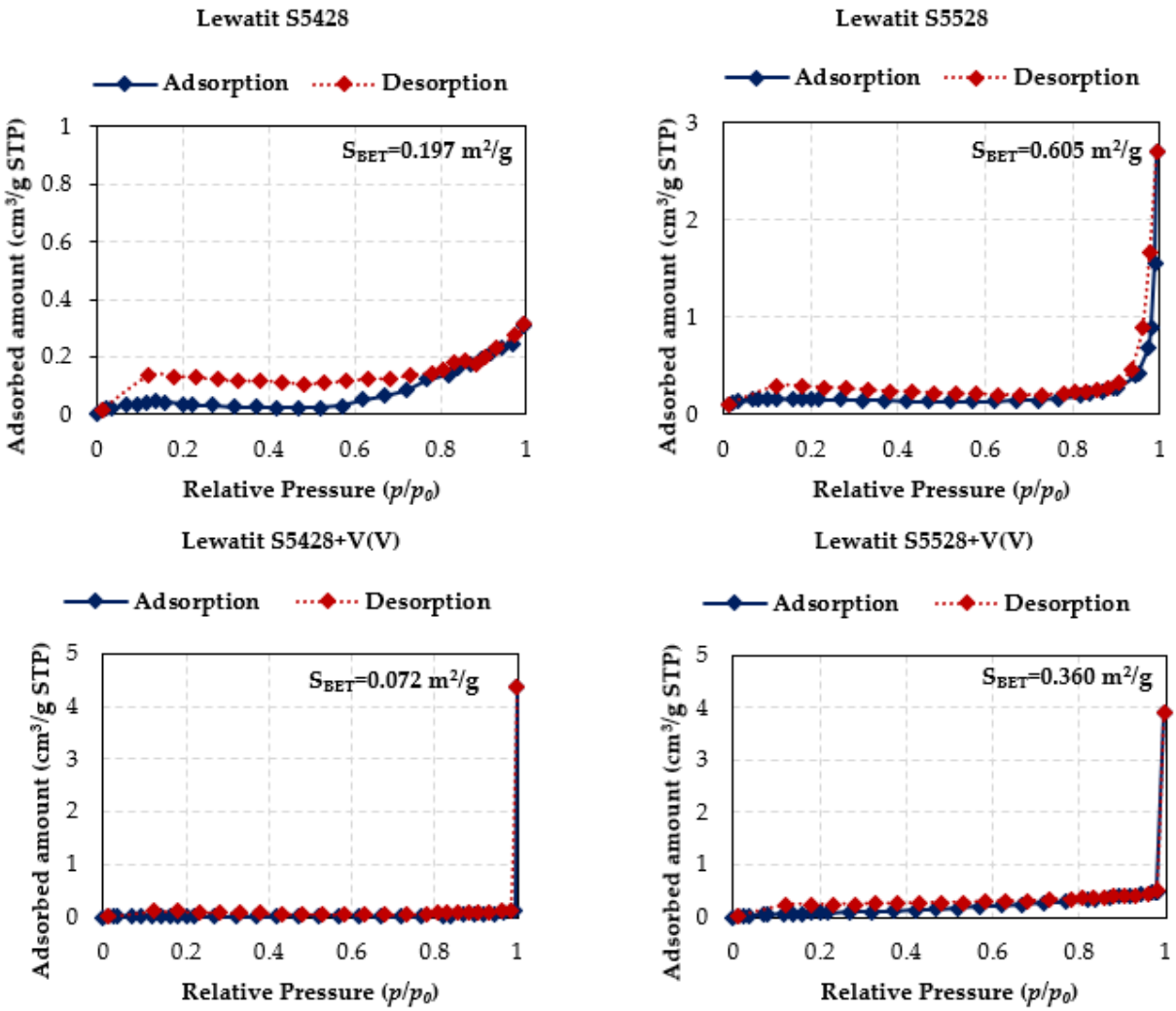


Figure 3. Low-temperature adsorption/desorption nitrogen isotherm of Lewatit S5428 and Lewatit S5528 before and after V(V) adsorption.

The macroporous anion-exchanger Lewatit S5428 exhibits a low nitrogen uptake and a weakly pronounced or absent hysteresis loop. This corresponds to an isotherm with features that are characteristic of materials with limited N_2-accessible porosity [56]. The low BJH adsorption surface area (0.172 m²/g) and very small pore volume (0.00048 cm³/g) were observed for Lewatit S5428 (Figure 4).

The isotherm shape did not change significantly after V(V) adsorption, reflecting the limited accessibility of its internal structure. The decrease in BET surface area indicates partial pore blockage in the polymer matrix, and the slight increase in BJH pore diameter (from 11.1 to 18.5 nm) is likely due to measurement artefacts arising from the very small pore volume or real structural expansion (Figure 5).

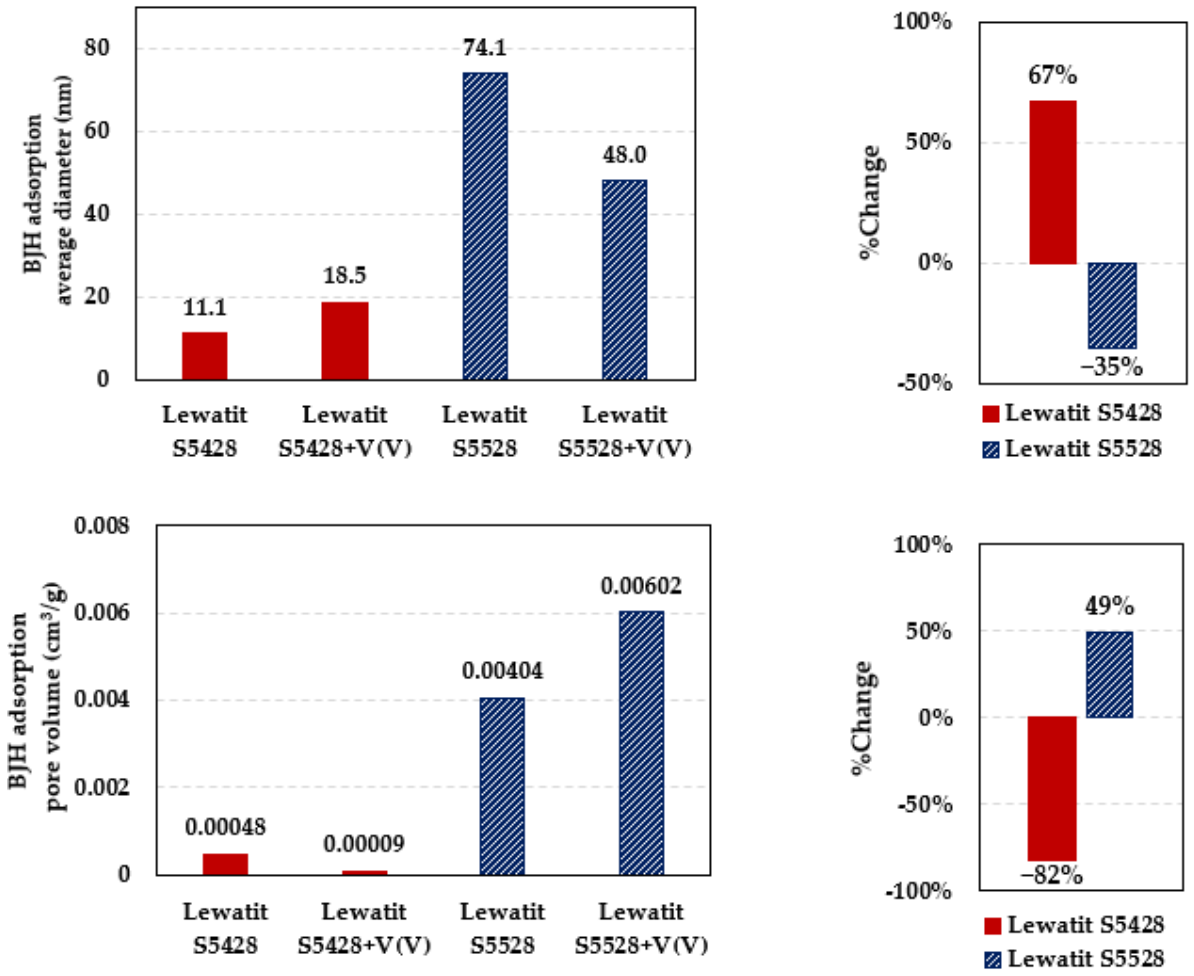


Figure 4. Comparison of average pore diameter and pore volume values obtained for Lewatit S5428 and Lewatit S5528, and these values change after V(V) adsorption.

The anion-exchanger Lewatit S5528 exhibits isotherms typical of macroporous materials and is characterized by higher BET surface area (0.605 m^2/g) and larger BJH adsorption surface area (0.218 m^2/g), as well as the higher pore volume (0.00404 cm^3/g) and wide pore diameter (74.1 nm) compared with Lewatit S5428 (Figure 4). The V(V) ion adsorption leads to Lewatit S5528 structure porosity changes. As was mentioned above, the BET surface area decreases to 0.3599 m^2/g due to partial pore blockage by adsorbed Vanadium(V) ions. In contrast, the BJH adsorption surface area increases substantially (to 0.501 m^2/g), accompanied by a decrease in pore diameter from 74.1 nm to 48.0 nm. These effects indicate that V(V) ion adsorption not only partially fills the pores but also leads to rearrangement and partial narrowing of the macropores (Figure 5). The formation of pore constrictions and a more complex pore network geometry found confirmation in the shape modification of the hysteresis loop after V(V) adsorption [56].

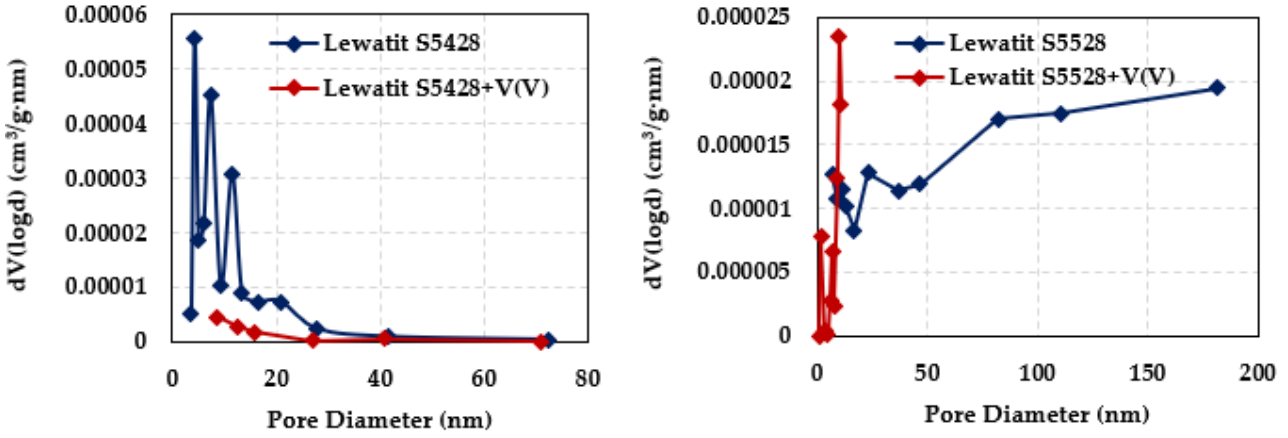
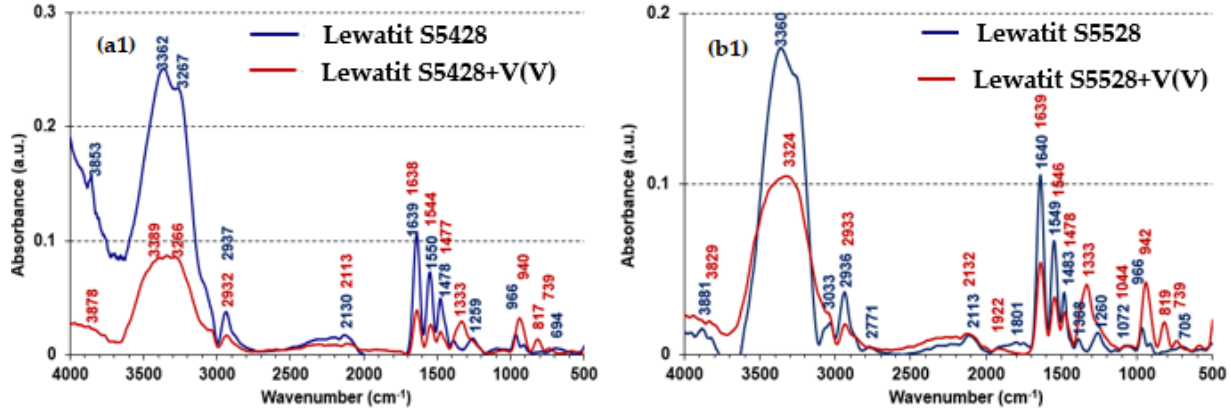


Figure 5. Pore-size distribution of the anion exchangers Lewatit S5428 and Lewatit S5528 before and after V(V) adsorption.

Fourier Transform Infrared Spectroscopy with Attenuated Total Reflectance (ATR/FT-IR) was used to identify the functional groups present in the structure of the anion exchangers Lewatit S5428 and Lewatit S5528, and to examine their possible interactions with Vanadium(V) ions during the adsorption process. Figure 6 presents the ATR/FT-IR spectra of the pure anion exchangers (before adsorption) and those loaded with V(V) for Lewatit S5428 (Figure 6(a1,a2)) and Lewatit S5528 (Figure 6(b1,b2)). It could be easily observed that, when comparing both spectra (before and after V(V) adsorption), the band shifts and the appearance of some new adsorption peaks related to the adsorbent-adsorbate interaction after the adsorption process are observed. The ATR-FTIR analyses of the anion exchangers Lewatit S5428 and Lewatit S5528 before adsorption show peaks characteristic of both their polymeric matrix type and their functional groups [57].



https://doi.org/10.3390/molecules31234308

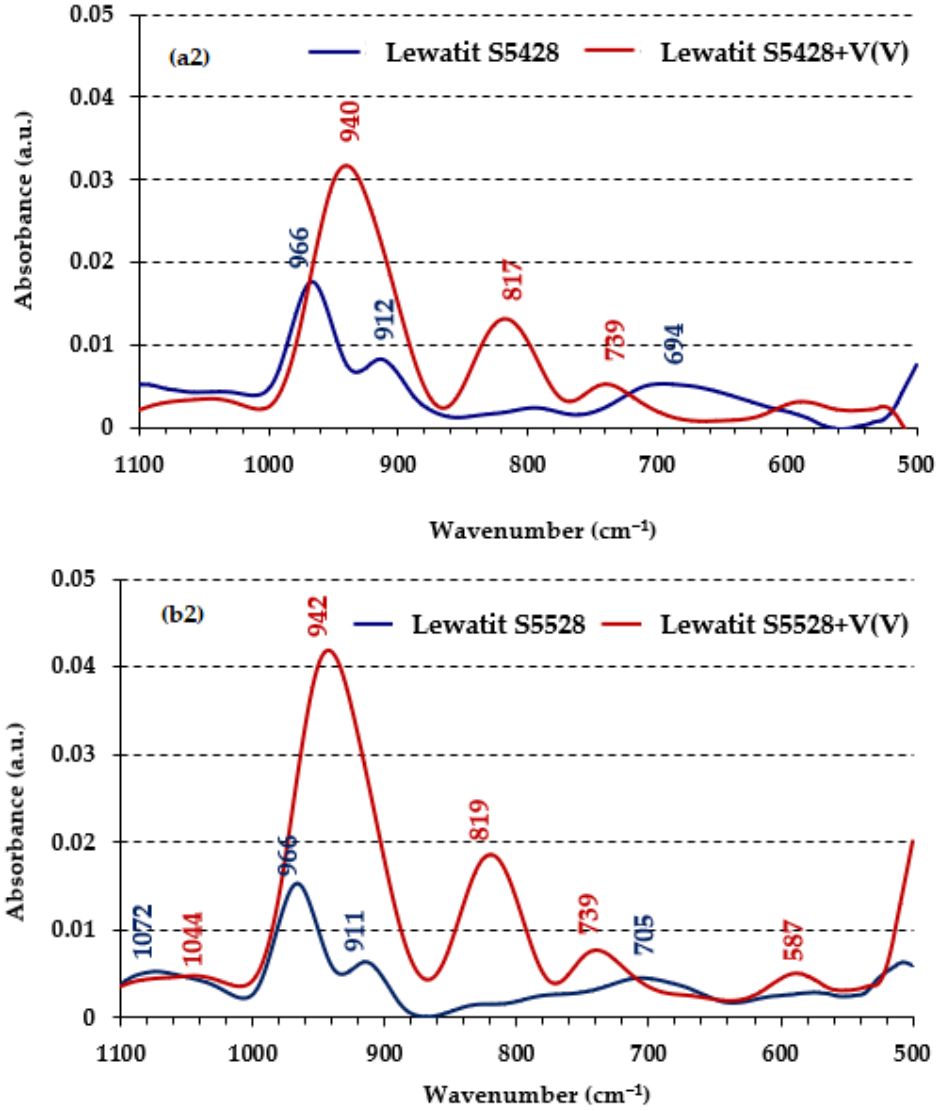


Figure 6. ATR-FTIR spectra of Lewatit S5428 and Lewatit S5528 before (blue line) and after V(V) adsorption (red line): spectra over the entire investigated wavenumber range (a1, b1), enlarged views of the spectra in the 500–1100 cm^{-1} range (a2, b2).

The high similarity of the FT-IR spectra of both anion exchangers before the adsorption process results from the presence of identical, strongly basic, type I functional groups, whose intense bands dominate the spectral structure. However, subtle differences in the high-wavenumber region confirm the presence of a different polymer matrix. In the 3200–3600 cm^{-1} wavelength range, the broad double band occurred at 3362 cm^{-1} and 3267 cm^{-1} for Lewatit S5428, and at around 3360 cm^{-1} and 3249 cm^{-1} for Lewatit S5528. The broad band in this region arises mainly from O–H stretching vibrations (ν(O-H)) of physically and hydrogen-bonded water molecules, with a minor contribution from N–H stretching vibrations of amino functional groups (ν(N-H)) [11,49,58,59]. After V(V) adsorption, this splitting disappears and the band transforms into a single band, while the N-H stretching vibration contribution remains overlapping. This broad peak shifted toward lower wavenumbers to 3324 cm^{-1} for Lewatit S5528, indicating reorganization of the hydrogen bond network caused by the replacement of water molecules by vanadate molecules at the active sites during adsorption (Figure 6(b1)). In the case of Lewatit S5428, the broad peak

intensity decreases, but it remains slightly asymmetric (Figure 6(a1)). It could indicate that, in the case of Lewatit S5428, the water was not fully removed from all the pores. In the region 3100–2800 cm^{-1}, Lewatit S5528 exhibits peaks at 3033 cm^{-1} and 2937 cm^{-1}, whereas Lewatit S5428 shows only a peak at 2936 cm^{-1}. The additional peak at 3033 cm^{-1} observed in Lewatit S5528 is likely due to aromatic or vinyl =C–H stretching or interactions with adsorbed water, reflecting subtle differences in matrix composition or surface hydration. The peaks at 2936–2937 cm^{-1} in both resins correspond to asymmetric C–H stretching vibrations of aliphatic $–CH_2$ and $–CH_3$ groups in the polyacrylic matrix, which shift to 2923 and 2937 cm^{-1} after adsorption [58]. In the region 1700–1500 cm^{-1}, both resins exhibit bands characteristic of the polyacrylic matrix and functional groups. For Lewatit S5428, bands at 1639 and 1550 cm^{-1} are observed, whereas Lewatit S5528 shows prominent peaks at 1640 and 1549 cm^{-1}. These bands can be attributed to overlapping contributions from aromatic C=C stretching vibrations, C=O stretching of carboxylate or ester groups, and N–H bending vibrations of amino functional groups ν(C-N) and δ(N–H) [11,60]. After V(V) adsorption, these bands remain but exhibit slight shifts and changes in intensity, suggesting interactions between vanadate species and the resins' functional groups. In the 1500–1250 cm^{-1} region, bands associated with C–H bending vibrations (at 1470 cm^{-1} for Lewatit S5428 and at 1483 cm^{-1} for Lewatit S5528) and C–N or C–O stretching modes are observed (ν(C-O), ν(C-N)) [60]. For Lewatit S5428, weak bands appear at 1259 cm^{-1}, while Lewatit S5528 exhibits more clearly resolved bands at 1260 cm^{-1}. After V(V) adsorption, a more intense band with slight broadening is observed at 1333 cm^{-1}, indicating interaction with vanadium species. Its peak is correlated with the stretching vibration of C-O, and the formation of vanadium complexes results from V(V) adsorption. The region 1000–900 cm^{-1} is particularly sensitive to changes associated with V(V) adsorption. Before adsorption, both Lewatit S5428 and S5528 exhibit a band at approximately 966 cm^{-1}, which is attributed to out-of-plane vibrations of the polymer backbone [11,59]. After V(V) adsorption, the band at approximately 940 cm^{-1} becomes more pronounced, particularly pronounced for Lewatit S5528 (Figure 6(b-2)). Absorption bands in this spectral region have been associated with stretching vibrations involving V–O bonds in Vanadium(V)-containing species. Therefore, the increased intensity of the band at approximately 940 cm^{-1} may be consistent with the presence of adsorbed vanadate species. However, because this region also contains vibrations associated with the polymer matrix, the assignment cannot be regarded as unequivocal evidence of a specific V–O or V=O bonding environment [59]. In conclusion, the ATR-FT-IR analysis indicates that the main characteristic bands of the polymer matrices are retained after V(V) adsorption, suggesting no major changes in the polymer backbone of the Lewatit resins detectable by this technique. Furthermore, the results show that V(V) adsorption is accompanied by distinct spectral changes in regions characteristic of the resin functional groups and potentially overlapping vanadium–oxygen vibrations [11]. The more pronounced band shifts and intensity changes observed for Lewatit S5528 suggest differences in the interactions between the adsorbed vanadium species and the resin. These differences may be associated with variations in polymer matrix structure, functional group accessibility, and hydration behavior; however, FT-IR data alone do not allow the strength or mechanism of these interactions to be determined quantitatively.

X-ray photoelectron spectroscopy (XPS) was used to identify the functional groups present on the adsorbents and to determine the interaction mechanism of V(V) ions with the Lewatit S5428 and Lewatit S5528. Figure 7 presents the XPS spectra of Lewatit adsorbents before and after V(V) loading. In Figure S4, additionally, XPS spectra of O 1s, V 2p, and N 1s before and after V(V) adsorption on Lewatit ion exchangers were also depicted.

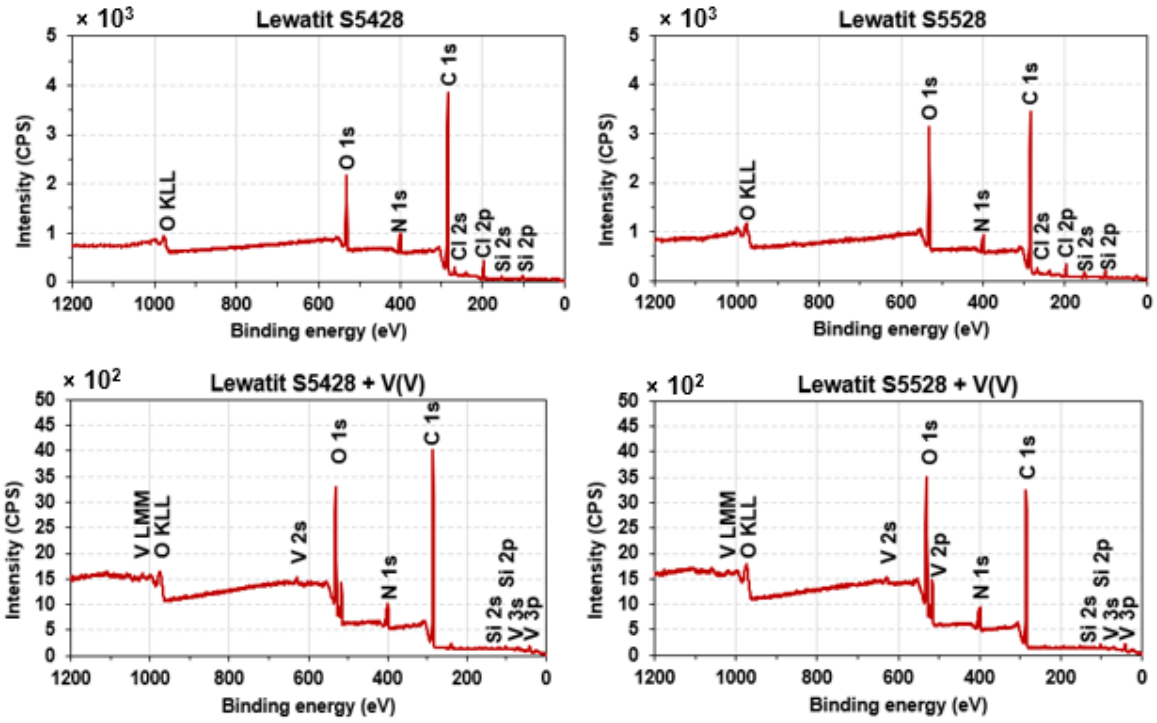


Figure 7. XPS spectra of Lewatit S5428 and Lewatit S5528 before and after V(V) loading.

Before adsorption, both resins exhibited XPS bands at identical binding energies: 285.0 eV for C 1s, 399.8 eV for N 1s, and 531.8 eV for O 1s [51,61–63]. In addition, signals at 102.0 eV and 197.3 eV were observed and assigned to Si 2p and Cl 2p, respectively. The atomic content % of C, N, O, and Cl before adsorption was 76.5, 6.1, 12.2, and 3.2% for Lewatit S5428, and 71.0, 5.0, 18.4, and 2.2% for Lewatit S5528. The XPS analysis of Lewatit ion exchangers before adsorption confirmed the resin components, including the polyacrylic (Lewatit S5528) and polyacrylamide (Lewatit S5428) matrices, as well as the chloride form. Although polyacrylic ion-exchange resins do not contain silicon as a structural component, trace amounts of Si (2.0–3.5% as silica/siloxanes) have been detected by surface-sensitive techniques such as XPS. This silicon could originate from residual silicon-containing additives, fillers, or surface contaminants, and its presence is not reflected by CHNS or SEM-EDX analysis. The presence of silicon in XPS, although not detected by SEM-EDX, indicates that silicon is present only in a trace form, localized at the surface, and does not affect the bulk composition of the polyacrylic resin. After V(V) adsorption on Lewatit, a significant increase in oxygen content is observed in both cases (Table 1). For Lewatit S5428, the increase was 11.4 percentage points, whereas for Lewatit S5528, it was 9.5 percentage points. A new peak at 530.1 eV (the total surface concentration of vanadium amounts to 23.3% for Lewatis S5428 + V(V), 24.8% for Lewatit S5528 + V(V)) corresponds to the formation of V-O bonds. In addition to the overall increase in the O 1s signal, the increases in the C=O and C-OH/C-O-C signals suggest that the resin surface is chemically interacting with V(V) [64,65]. This increase is greater for Lewatit S5528, indicating that this surface may have a higher number of adsorption sites. Moreover, V 2p in the range of 515.7–524.4 (Lewatit S5428) and in the range of 515.6–524.6 eV (Lewatit S5528) appeared after V(V) adsorption. The XPS spectra of the V 2p region for Lewatit resins after V(V) adsorption suggest the presence of vanadium species corresponding predominantly to V(V), with a minor contribution tentatively assigned to V(III). The spectra exhibit the characteristic doublet composed of V $2p_{3/2}$ and V $2p_{1/2}$ components, with a separation of approximately 7.3–7.5 eV, consistent with literature values for vanadium oxides [66]. The V

$2p_{3/2}$ peak located at approximately 517.1 eV for both resins and the accompanying V $2p_{1/2}$ peak at 524.4 eV for Lewatit S5428 + V(V) and 524.6 eV for Lewatit S5528 + V(V) are characteristic of V(V) species, whereas the V $2p_{3/2}$ components at approximately 515.7 eV and 515.6 eV, and the corresponding V $2p_{1/2}$ components at 523.1 eV and 522.9 eV, may be assigned to V(III) species, although this assignment should be considered tentative due to uncertainties associated with spectral deconvolution (Figure S4). Furthermore, partial reduction of vanadium species induced by X-ray irradiation during XPS measurements cannot be excluded, as previously reported for vanadium-containing materials [67,68]. Therefore, the minor V(III)-like contribution does not provide conclusive evidence of V(V) reduction during the adsorption process (Figure S4, Table 1). Quantitative analysis indicates that, for both resins, V(V) is the dominant species, accounting for approximately 89.4% for Lewatit S5428 and 92.5% for Lewatit S5528 of the total vanadium detected at the surface, whereas V(III) accounts for roughly 7.5–10.6% (Table 1). Despite the difference in total V loading, the relative distribution of oxidation states remains nearly identical, indicating a similar adsorption mechanism. Moreover, the predominance of V(V) species, together with the disappearance of the Cl 2p signal of counter-ions, confirms that the adsorption process proceeds mainly via an anion-exchange mechanism involving protonated surface functional groups (stoichiometric anion exchange as the governing mechanism).

Table 1. Binding energy of the deconvoluted XPS spectra of ion-exchange resin surfaces before adsorption of V(V) ions (Lewatit S5428 and Lewatit S5528) and after adsorption of V(V) ions (Lewatit S5428 + V(V) and Lewatit S5528 + V(V)).

Element	Peak	Lewatit S5428		Lewatit S5428 + V(V)		Lewatit S5528		Lewatit S5528 + V(V)	
		Binding Energy (eV)	Content (%)	Binding Energy (eV)	Content (%)	Binding Energy (eV)	Content (%)	Binding Energy (eV)	Content (%)
C 1s	-	285.0	76.5	285.0	68.0	285.0	71.0	285.0	63.1
	C-C/C-H	285.0	59.9	285.0	60.0	285.0	58.8	285.0	53.4
	C-OH/C-O-C C=O	286.4	29.6	286.4	30.4	286.5	29.8	286.3	35.8
	COOR	287.9	7.6	287.9	6.7	287.9	6.2	287.9	9.0
		289.3	2.9	289.3	2.8	289.0	5.2	289.0	1.9
N 1s	-	399.8	6.1	399.8	7.2	399.8	5.0	399.0	7.9
	Amine	400.0	52.9	399.8	45.9	399.9	55.0	399.5	47.1
	N-O/-NH^+=	403.0	47.1	402.7	40.5	402.8	45.0	402.3	40.9
	Nitrates	-	-	406.5	13.6	-	-	406.2	12.0
O 1s	-	531.8	12.2	531.8	23.6	531.8	18.4	531.0	27.9
	C=O	531.4	23.7	531.3	19.8	531.2	21.1	531.3	19.7
	C-OH/O-C-O-	532.4	49.9	532.2	41.8	532.3	53.8	532.2	41.5
	C-O	533.5	21.0	533.4	13.6	533.4	23.4	533.4	13.1
	H_2O/O_2	534.9	5.5	534.8	1.6	534.9	1.7	534.8	0.9
	V-O	-	-	530.1	23.3	-	-	530.1	24.8
Si 2p	-	102.0	2.0	102.0	1.3	102.0	3.5	102.0	1.1
Cl 2p	-	197.3	3.2	-	-	197.3	2.2	-	-
V 2p 3/2	V(III)	-	-	515.7	10.6	-	-	515.6	7.5
V 2p 1/2	V(III)			523.1	0.0			522.9	0.0
V 2p 3/2	V(V)	-	-	517.1	89.4	-	-	517.1	92.5
V 2p 1/2	V(V)			524.4	0.0			524.6	0.0

The point of zero charge (pH_{PZC}) is a key property of ion-exchange resin surfaces, generally defined as the pH at which the net charge of the total particle surface is equal to zero or neutral. This value could influence both the chemical speciation of the metal ions

in solution and the ionization of active sites of the sorbent. The sorbent's surface charge may significantly impact its functionality. This is due to the potential for protonation and deprotonation of adsorbent functional groups, which can affect adsorption efficiency. The impact of pH on solution properties is a crucial factor in this regard. The elucidation of the adsorption mechanism may be facilitated by this understanding [69]. The point of zero charge (pH_{PZC}) for Lewatit S5428 and Lewatit S5528 was obtained by the pH-drift method [70,71]. The results are illustrated in Figure S5. As shown in Figure S5 (see Supplementary Materials), the anion-exchange resins under discussion have pH_{PZC} values of 6.59 for Lewatit S5528 and 7.02 for Lewatit S5428. In the region above the pH_{PZC} value (pH > pH_{PZC}), the anion exchangers' surface becomes negatively charged, while below the pH_{PZC} value (pH < pH_{PZC}), the surface is positively charged. In the context of vanadium adsorption, it has been demonstrated that vanadium anions, such as VO_3^- and HVO_4^{2-}, exhibit effective adsorption at pH values below the point of zero charge. At these pH values, electrostatic attraction between the positively charged anion-exchange resin surface and vanadium anions is enhanced, thereby facilitating adsorption [69,72].

The specifications of Lewatit S5428 and Lewatit S 5528 adsorbents are summarized in Table 2

Table 2. The characteristics of anion-exchange resins used to remove Vanadium(V) from aqueous solutions [47,48,73].

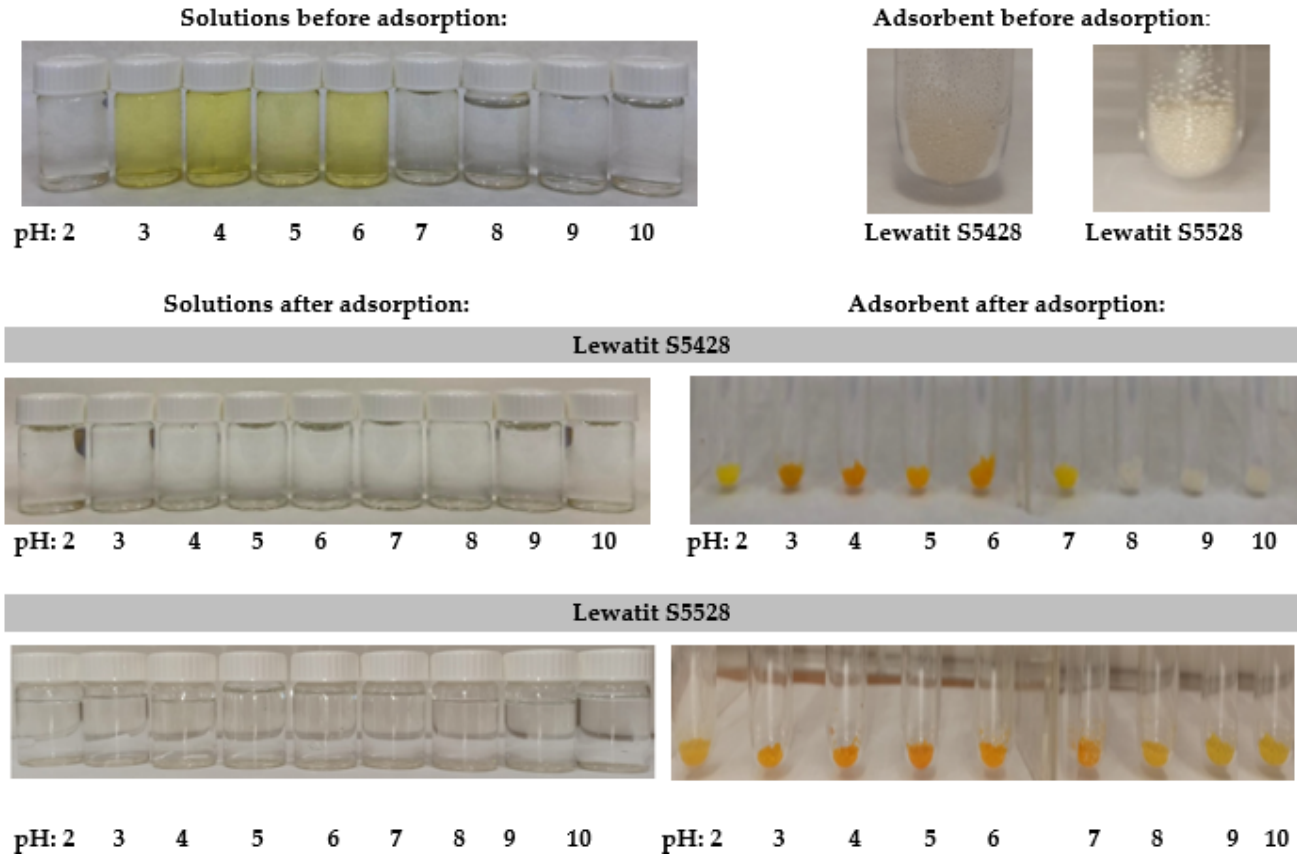
Property	Lewatit S5428	Lewatit S5528
Type	strongly basic anion-exchange resin	strongly basic anion-exchange resin
Matrix	Crosslinked polyacrylamide	Crosslinked polyacrylate
Structure	macroporous	macroporous
Functional group	Quaternary ammonium, Type I	Quaternary ammonium, Type I
Commercial form	Chloride	Chloride
Appearance	White, opaque	White, opaque
Bead size (mm)	0.4–1.6, > 90%	0.4–1.6 (d50)
Effective size (mm)	0.5–0.65	0.5–0.65 (d10)
Uniformity coefficient	max. 1.8	max. 1.8
Total capacity min. (val/L)	0.85	0.85
Operating temperature (max.°C)	80	80
Operating pH range	0–14	0–12
Water retention (wt. %)	63–68	66–72
Volume change ($Cl^- \rightarrow OH^-$)	–	max. 25%
Bulk density (g/L)	725	720
Density approx. g/ml	1.06	1.06
pH_{PZC}	7.02	6.59
Additional information	– Demineralization of aqueous solutions (fruit juices, whey, food acids). – Removing of organic matter.	– Food grade ion exchanger. – Special bead size distribution for use in the co-current and counter-current systems. – Is suitable for the decolorization of syrups from sugar production for example cane sugar, solutions of organic products, e. g. glycerin, amino acids. – Highly recommended for rapid removal of a relatively high concentration of organic substances.

2.2. Lewatit Anion Exchangers Adsorption Behaviour Towards V(V) Ions—Study on Static Adsorption Performance

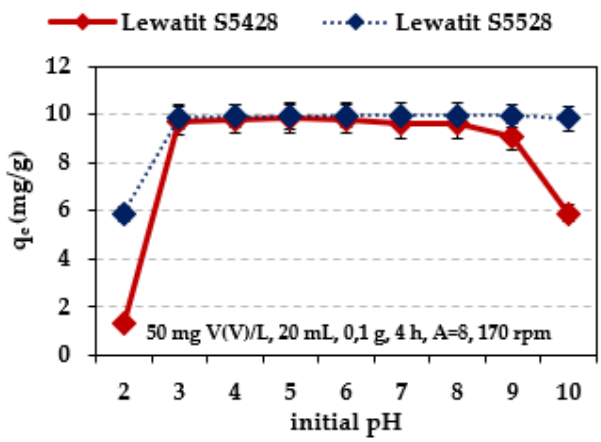
2.2.1. Effect of Solution pH on Adsorption

The effect of the initial pH on V(V) adsorption was investigated over the range of 2 to 10 at an initial solution concentration of 50 mg/L, a V/m of 20 mL:0.1 ± 0.0002 g, an adsorption time of 4 h, and a temperature of 25 °C. The experimental results for both Lewatit resins are shown in Figure 8.

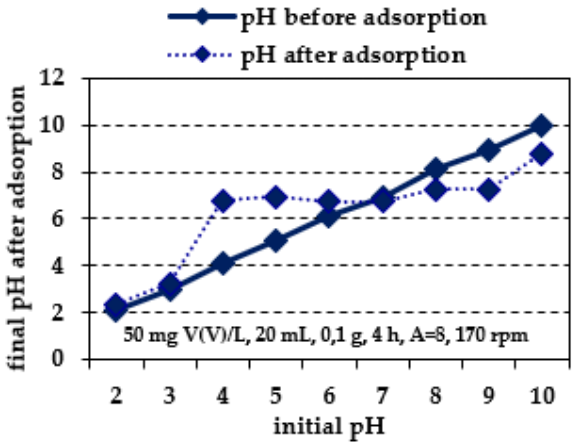
As depicted in Figure 8, the adsorption capacity of Lewatit S5428 and Lewatit S5528 initially increases with increasing pH. The adsorption capacity reaches its maximum at pH 5–6 (0.1 g of sorbent) then slightly decreases, especially for Lewatit S5428.



(**a**)



(**b**)



(**c**)

https://doi.org/10.3390/molecules31234308

Figure 8. Solutions and sorbents before and after V(V) adsorption on Lewatit S5428 and Lewatit S5528 (**a**), and the effect of initial pH on V(V) adsorption (**b**) with its changes before and after adsorption for Lewatit S5528 (**c**).

The obtained experimental adsorption capacities were 9.97 mg/g (Lewatit S5528) and 9.85 mg/g (Lewatit S5428). The adsorption capacity increases with increasing solution pH, reflecting that V(V) exists in different forms at different pH values. The vanadium species, such as cationic, neutral, and anionic, as well as the other mono- or poly-vanadate species, depending on pH, are presented in Figure S6 [34,74]. Monomeric vanadium species prevail in highly dilute solutions, while increasing vanadium concentration promotes their condensation into oligomeric and polymeric forms, resulting from protonation and condensation reactions [75]. Under strongly acidic conditions, V(V) exists mainly as a cation, such as $[VO_2]^+$ and, to a lesser extent, $[H_2V_{10}O_{28}]^{4-}$ [76]. In such conditions, the anion-exchange resins cannot adsorb cationic species; also, the pH values at the lower side indicate adsorption, which is lesser due to the exchange competition between hydrogen ions and vanadate ions for adsorption sites. However, the distribution of vanadium species depends not only on pH but also on the total vanadium concentration. At the investigated concentration of 50 mg V(V)/L, both monomeric and polynuclear vanadium species may contribute to the adsorption process [34]. For pH below pH_{PZC} of adsorbents (6.59 for Lewatit S5528, 7.02 for Lewatit S5428), the surface is positively charged; therefore, the repulsion of the positively charged adsorbent surface and the positively charged vanadium species could proceed, resulting in low adsorption capacities. Moreover, at low pH, positively charged ionic groups can only adsorb vanadate anionic groups, such as $[H_2V_{10}O_{28}]^{4-}$ which do not constitute a major component of the solution. With the pH value increases, the fraction of $[VO_2]^+$ decreases, and the poly-vanadate species of anionic charge are dominant; therefore, the adsorption capacity increases ($[H_2V_{10}O_{28}]^{4-}$, $[HV_{10}O_{28}]^{5-}$, and $[V_{10}O_{28}]^{6-}$) due to vanadium anions exchanging with the counter ions of the anion-exchange resins [77,78]. At pH 5–6, the combination of anionic vanadium species and favorable interactions with positively charged/quaternary ammonium sites results in the highest adsorption. At pH 6–9, the dominant species are HVO_4^{2-} and $H_2VO_4^-$, whereas at pH > 10–12, VO_4^{3-} is dominant (Figure S6). At pH > pH_{PZC}, electrostatic repulsion can occur between the negatively charged adsorbent surface and the anionic vanadate species, thereby hindering vanadate adsorption. Adsorbent surface and the anionic vanadate species, thereby hindering vanadate adsorption [78]. A more significant decrease in adsorption observed at pH > 8 may be associated with changes in vanadium speciation, as well as competition of vanadium and hydroxide due to increasing concentration of hydroxide ions [74]. Moreover, a more pronounced decrease in adsorption was observed for Lewatit S5428 at pH >8, and differences in the physicochemical properties of the resins, especially their polymer matrices, differ (Lewatit S5428 crosslinked polyacrylamide, whereas Lewatit S5528 contains a crosslinked polyacrylate matrix). These differences may influence resin hydration, the accessibility of ion-exchange sites, and the transport of vanadate species within the polymer network [49,74]. Despite only slight changes in adsorption capacity (q_e), especially for Lewatit S5528, across the pH range, and taking into account the highest percentage removal (%R) values, pH 6 was chosen as the optimum for subsequent studies. This selection provides favorable adsorption conditions for both resins and allows their performance to be compared under the same experimental conditions. At pH 5–6, the combination of anionic vanadium species and favorable interactions with positively charged/quaternary ammonium sites results in the highest adsorption. It is worth emphasizing that these anion exchangers can be applied over a wide pH range, which represents one of their significant advantages [79]. This feature enables their application under vari-

ous operating conditions, depending on the specific objectives of the study and the requirements of the treatment process. The changes in pH values of the aqueous solutions before and after V(V) adsorption onto Lewatit S5528 are presented in Figure 8c. The observed variations indicate that the adsorption process was accompanied by significant changes in the acid–base equilibrium of the solution. For initial acidic solutions (pH 2.0–3.0), a slight increase in pH was observed after adsorption, from 2.10 to 2.35 and from 3.00 to 3.24, respectively. This behavior may be attributed to the consumption of protons from the solution during the adsorption process, possibly associated with the exchange of counter-ions, and interactions between vanadium species and the functional groups of the anion exchanger. A pronounced increase in pH was observed for solutions with initial pH values of 4.0–5.0, where the pH increased to 6.76 and 6.93, respectively. For initial pH values above 6, the pH after adsorption remained relatively stable or slightly decreased (from 6.90 to 6.74, from 8.11 to 7.25, and from 8.90 to 7.28). The decrease observed in alkaline solutions may result from the formation of protonated vanadate species and redistribution of acid–base equilibria during adsorption. At the highest initial pH (9.95), the final pH decreased to 8.77. Overall, the adsorption of V(V) onto Lewatit S5528 caused a shift of the solution pH toward neutral values. This effect suggests that the anion-exchange resin participates not only in electrostatic interactions with vanadate anions but also influences the acid-base equilibrium balance of the aqueous phase [80].

Literature findings concerning pH effect on vanadium ions adsorption presented in Table 3 indicate that the pH dependence of V(V) adsorption varies considerably among ion exchangers and cannot be explained by acid–base conditions alone [29–40,42–44]. In particular, the data summarized in Table 3 show that strongly basic anion exchangers can exhibit different adsorption behavior under alkaline conditions. Literature findings concerning the effect of pH on V(V) adsorption, presented in Table 3, indicate that pH is one of the factors that significantly affect the adsorption of V(V) ions [29–40,42–44]. However, the influence of pH varies considerably among the investigated ion exchangers. In particular, the data summarized in Table 3 show that V(V) adsorption has been investigated over a wide range of pH values, and that the adsorption efficiency depends on the type of ion exchanger used. Moreover, strongly basic anion exchangers can exhibit different adsorption behavior under alkaline conditions. Literature data indicate that the optimum pH for vanadium adsorption was 4 for Amberjet™ 4200 Cl anion exchanger [77], 5 for hybrid ion exchanger (fibrous PONF-g-GMA with IRA-96 anion exchangers) [36], 3–9 for nano-hydrous zirconium oxide-modified anion-exchange resin [81], 6 for weakly basic Purolite A830, weakly basic/chelating Purolite S984, strongly basic Lewatit MonoPlus SR7, Purolite A400TL, Dowex PSR2, Dowex PSR3 anion exchangers [41], 4 for weakly basic/chelating Lewatit MonoPlus TP220, and Dowex M4195 ion exchangers [40], and it is in good correlation with our observation.

Table 3. Comparison of ion-exchange resins applied for removing V(V) from aqueous solutions.

Ion Exchanger	Type of Solutions	pH	Adsorption Capacity (q_e) or Percentage Removal (%R)	Additional Information	Ref.
Natural ion exchanger *	Model and industrial effluents (acidic)	pH 3 (1–6)	%R = 92% (pH 3); %R = 86.32–94% (283–323 K); %R = 83.97–96.63% (0.5–5 g); %R = 85.08–91% (5–60 min); %R = 64.8–80.1% (C_0 = 2 mg V/L); %R = 80.1%, pH 3, 5 g, 60 min	-	[30]
Amberlite IRA-400	Model aqueous solutions	V(V): 6 Mo(VI): 4	Mo(VI): q_e = 208, IRA-743, V(V): q_e = 177 mg/g, IRA-400	Elution: 6 mol/L H_2SO_4, 1 mol/L Na_2CO_3	[32]

(SBA, Cl^-), Amberlite IRA-743 (ChIE)		(2–14)			
Nano-hydrous zirconium oxide-modified anion-exchange resin (HZrO@D201)	Model aqueous solutions	3–9	q_e = 118.1 mg/g	Surface modification improves selectivity for vanadate	[31]
Amberlite IRA-400 (SBA, Cl^-)	The bauxite residue leachate enriched with V_2O_5	11.5–13	q_e ~9.8 mg/g (Langmuir, pH 13); $\%R$ > 90%	Flow rate: 6 mL/min; %D > 70% (2 mol/L NaOH)	[29]
Amberjet™ 4200 (SBA, Cl^-)	Ni and V removal from ammoniacal industrial wastewater (Ni 2–4, V 40–50 mg/L)	7–9	Ni: $\%R$ = 100% (pH 5.5–9, 2–10 g/L), q_e = 4.36 mg/g, pH 7; V: $\%R$ > 89% (pH 7, 1–10 g/L), q_e = 48.9 mg/g, pH 7; Column studies: Ni: $\%R$ = 100%, V: $\%R$ = 92–98% (3 cycles) at pH 7–9	$\%D$ = 72–96% (V, 2.5 mol/L NaOH), $\%D$ = 94% (Ni, 1 mol/L H_2SO_4)	[36]
Dowex M4195 and Lewatit MonoPlus TP220 (WBA, ChIE)	Model and real effluents from leaching spent catalyst	4 (2–10)	M4195: $\%R$ = 98.2%, 0.1 g, 99.3%, 0.5 g; C_w = 0.007 g/mL (C_0 = 50 mg V(V)/L), q_e = 209 mg/g—Langmuir; TP220: $\%R$ = 94.9%, 0.1 g, 97.8%, 0.5 g; C_w = 0.04 g/mL (C_0 = 50 mg V(V)/L), q_e = 248 mg/g—Langmuir	Flow rate: 4 mL/min; Elution: 0.1–1 mol/L NaOH, HCl; M4195: $\%D$ = 30.6–45.6%; TP220: $\%D$ = 30.4–47% (NaOH)	[39]
Purolite S984 (ChIE, WBA); Purolite A830 (WBA, Cl^-); Lewatit MonoPlus SR7, Purolite A400TL, Dowex PSR2, Dowex PSR3 (SBA, Cl^-); Lewatit AF5 (without FG)	Model and real effluents from leaching spent catalyst	6 (2–10)	S984: q_e = 221.4 mg/L, C_w = 25.6 g/mL; A830: q_e = 202 mg/L, C_w = 17.7 g/mL; A400TL: q_e = 200.4 mg/L, C_w = 12 g/mL, C_0 = 200 mg/L); real solutions: S984: $\%R$ = 98%, R2; A830: $\%R$ = 80.6%, R2; A400TL: $\%R$ = 67.8%, R4	Column studies selectivity series: S984 > A830 > A400TL > SR7 > PSR3 > PSR2 > AF5 (C_0 = 100 mg/L); Flow rate: 4 mL/min; Elution: 0.1–1 mol/L NaOH, HCl; $\%D$ close to 100% using NaOH	[40]
Amberlite® IRA958, Dowex® 1 × 2 (SBA, Cl^-)	Spent vanadium catalyst leachers by KOH	8 (8–14)	$\%R$ = 9%, pH 14 (both SBA) $\%R$ = 67% (IRA 958), pH 12; $\%R$ = 52% (1 × 2), pH 12; $\%R$ = 97%, pH 8, (both SBA); $\%R$ = 98% and 97% (5 mL); $\%R$ = 85% and 90% (25 mL)	-	[44]
Amberlite IR—120 plus, Dowex 50W X4-100, Dowex 50W X4 (SAC, H^+)	Spent vanadium catalyst leachers by H_2SO_4	-	Fe: $\%R$ = 97.8% (IR—120), 99.8% (50W X4-100, 100% (50W X4), V lost: 30.1, 37.1, 9.5% for J1, J2 and J3	Flow rate: 2 mL/min; Elution: 2 mol/L HCl	[33]

Amberlite IRA-904 modified with TCPP	Tap water, pond water	3–11	$\%R$ = 95 + 2.5% − 98.4 + 2.3%	Pre-concentration factor = 110	[39]
TA-62, (SBA, OH^-)	Aqueous media	6–7	$\%R$ = 97.5% (0.1 g of sorbent) $\%R$ > 99.9% (0.25 g of sorbent)	C_0 = 40 mg/L, Phase contact time: 3 h	[34]
D314, (WBA, Cl^-)	Vanadium containing chromate solution	2.5–6.5	$\%R_V$ = 23.1% (14 h) $\%R_{Cr}$ = 1.8% (14 h) The adsorption of V increase-with pH decrease from 6.5 to 2.5	V/Cr can be completely separated, Separation coefficient: 16.52 (pH 6.5), Elution: 2 mol/L NaOH, $\%D$ = 99.0%	[44]
Resin 717 (SBA, OH^-)	Alkaline media	9–10	$\%R_{V(V)}$ = 90.6% (15 min) $\%R_{Si(IV)}$ = 33.5% (15 min) $\%R_{Al(III)}$ = 21.6% (15 min) $\%R$ = 86.3% (23 °C), 87.3% (45 °C), 88.5% (58 °C) $\%R$ increase from 61.6% to 86.3% with pH values decrease from 10.39 to 9.06	Elution: 2 mol/L NaOH, $\%D_{V(V)}$ = 81.7% (5 min) $\%D_{Si(IV)}$ = 99.1% (5 min) $\%D_{Al(III)}$ = 99.3% (5 min)	[35]
Resin 201 *7 (SBA, Cl^-)	Vanadium waste liquid (separation process of vanadium, titanium magnetite)	6–8	q_e = 1.6 g/L	40 °C, phase contact time: 20 min	[42]
Resins D851 (ChIE), D201 (SBA, Cl^-)	High acidic wastewater	1.5	D851: $\%R$ > 98% (V(IV) and V(V)), q_e = 162 mg/g (V(IV)) D201: $\%R$ < 40% (V(IV)) and 60% (V(V)), q_e = 104 mg/g (V(IV))	Phases contact time: 60 min	[43]
Resins D453, D301FC, ZGA414 (WBA), D202, ZGA351 (SBA)	Leach solutions form roasted stone coal by the sulfuric acid (V, Fe(III), Fe(II), Al(III) and Mg(II))	2.5 2	ZGA414: $\%R$ = 99.9% (V(V)) $\%R$ = 17% (V(IV)) $\%R$ increase with pH increase	Column studies: real solutions—V(V) adsorption affected by Fe(III), addition of $NaClO_3$ causes Fe(III) increase and led to V(V) adsorption decrease and the blocking of resin at pH 2.5	[38]
Resins DDAS, CUW or CW-2 (ChIE, H^+, Na^+)	Ammonium molybdate solution	7.4	$\%R_v$ > 99.5% $\%R_{Mo}$ > 0.27%	Phases contact time: 60 min, ambient temperature, Elution: 5% $NH_3 \cdot H_2O$, Flow rate: 15 mL/h (max. concentration in eluate: 22 g V/L, 0.8 Mo g/L)	[37]

SBA—the strongly basic anion-exchange resin, * Tamarindus indica seeds treated with 39% formaldehyde and 0.1 mol/L H_2SO_4, 80 °C, for 30 min, $\%D$—the desorption efficiency, SAC—the strongly acidic cation exchanger, WBA—the weakly basic anion exchangers, ChIE—the chelating ion exchangers, R2—leaching solutions: 5% m/m H_2SO_4, R4—15% m/m KOH, C_w—the working ion-exchange capacities (column studies), TCPP—5,10,15,20-tetrakis (4-carboxyphenyl) porphyrin, FG—the functional groups, CUV—modified hydrophilic polymers grafted to amorphous silica gel.

2.2.2. Effect of Adsorbent Mass on Adsorption

Sorbent dosage is an important factor influencing adsorption, as it determines the number of available active sites, the effective surface area, and the overall process cost. In general, increasing the amount of sorbent increases adsorption efficiency by increasing the availability of active sites for binding [82,83].

In the next stage, the influence of the anion exchanger dose on the V(V) ion removal efficiency from solutions at the optimum pH for Lewatit S5428 and Lewatit S5428, while maintaining the other experimental conditions constant, was investigated. A given amount of anion exchanger (0.01—0.1 g) was mechanically mixed (A = 8, 170 rpm) with 20 mL of the V(V) solution at pH = 6.0 for 4 h. The results of adsorbent mass effect on V(V) adsorption efficiency were depicted in Figure 9 and compared with other adsorbents. The initial V(V) concentration was 33 mg/L for Lewatit S5528 and 41.9 mg/L for Lewatit S5428. The adsorption capacities and percentage removal were calculated using the actual initial V(V) concentration determined for each system.

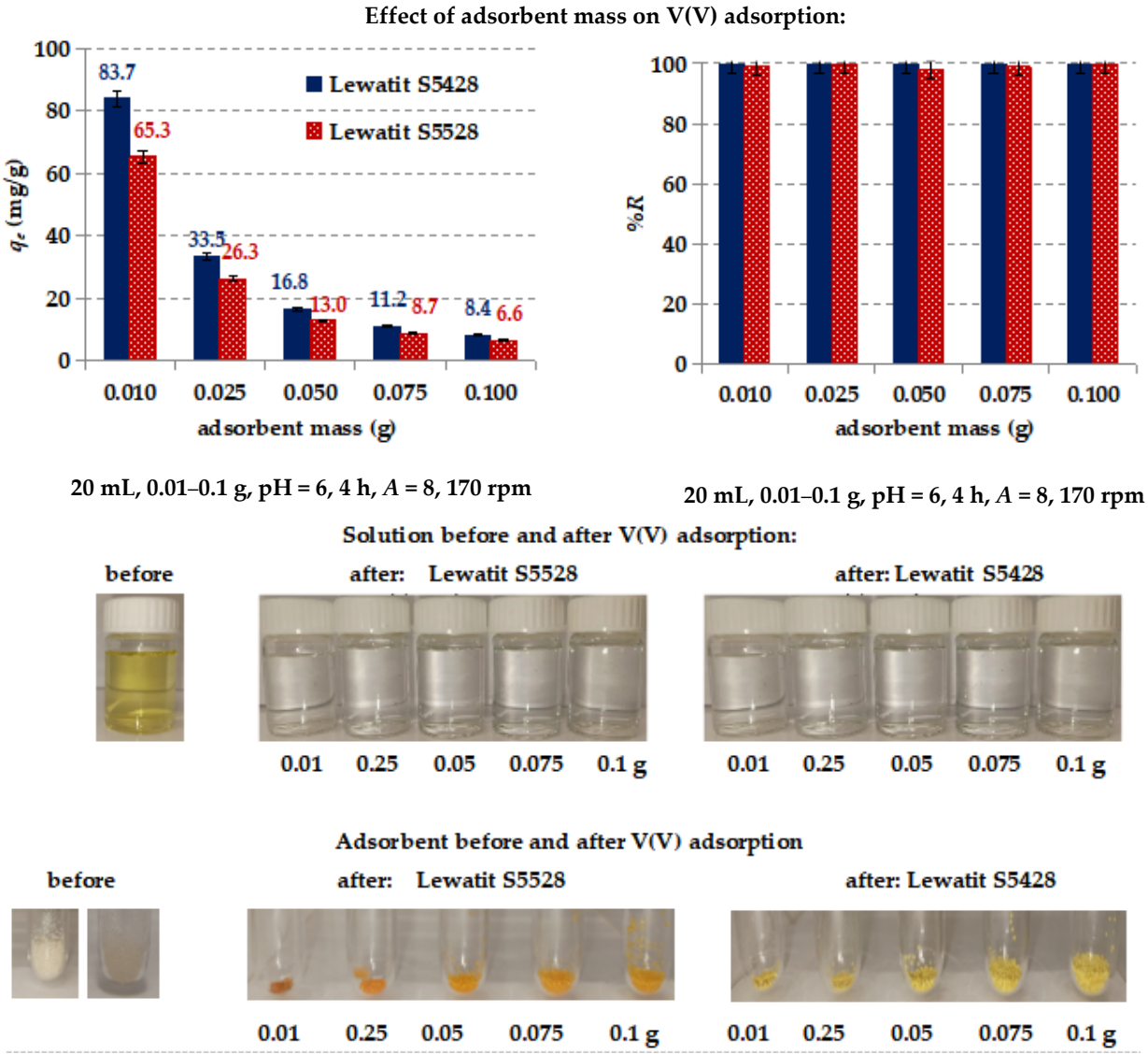


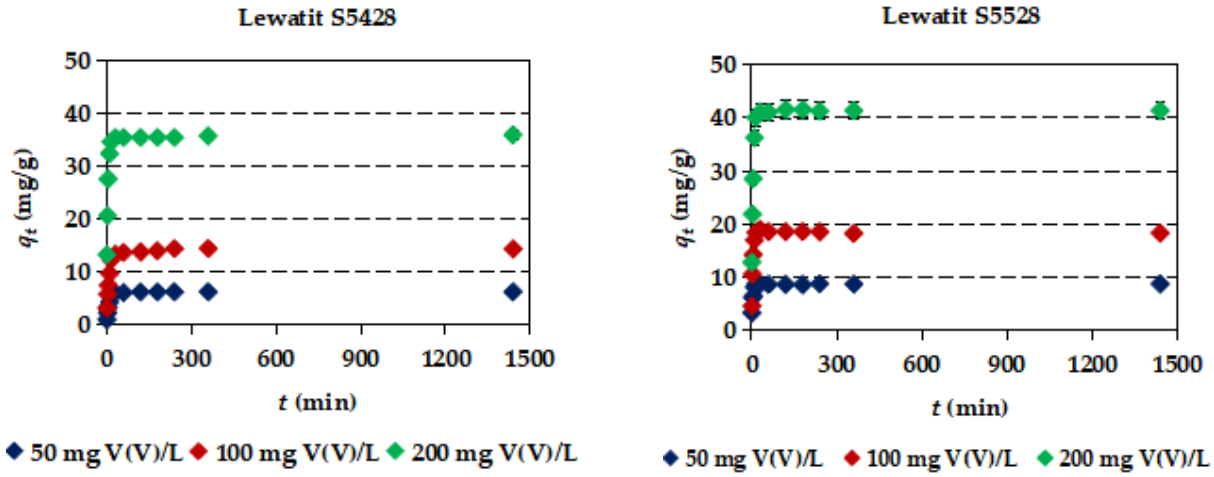
Figure 9. Effect of Lewatit S5428 and Lewatit S5528 mass on V(V) adsorption and solutions and sorbents before and after V(V) adsorption on Lewatit S5428 and Lewatit S5528 (50 mg V(V)/L, 20 mL, 0.01–0.1 g, pH = 6, 4 h, A = 8, 170 rpm).

https://doi.org/10.3390/molecules31234308

The obtained results suggest that the percentage removal values of the V(V) are high for both adsorbents (98–100%) and slightly increased from 98.1% (0.01 g dosage, Lewatit S5528) and 99.7% (0.01 g dosage, Lewatit S5428) to 99.7% (0.1 g dosage, Lewatit S5528) and 100% (0.1 g dosage, Lewatit S5428). Increasing the anion exchanger dosage resulted in only a slight improvement in V(V) removal efficiency, with values approaching a plateau close to complete removal. The decrease in adsorption capacity (q_e) with increasing anion exchanger dosage is attributed to the fixed amount of V(V) ions, which could be adsorbed among a larger number of available adsorption sites. At higher resin dosages, although the removal efficiency increases due to the availability of more active sites, a significant fraction of these sites remains unsaturated, resulting in a lower amount of adsorbed vanadium per unit mass of resin. Although lower resin dosages were sufficient to achieve high V(V) removal efficiencies for Lewatit resins, a dosage of 0.1 g was selected for subsequent experiments to maintain consistency with comparative studies performed using other anion exchangers. Comparing the %*R* obtained for Lewatit S5428 and Lewatit S5528 at 0.1 g of adsorbent mass, these values were comparable or higher compared to Dowex PSR3 (%*R* = 97.7%), Purolite A830 (%*R* = 97.4%), Lewatit MonoPlus SR7 (%*R* = 97%), Purolite S984 (%*R* = 88.2%), Purolite A400TL (%*R* = 88%), Dowex PSR2 (%*R* = 45.5%), and Lewatit AF5 (%*R* = 19.8%) [41].

2.2.3. Effect of Phase Contact Time—Adsorption Kinetics

To investigate the fast of V(V) ion adsorption on the Lewatit S5528 and Lewatit S5428 adsorbents, the effect of the phase contact time was examined on sorption effectiveness from solutions with varying initial concentrations equal to 50, 100, and 200 mg V(V)/L. Figure 10 depicts the variations in the effectiveness of removing V(V) ions in the sorption systems under consideration at the following experimental conditions: 20 mL, 0.1 g, pH = 6, *t* = 1 min to 24 h, *A* = 8, 170 rpm. Although adsorption equilibrium was reached after approximately 15–240 min contact time, experiments were continued for up to 24 h to confirm the stability of the equilibrium state and maintain consistent experimental conditions, which allowed for comparison with other ion-exchange materials tested under the same conditions.



https://doi.org/10.3390/molecules31234308

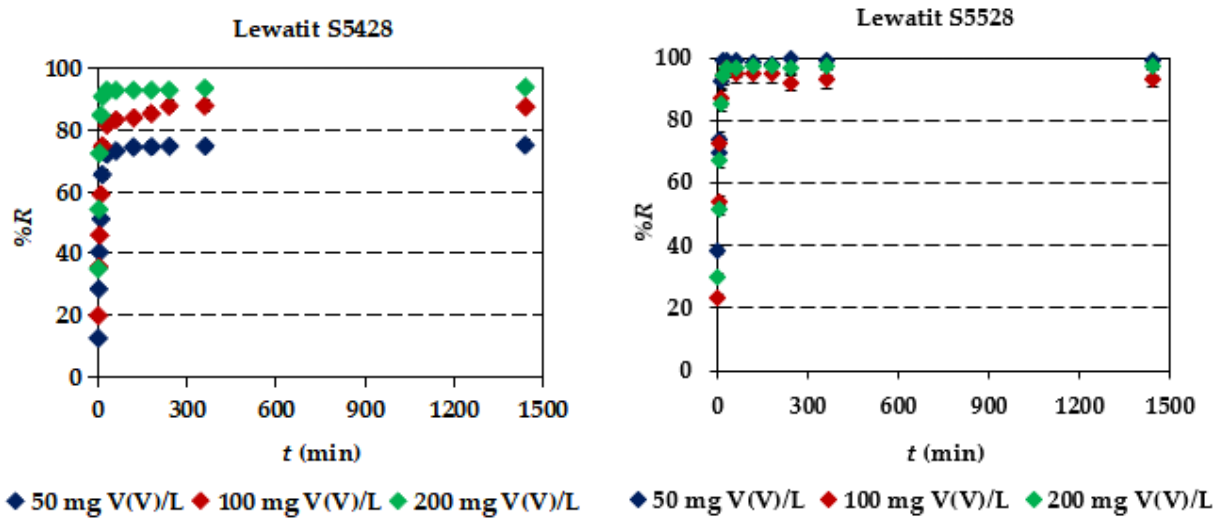


Figure 10. Effect of phase contact time on V(V) adsorption on Lewatit S5428 and Lewatit S5528 (0.1 g, 20 mL, 50, 100, 200 mg V(V)/L, pH = 6, t = 1 min–24 h, A = 8, 170 rpm).

During the adsorption with the increasing phases contact time, the amount of V(V) ions adsorbed increased until the system reached equilibrium. The equilibrium time is the earliest contact time, after which changes in adsorption capacity fulfill the criteria: (a) the differences between consecutive measurements did not exceed 2%, (b) all adsorption capacity (q_t) values measured at and after the assumed equilibrium time (t_{eq}) must differ by no more than 2% from the value obtained at the final measurement (1440 min), and (c) no systematic increase or decrease in adsorption capacity was observed on the kinetic curve. With the initial concentration increased from 50 to 100 mg/L, the time required to reach equilibrium also increased for both resins and decreased for solutions of 200 mg/L concentration. For Lewatit S5428, the equilibrium time was in the range from 30–240 min, whereas for Lewatit S5528, it was in the range from 15 min to 60 min. A similar observation was also made in the systems of V(V) ions—macroporous ion exchangers with the N-methyl-D-glucamine groups (the polystyrene matrix cross-linked with divinylbenzene), where the initial concentration (10, 25, 50, 100 mg V(V)/L) affects the equilibrium establishment [83]. In all solutions under discussion, a two-stage adsorption process was observed [18,83]. The first stage is characterized by a rapid increase in V(V) removal, driven by the abundance of active sites on the adsorbent surface. In the second stage, the adsorption efficiency changes only slightly as the active sites become saturated and the system approaches equilibrium [18]. The obtained results are compared to those from the literature [18,32,83–87]. The time required to reach equilibrium varied with the type of adsorbent and is in the range from 5 min to 36 h (strongly basic anion exchangers: e.g., Amberlite IRA-400, 5 or 60 min [32,85], D296, 12 h [86] ion exchangers with the N-methyl-D-glucamine groups, 120 min [83], N235 impregnated resin (NIRs), 6 and 10 h [84], di-(2-ethylhexyl) phosphoric acid -tributyl phosphate impregnated resin, 36 h [87]). Two-stage V(V) ion adsorption has also been documented in previous studies [18,40,41,83]. The percentage removal of V(V) values increase with the phase contact time increase, e.g., form 12.5% (t = 1 min) to 75.2% (1440 min) (50 mg/L), from 19.8% (t = 1 min) to 87.6% (1440 min) (100 mg/L), and from 35% (t = 1 min) to 94.0% (t = 1440 min) (200 mg/L) for Lewatit S5428. The %R achieved was usually 75–94% for Lewatit S5428 and 96–100% for Lewatit S5528.

The obtained kinetic data of V(V) were fitted to the following kinetic models: the pseudo-first (PFO) [88] and pseudo-second order (PSO) [89], as well as intraparticle diffusion (IPD) [90] models described in Section 3.5. The kinetic parameters obtained from the slope and intercept of the curve, using linear (L) and non-linear (NL) regression, are shown in Table 4.

Table 4. Comparison of kinetic parameters obtained during the V(V) adsorption on Lewatit resins.

	Parameters	**Lewatit S5428**			**Lewatit S5528**		
		50 mg/L	**100 mg/L**	**200 mg/L**	**50 mg/L**	**100 mg/L**	**200 mg/L**
	$q_{e,\ exp}$ (mg/g)	6.30	14.45	35.93	8.82	18.96	41.51
PFO-L	$q_{e,\ cal}$ (mg/g)	1.32	5.31	3.65	0.60	1.02	4.39
	k_1 (1/min)	0.014	0.020	0.010	0.011	0.003	0.012
	R^2	0.708	0.914	0.499	0.397	0.033	0.550
PFO-NL	$q_{e,\ cal}$ (mg/g)	6.08	13.41	34.62	6.08	13.41	34.62
	k_1 (1/min)	0.167	0.198	0.384	0.167	0.198	0.384
	R^2	0.983	0.949	0.956	0.955	0.976	0.931
	R^2_{adj}	0.980	0.937	0.946	0.945	0.971	0.915
	MPSD	0.039	0.132	0.061	1.967	1.248	0.204
PSO-L	$q_{e,\ cal}$ (mg/g)	6.32	14.49	35.96	8.77	18.35	41.54
	k_2 (g/mg min)	0.054	0.019	0.017	0.124	0.120	0.016
	R^2	1.000	1.000	1.000	1.000	1.000	1.000
	h	0.913	0.928	0.687	0.913	0.928	0.687
PSO-NL	q_e (mg/g)	6.57	15.11	28.84	8.98	15.11	42.54
	k_2 (g/mg min)	0.030	0.014	0.003	0.070	0.014	0.010
	MPSD	0.024	0.060	2.801	0.015	1.276	0.022
	R^2	0.981	0.988	0.782	0.970	0.863	0.975
	R^2_{adj}	0.976	0.985	0.734	0.963	0.833	0.969
IPD	q_e (mg/g)	6.35	14.69	35.93	8.78	18.17	41.53
	k_{i1} (mg/g min$^{0.5}$)	1.494	3.048	7.446	1.770	4.683	9.522
	C_1	−0.27	0.41	7.85	2.35	1.77	5.05
	R_1^2	0.986	0.994	0.938	0.920	0.917	0.974
	k_{i2} (mg/g min$^{0.5}$)	0.006	0.029	0.017	0.002	0.015	0.014
	C_2	6.13	13.58	35.28	8.72	18.83	40.99
	R_2^2	0.496	0.575	0.858	0.134	0.588	0.807

Moreover, the applicability of the kinetic models for the description of the adsorption of V(V) ions on the Lewatit anion exchangers to the aforementioned equations of PFO, PSO, and IPD models is graphically represented in Figure S7 for Lewatit S5428 and Figure S8 for Lewatit S5528 (Supplementary Materials), and the IPD plots q_t (mg/g) versus $t^{0.5}$ is depicted in Figure 11.

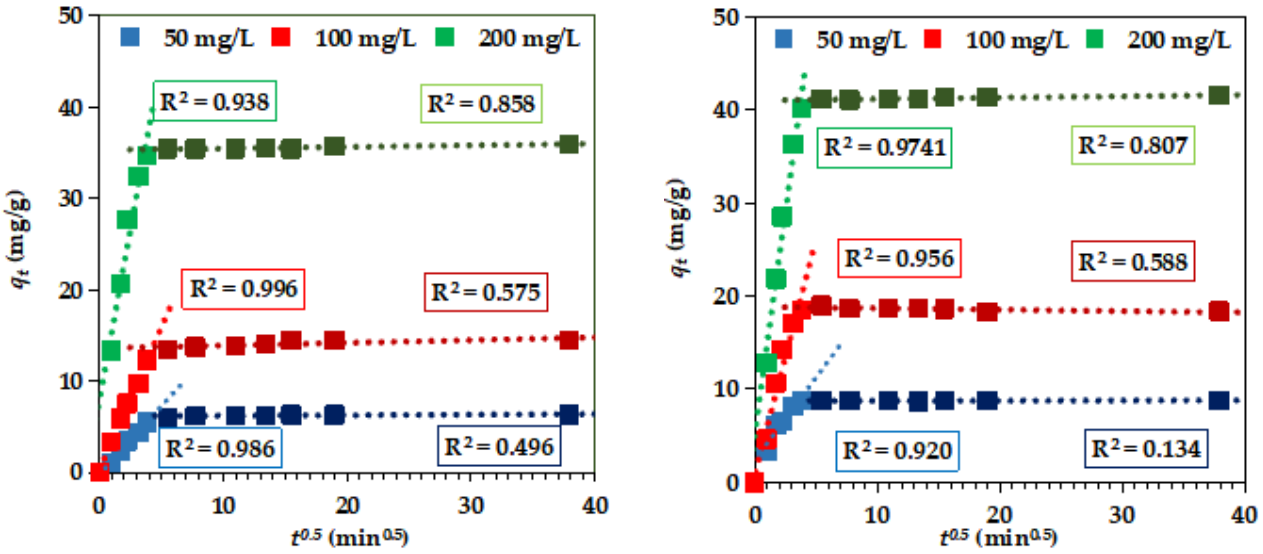


Figure 11. IPD plots obtained during V(V) adsorption on Lewatit S5428 and Lewatit S5528 (light green, red, blue - part 1; dark green, red, blue - part 2).

The comparison of kinetic parameters for the most widely used pseudo-first- and pseudo-second-order models suggests that the adsorption of V(V) ions onto Lewatit resins follows a pseudo-second-order mechanism. This conclusion is supported by the high R^2 values, which are higher for the pseudo-second-order model for both resins (R^2 = 1.000) than for the pseudo-first-order model (up to 0.914-NL and up to 0.983-L), as shown in the fitting plots presented in the Supplementary Materials (Figure S7 and S8). Moreover, the calculated equilibrium capacities $q_{e,\,cal}$, according to the PFO and PSO kinetic models, were compared with the experimental equilibrium capacities, $q_{e,\,exp}$. It was found that the $q_{e,\,cal}$ values are consistent with the $q_{e,\,exp}$ ones (PSO-L). These values differ by a maximum of 0.03 (PSO-L, Lewatit S5428) and 0.61 (PSO-L, Lewatit S5528). In contrast, the $q_{e,\,cal}$ (PSO-NL), $q_{e,\,cal}$ (PFO-L), and $q_{e,\,cal}$ (PFO-NL) values were slightly (PSO-NL) or significantly lower than the $q_{e,\,exp}$ values (PFO-L and PFO-NL). The k_2 rate constant values determined using the PSO model indicate that the adsorption rate decreased with increasing initial V(V) concentrations from 50 to 200 mg/L. This trend indicates that the adsorption process becomes slower at higher initial concentrations.

According to the Weber-Morris model, if the plot of q_t versus $t^{0.5}$ is linear and passes through the origin, the intraparticle diffusion is the only rate-limiting step. On the contrary, if the plot does not pass through the origin, the adsorption processes follow the intraparticle diffusion and also the film diffusion, which is connected with the thickness of the boundary layer [88]. Particularly during the initial reaction phase, external mass transfer may be significant. In the IPD plots based on the kinetic data for V(V) adsorption on Lewatit resins, two adsorption steps could be distinguished (Figure 11). At the beginning of the film diffusion, where V(V) ions are captured by the external surface sites of the Lewatit ion exchanger, the process occurs. Then, the V(V) ion adsorption process slows, and metal ions diffuse into internal pores of the Lewatit resin (intraparticle diffusion), and the system approaches equilibrium. The high values of the determination coefficient for the first linear segment (R_1^2 = 0.917–0.994) indicate that the model fits the experimental data well. At the same time, the lower values of R_2^2 (0.134–0.858) indicate a weaker fit for the second segment. Such multilinearity was also reported previously in the literature for V(V) adsorption systems [40,41,83]. The IPD q_t versus $t^{0.5}$ plot does not pass through the

origin (see C_1 and C_2 presented in Table 4), indicating that the V(V) adsorption mechanism is mixed. Based on that, we can conclude that adsorption kinetics are influenced not only by intraparticle diffusion but also by film diffusion.

2.2.4. Effect of Concentration—Equilibrium Studies

Equilibrium studies and data adsorption isotherm modelling were conducted to identify the possible interaction mechanisms between V(V) ions and Lewatit S5428 and S5528, as well as to determine their maximum adsorption capacities. The adsorption data were analyzed using the following isotherm models: (1) the Langmuir model, which assumes a uniform surface with monolayer adsorption and no interactions between adsorbed species [91–93], (2) the Freundlich model, which is empirical and describes multilayer adsorption on heterogeneous surfaces [91,92,94], (3) the Temkin model which considers a uniform distribution of binding energies and assumes that the heat of adsorption decreases linearly as surface coverage increases [91,92,95,96], and (4) the Dubinin–Radushkevich model, also empirical, which is commonly applied to the adsorption of vapors on solid surfaces and can be used to describe heterogeneous systems involving both solid and liquid phases [91,92] described in Section 3.5, Equations (35)–(44). The initial concentration of V(V) ions in the vanadium-plus-ion exchanger systems ranged from 50 to 1000 mg/L. Figure 12 displays the equilibrium data for V(V) ion adsorption on Lewatit resins at ambient temperature (blue rhombuses), along with the fitting plots for the Langmuir, Temkin, Freundlich, and Dubinin-Radushkevich isotherm models using linear (L) and non-linear (NL) regression. The parameter value for the calculated isotherm models, obtained from the C_e/q_e vs C_e, log q_e vs log C_e, q_e vs ln C_e, and ln q_e vs ε^2 plots, are reported in Table S2. The determination coefficient (R^2), the Marquardt's percent standard deviation ($MPSD$), and adjusted R-squared (R^2_{adj}) values were calculated based on the following equations [97]:

$$R^2 = 1 - \frac{\sum \left(q_{e\,exp} - q_{e\,cal}\right)^2}{\sum \left(q_{e\,exp} - q_{e\,mean}\right)^2} \quad (1)$$

$$MPSD = \sum_{i=1}^{n} \left(\frac{q_{e\,exp} - q_{e\,cal}}{q_{e\,exp}}\right)_i^2 \quad (2)$$

$$R^2_{adj} = 1 - \left[\frac{(1 - R^2)(n - 1)}{n - k - 1}\right] \quad (3)$$

where: $q_{e\,exp}$ (mg/g) is the amount of V(V) adsorbed at equilibrium, $q_{e\,cal}$ (mg/g) is the amount of V(V) adsorbed, $q_{e\,mean}$ (mg/g) is the adsorption capacity from experiment measured obtained from $q_{e\,exp}$ values, n is the number of data points, and k is the number of independent regressors.

V(V) ion adsorption increased with increasing initial V(V) concentration, reaching a plateau at higher concentrations. The maximum experimental adsorption capacities for V(V) were 181.20 mg/g for Lewatit S5428 and 226.30 mg/g for Lewatit S5528 (ambient temperature). Comparing the maximum monolayer adsorption capacities obtained from the Langmuir model (Q_0), which are 206.59 mg/g (L) and 154.06 mg/g (NL) for Lewatit S5428, and 261.94 mg/g (L) and 154.06 mg/g (NL) for Lewatit S5528, with the experimental adsorption capacity values, it can be concluded that there is little agreement between them. Moreover, the determination coefficient (R^2) obtained for the Langmuir model is in the range of 0.903–0.962 for both the L and NL regressions. This suggests that the Langmuir model does not describe the adsorption data well and that the monolayer adsorption of V(V) on the Lewatit resin surface is not the dominant process. The Langmuir constant k_L

reflects the affinity between the adsorbent and adsorbate. Higher k_L values indicate stronger interactions, whereas lower values indicate weaker adsorbate binding. The Langmuir k_L constants were within the range 0.037–0.102 L/mg for both resins. The Freundlich adsorption model fits the experimental data better, as indicated by higher determination coefficients: 0.994 (L) and 0.997 (NL) for Lewatit S5428, and 0.996 (L) and 0.992 (NL) for Lewatit S5528; a higher adjusted determination coefficient: (R^2_{adj} = 0.996 (NL) and 0.989 (NL)); and lower MPSD values (0.137 (NL) and 0.029 (NL)) compared with the Langmuir model (R^2 = 0.923 (NL) and 0.903 (NL); R^2_{adj} = 0.893 (NL) and 0.871 (NL); MPSD = 0.408 (NL) and 0.670 (NL), respectively). Due to the smaller values of the determination coefficients for Temkin (0.919–0.928) and Dubinin-Raduchkievich (0.391–0.621) (Table S2), as well as the shape of the isotherms (Figure 12), the Temkin and Dubinin-Raduchkievich models proved to be inadequate to describe the adsorption process in the V(V)-Lewatit S5428 and S5528 systems. The mean free energy of adsorption (E), calculated using the Dubinin–Radushkevich model, ranged from approximately 0.84 to 1.09 kJ/mol. The mean free energy of adsorption (E) ranged from 0.839 to 1.097 kJ/mol. These values are below 8 kJ/mol, suggesting that physical interactions could play a role during V(V) adsorption [98,99]. However, this interpretation should be treated with caution due to the relatively poor fit of the Dubinin–Radushkevich model. Moreover, relatively high values of Marquardt's percent standard deviation (*MPSD*) were obtained for both the Dubinin–Radushkevich (1.387 and 2.233) and Temkin (0.516 and 1.000) models, indicating their limited suitability for describing the adsorption process. In the Langmuir model, the MPSD values (0.480 and 0.670) were also higher than those calculated for the Freundlich model (0.137 and 0.029). The significantly lower error values for the Freundlich model suggest that it provides the best fit to the experimental data and most accurately represents the adsorption behaviour. The $1/n$ parameter describing the intensity of adsorption was in the 0–1 range and indicates favourable adsorption. The obtained results are consistent with literature data, where the Freundlich model frequently provides the best fit for V(V) adsorption on various adsorbents. For example, the vanadium adsorption on Amberlite IRA-400 from the post-closure effluent (1) (pH 11.5) and operating bauxite residue disposal areas leachate (2) (pH 13.3) was described better by the Freundlich model (1: k_F = 0.547; n = 2.383; R^2 = 0.999 and 2: k_F = 0.285; n = 1.050; R^2 = 0.993) than the Langmuir one (1: q_{max} = 1.135 mg/g; b = 3.218 L/mg; R^2 = 0.859 and 2: q_{max} = 9.759 mg/g; b = 0.060 L/mg; R^2 = 0.919) [29]. Similarly, vanadium adsorption on Tulsion A-62 (F: k_F = 15.33 mg/g; n = 3.2 L/g; R^2 = 0.980, L: q_{max} = 36.9 mg/g; k_L = 0.585 1/mol; R^2 = 0.964) [34] and Amberlite IRA743; Lewatit MK51; Purolite S110; Purolite S108 (L: q_{max} = 66.42–77.03 mg/g; R^2 = 0.992–0.997; F: R^2 = 0.958–0.998) [80] follows the Freundlich model. In the present study, the Freundlich model better described the adsorption of V(V) onto Lewatit S5428 and Lewatit S5528, suggesting a heterogeneous adsorption mechanism and possible multilayer formation.

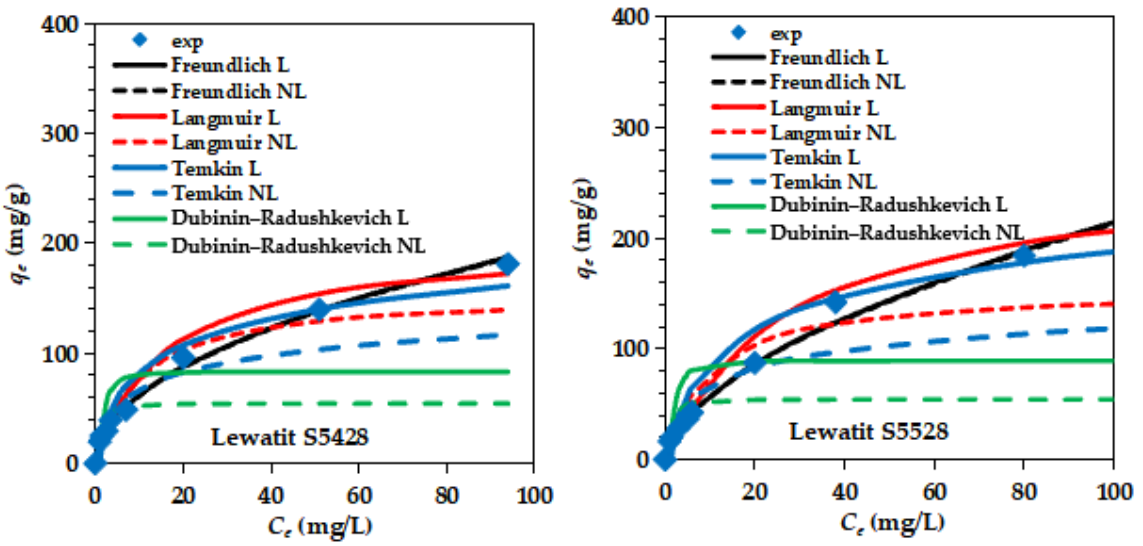


Figure 12. Effect of initial concentration on V(V) adsorption on Lewatit S5428 and Lewatit S5528 (0.1 g, 20 mL, pH = 6, t = 24 h, A = 8, 170 rpm) and fitting of the Langmuir, Freundlich, Temkin, and Dubinin–Radushkevich models.

2.2.5. Effect of Temperature and Thermodynamic Studies

The effect of temperature (295, 203, 333 K) on V(V) was analyzed, and the thermodynamic parameters, including Gibbs free energy change ($\Delta G°$), enthalpy change ($\Delta H°$), and entropy change ($\Delta S°$), were calculated according to Equations (45)–(47). The description of the meaning of each parameter is provided in Subchapter 3.5. The temperature affects the adsorption capacities slightly. About 1–2% changes of adsorption capacities were observed: Lewatit S5428 (180.7 mg/g (298 K), 179.3 mg/g (313 K), 177.6 mg/g (333 K)) and Lewatit S5528 (226.3 mg/g (298 K), 225.5 mg/g (313 K), 224.7 mg/g (333 K)). The enthalpy ($\Delta H°$, kJ/mol) and entropy ($\Delta S°$, J/mol K) changes were estimated using the slope and intercept of linear plots of ln Kc versus $1/T$ (the Van't Hoff plot).

Dependence of ln Kc versus $1/T$ is presented in Figure S9, whereas the calculated thermodynamic parameters for both anion exchangers are presented in Table 5.

Table 5. Thermodynamic parameters obtained during V(V) adsorption onto Lewatit S5428 and Lewatit S5528.

Temperature	$\Delta G°$ (kJ/mol)	$\Delta H°$ (kJ/mol)	$\Delta S°$ (J/mol K)	R^2
Lewatit S5528				
298 K	−18.69			
308 K	−19.53	−1.68	57.04	0.997
318 K	−20.68			
Lewatit S5428				
298 K	−18.65			
308 K	−19.39	−3.85	49.67	1.000
318 K	−20.39			

The negative $\Delta G°$ values (−18.65 to −20.39 kJ/mol for Lewatit S5428 and −18.69 to −20.68 kJ/mol for Lewatit S5528) confirm the spontaneity and feasibility of V(V) adsorption. The more negative the $\Delta G°$ value, the greater the driving force of the process and the

greater the spontaneity of adsorption indicating that the process becomes thermodynamically more favorable at higher temperatures [34,53]. For the Lewatit S5428 and Lewatit S5528 anion exchangers, the ΔG° values become slightly more negative with increasing temperature. Values around −18 to −21 kJ/mol indicate a relatively thermodynamically favorable process, dominated by electrostatic interactions and ion-exchange rather than stable chemical bonds. Secondly, the negative enthalpy change value (ΔH°) being −1.68 kJ/mol for Lewatit S5528 and −3.85 kJ/mol for Lewatit S5428 indicates that the adsorption process of V(V) ions on anion exchangers was exothermic and involving weak interactions rather than the formation of strong chemical bonds [100]. Finally, the positive entropy value (ΔS°) confirms that the system becomes less ordered after adsorption than before. The positive ΔS° values (57.04 and 49.67 J/mol·K for Lewatit S5528 and Lewatit S5428, respectively) indicate an increase in the disorder of the system during adsorption. Although the negative ΔH° values indicate the exothermic nature of adsorption, the increasingly negative ΔG° values with increasing temperature do not contradict this observation. This behavior results from the predominantly entropy-driven nature of the process. According to the Gibbs free energy relationship ($\Delta G^\circ = \Delta H^\circ - T\Delta S^\circ$), the contribution of the positive entropy term ($-T\Delta S^\circ$) becomes increasingly favorable as temperature rises, outweighing the relatively small negative enthalpy contribution. Consequently, adsorption becomes thermodynamically more favorable at higher temperatures despite its exothermic character. The positive entropy change may be mainly attributed to the release of structured hydration water molecules (desolvation) and the displacement of hydrated chloride counterions into the bulk solution during polyvanadate exchange, resulting in increased disorder at the solid–solution interface. Therefore, it can be concluded that the adsorption process of V(V) ions on Lewatit anion exchangers is spontaneous and exothermic, with its thermodynamic favorability predominantly governed by entropy. Obtained results are consistent with other adsorption systems, e.g., V(V) adsorption on $SiO_2Fe_xO_y$ sample, where ΔG° values were negative (−4.75 kJ/mol for 298 K, −5.57 kJ/mol for 308 K and −6.4 kJ/mol for 318 K), whereas ΔH° = 19.76 kJ/mol and ΔS° = 82.28 J/mol·K were positive [101]. Feasible and spontaneous V(V) adsorption (ΔG° = −8.0 kJ/mol for 303 K, −9.2 kJ/mol for 313 K and −10.40 kJ/mol for 323 K), the endothermic nature (ΔH° = 28.31 kJ/mol), and the increase in randomness at the solid–solute interface (ΔS° = 120 J/mol·K) were observed during the adsorption of vanadium on Tulsion A-62(MP) [34]. Vanadium adsorption on Lewatit MonoPlus MP600 resin of the quaternary amine, type II functional groups shows negative values of ΔG°, which are −26,39 kJ/mol for 298 K, −27.95 kJ/mol for 303 K, and −29.51 kJ/mol for 313 K, as well as positive values of ΔH° and ΔS° (ΔH° = 19.39 kJ/mol, ΔS° = 156.23 J/mol·K) [102]. The adsorption thermodynamic parameters during vanadium adsorption onto 312 resin were ΔH° = 9.26 kJ/mol, ΔS° = 53.59 J/mol*K and ΔG°_{298} = −6.71 kJ/mol, indicating the spontaneous and endothermic adsorption [103]. Although these literature examples confirm that vanadium adsorption is generally thermodynamically favorable, the differences in the signs and magnitudes of ΔH° and ΔS° demonstrate that the adsorption mechanisms and their dependence on temperature may vary considerably depending on the sorbent properties and experimental conditions. Therefore, direct comparison of ΔG° values should be treated with caution, as differences in sorbent functionality, solution chemistry, and standard-state conventions may affect the calculated thermodynamic parameters. As was pointed out by Peng et al. [99], thermodynamic analysis is useful for studying the reaction mechanism during adsorption. When ΔG° values range from 0 to −20 kJ/mol, physical interactions (physisorption), such as electrostatic forces, van der Waals forces, or ion exchange, dominate. For values below −20 to −80 kJ/mol, a mixed mechanism—physisorption and chemisorption—is indicated, while values between −80 and −400 kJ/mol indicate chemisorption with the formation of stronger chemical bonds. However, ΔG° values alone cannot unequivocally determine the adsorption mechanism

and should be interpreted together with other thermodynamic parameters and complementary characterization results. Although these $\Delta G°$ values lie near the boundary (−20 kJ/mol), they are often associated with mixed physisorption –chemisorption regimes [99]. The very low enthalpy changes $\Delta H°$ = −3.85 and −1.68 kJ/mol (which are substantially lower in magnitude than the values typically associated with strong chemical interactions) do not provide evidence for significant covalent or coordinate bond formation. Instead, the process is primarily entropy-driven ($\Delta S°$ = 49.67 and 57.04 J/(mol·K)), resulting from the displacement of structured hydration water (desolvation) and the release of multiple hydrated Cl^- counterions into the bulk solution upon polyvanadate exchange. Thus, the thermodynamic behavior is consistent with an entropy-driven, electrostatically governed ion-exchange mechanism.

2.2.6. Desorption Studies

The practical application of the sorbent is influenced by several factors, including the potential for V(V) desorption and its reuse. On the other hand, desorption yield depends on the adsorption mechanism type, the desorption agent type, and concentration, regeneration time, or temperature [41]. Desorption of loaded vanadium was carried out by using the 0.1, 0.25, 0.5, and 1 mol/L HCl and 0.1, 0.25, 0.5, and 1 mol/L NaOH solutions under the experimental conditions: W = 0.1 ± 0.0005 g, V = 20 mL, pH = 6, 170 rpm, A = 8, T = 295 K, t = 4 h. The desorption results are presented in Figure 13. Despite the higher concentrations of HCl or NaOH, they may improve vanadium desorption [102]. However, the additional benefit is often limited compared with the increased operational costs and the risk of polymer matrix degradation [80]. According to the manufacturer's recommendations, Lewatit S5528 and S5428 resins can be effectively regenerated using moderate concentrations of NaOH (2–6 wt.%) or NaCl solutions (approximately 10 wt.%) [48]. Therefore, up to 1 mol/L of eluent concentration was selected in this study. In particular, the use of 1 mol/L of NaOH is consistent with the manufacturer's recommendation for Lewatit S5428, where NaOH at approximately 4 wt.% is suggested as an effective regenerant. Although NaOH is the eluting agent recommended by the manufacturer, 1 mol/L of HCl was also investigated due to the ability of chloride ions to act as counter-ions in strongly basic anion-exchange resins, facilitating the replacement of sorbed vanadate species.

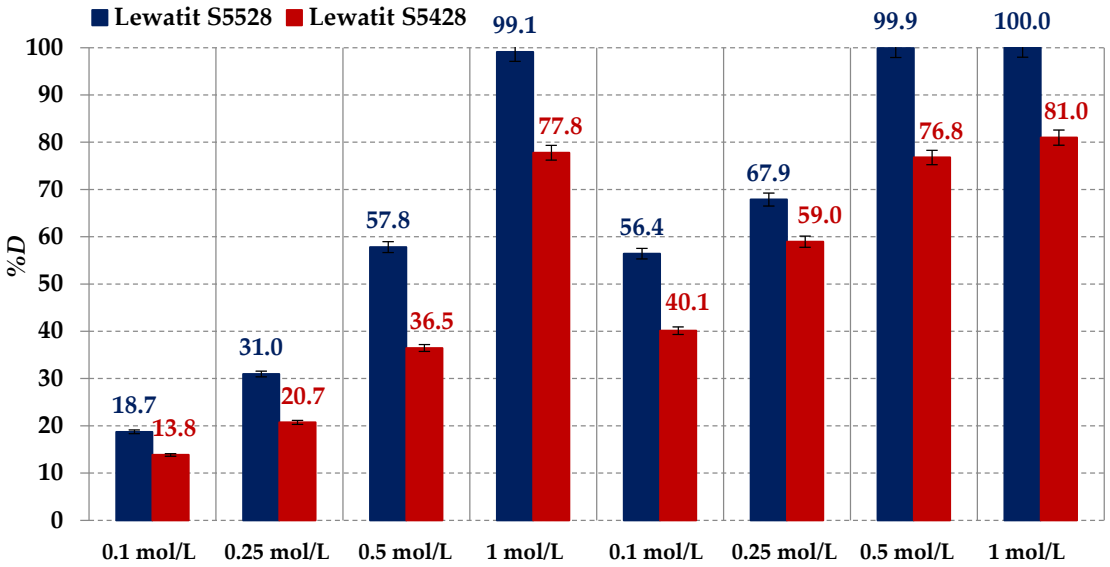


Figure 13. Desorption yield of V(V) from Lewatit S5428 and Lewatit S5528.

https://doi.org/10.3390/molecules31234308

The V(V) adsorption was slightly higher for Lewatit S5528 (with a %*S* above 99%) than for Lewatit S5428 (with a %*S* close to 92%). The desorption yield increased with increasing HCl and NaOH concentration, reaching a maximum at 1 mol/L. Additionally, 1 mol/L HCl and 1 mol/L NaOH ensure 90–100% desorption for Lewatit S5528, whereas in the case of Lewatit S5428, the desorption was slightly lower and reached 77.8% by using 1 mol/L HCl and 81% by using 1 mol/L NaOH, indicating a stronger affinity. The lower desorption observed with 1 mol/L HCl (99.1% for Lewatit S5528 and 77.8% for Lewatit S5428) compared to 1 mol/L NaOH (100% for Lewatit S5528 and 81%% for Lewatit S5428) is directly related to vanadium speciation. Strongly acidic conditions preserve stable polyvanadate clusters that possess high affinity for quaternary ammonium sites and are not fully displaced by chloride counterions. In contrast, alkaline conditions of 1 mol/L NaOH, corresponding to approximately 3.85 wt.%, are consistent with the manufacturer's ~4 wt.% recommendation) and promote depolymerization into simple orthovanadate oxyanions, allowing efficient displacement by hydroxide ions. With NaOH concentration increases, the amount of OH^- anions also increases, forcing the depolymerization of decavanadates back into simple orthovanadate monomers VO_4^{3-} and V_{10} clusters, breaking the multi-centre binding, resulting in a highly efficient desorption yield ($H_2V_{10}O_{28}^{4-} \rightarrow 10\ VO_4^{3-}$) while maintaining its valence state unchanged. Although these batch tests identified 1 mol/L NaOH as an effective stripping agent, long-term resin stability across multiple exhaustion –regeneration cycles was not investigated in this work and will be addressed in future dynamic column studies.

The literature data are consistent with our studies and indicate that vanadium could be effectively desorbed from other strongly and weakly basic ion exchangers such as D296 resin (6 mol/L HCl, %*D* = 98.68%) [86], D201 (5% NaOH + 10% NaCl, %*D* = 91.2%) [20], Amberlite IRA40 (2 mol/L NaOH, %*D* = 57 − 72%, 30 min) [85], 201 *7 (2 mol/L NaOH, %*D* = 81.7%, 5 min) [35], and 201 *7 (3 mol/L NaOH, %*D* > 95%) [104], etc. Moreover, desorption experiments of vanadium from Lewatit MonoPlus MP600 using aqueous HCl and NaOH solutions from 1.0 to 3.0 mol/L indicated that desorption yield and rates increase with the desorption solution concentration increases, yielding over 80% desorption for vanadium after 240 min of phases contact time [102].

2.2.7. Column Experiment Results

From a technological point of view, vanadium adsorption studies using the column method are more useful than those using the static method. Therefore, adsorption studies in a continuous system with solutions of various initial concentrations (50, 100, and 200 mg/L) were conducted at pH 6 and a solution flow rate of 0.4 mL/min. The dynamic method requires determining the breakthrough curve shape and the working ion-exchange capacity under given conditions. The breakthrough curves were plotted, taking into account the variation in V(V) concentration in the aqueous solution (C/C_0) as a function of the volume of effluent (Figure 14). When the V(V) concentration reached $0.01C_0$, the breakthrough point was observed, and V(V) ions appeared in the eluate. The ion exchanger reached saturation when the effluent concentration equaled the initial concentration. Based on the breakthrough curves, the following column parameters were determined: (a) the weight distribution coefficient (D_w), (b) the bed distribution coefficient (D_b), and (c) the working ion-exchange capacity (C_w) (mg/mL) and (C_w) (mg/g) and collected in Table 6 using equations 26–28 presented in Section 3.4.

The breakthrough curves for the initial V(V) concentrations of 50 and 100 mg/L and the 10 mL bed volume at a flow rate of 0.4 mL/min follow the characteristic S-shaped profile. The volume at which the breakthrough points (at $C/C_0 = 0.01$($C/C_0 = 0.05$)) were observed was equal to 1000–500 mL (1880–4135 mL) for Lewatit S5428 and 1200–2750 mL

(2700–5450 mL) for Lewatit S5528, at the initial concentrations from 50 to 200 mg/L, respectively.

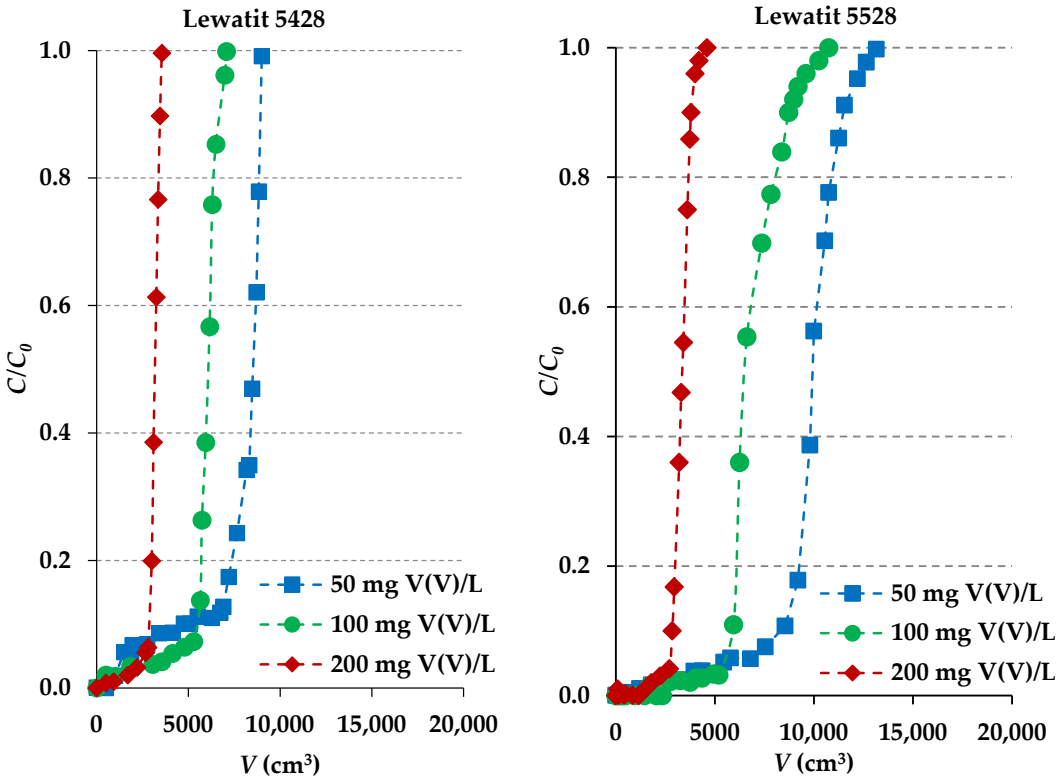


Figure 14. The column studies—breakthrough curves obtained during the V(V) ions adsorption on Lewatit S5428 and Lewatit S5528, and comparison of adsorption parameters.

Table 6. Comparison of column parameters obtained for Lewatit S5428 and Lewatit S5528.

C_0 (mg/L)	Adsorbent	C_w (mg/mL)	C_w (mg/g)	D_w	D_b	Adsorbent	C_w (mg/mL)	C_w (mg/g)	D_w	D_b
50	**Lewatit S5428**	5.0 (9.4)	19.94 (37.48)	3394.7	851.4	**Lewatit S5528**	6.0 (27.3)	33.33 (151.67)	5512.2	992.2
100		5.0 (41.4)	19.94 (165.07)	2424.6	608.1		27.5 (52.0)	152.78 (288.89)	3594.4	647.0
200		10.0 (44.0)	39.87 (175.44)	1263.2	316.8		28.0 (54.0)	155.56 (300.0)	1858.9	334.6

C_w for $C/C_0 = 0.01$ value without brackets, for $C/C_0 = 0.05$ value in round brackets.

The working ion-exchange capacities are higher for Lewatit S 5528 (6.0–28.0 mg/mL) compared to Lewatit S5428 (5.0–10 mg/mL), which is consistent with the trend observed in the static method and indicates a higher practical bed capacity, which translates into the ability to purify a larger volume of solution before the resin is exhausted. The column breakthrough curves (Figure 14) support the better overall dynamic performance of Lewatit S5528. The volume of solution treated until complete breakthrough ($C/C_0 = 1.0$) was 13 150, 10 750, and 4600 cm^3 for Lewatit S5528 at initial V(V) concentrations of 50, 100, and 200 mg/L, respectively. The corresponding values for Lewatit S5428 were approximately 9000, 7070, and 3550 cm^3, respectively. Thus, Lewatit S5528 enabled a larger volume of solution to be treated before complete breakthrough at all investigated concentrations.

Considering the resin bed volume of 10 mL, the number of bed volumes (BV) treated before complete breakthrough (C/C_0 = 1.0) were approximately 900, 707, and 355 BV for Lewatit S5428 and 1315, 1075, and 460 BV at initial V(V) concentrations of 50, 100, and 200 mg/L, respectively. These results confimed that Lewatit S5528 provides a higher dynamic treatment capacity than Lewatit S5428 under the investigated conditions. The difference was particularly pronounced at the initial V(V) concentration of 50 mg/L. It should also be noted that the breakthrough behaviour depended on the initial V(V) concentration. At 200 mg/L, the increase in C/C_0 occurred relatively rapidly for both resins, indicating faster exhaustion of the resin beds under higher V(V) loading. Nevertheless, Lewatit S5528 allowed a larger total volume of solution to be treated before complete breakthrough. From a practical perspective, the higher number of bed volumes achieved with Lewatit S5528 indicates its greater potential for continuous-flow treatment of V(V)-containing solutions. For all investigated initial V(V) concentrations, Lewatit S5528 exhibited higher D_w and D_b values than Lewatit S5428. The D_w values for Lewatit S5528 increased from 1858.9 to 5512.2, compared with 1263.2–3394.7 for Lewatit S5428, while the corresponding D_b values ranged from 334.6 to 992.2 and from 316.8 to 851.4, respectively, indicating better dynamic performance and more effective utilization of Lewatit S5528 under the investigated column conditions.

Comparing the working ion-exchange capacities obtained for V(V) ions, the selectivity series were as follows: for systems with an initial V(V) concentration C_0 = 50 mg/L: Lewatit MonoPlus TP220 (40.0 mg/mL) > Purolite S984 (7.0 mg/mL) ≈ Dowex M4195 (7.0 mg/mL) > Lewatit S5528 (6.0 mg/mL) > Lewatit S5428 (5.0 mg/mL) > Purolite A400TL (4.5 mg/mL) > Purolite A830 (3.5 mg/mL) > Lewatit MonoPlus SR7 (1.0 mg/mL) > Dowex PSR3 (0.3 mg/mL) > Dowex PSR2 (0.1 mg/mL) > Lewatit AF5 (0.0 mg/mL); for systems of initial V(V) concentration C_0 = 100 mg/L: Lewatit MonoPlus TP220 (28.4 mg/mL) ≈ Lewatit S5528 (27.5 mg/mL) > Purolite S984 (23.0 mg/mL) > Purolite A830 (9.5 mg/mL) > Purolite A400TL (8.0 mg/mL) > Dowex M4195 (7.0 mg/mL) > Lewatit S5428 (5.0 mg/mL) > Lewatit MonoPlus SR7 (1.0 mg/mL) ≈ Dowex PSR3 (0.5 mg/mL) > Dowex PSR2 (0.3 mg/mL) > Lewatit AF5 (0.0 mg/mL); for systems of initial V(V) concentration C_0 = 200 mg/L: Lewatit S5528 (28.0 mg/mL) ≈ Purolite S984 (25.6 mg/mL) > Lewatit MonoPlus TP220 (18.0 mg/mL) ≈ Purolite A830 (17.7 mg/mL) > Purolite A400TL (12.0 mg/mL) > Lewatit S5428 (10.0 mg/mL) > Dowex M4195 (2.0 mg/mL) > Lewatit MonoPlus SR7 (1.0 mg/mL) ≈ Dowex PSR3 (0.5 mg/mL) ≈ Dowex PSR2 (0.4 mg/mL) > Lewatit AF5 (0.0 mg/mL) [40,41]. Compared to the other sorbents tested, Lewatit S5528 was among the most effective materials, achieving some of the highest values of working ion-exchange capacity (C_w), ranking second at the initial V(V) concentration of 50 mg/L and approximately equal to Lewatit MonoPlus TP220 at 100 mg/L. At 200 mg/L, it exhibited the highest working ion-exchange capacity among the compared materials. Lewatit S5428, on the other hand, demonstrated moderate adsorption efficiency, with lower working ion-exchange capacities than Lewatit S5528 at all investigated initial V(V) concentrations, indicating its limited suitability for V(V) ion removal compared to the most effective chelating resins. Overall, the comparison demonstrates the better performance of Lewatit S5528 in terms of working ion-exchange capacity, particularly at initial V(V) concentrations of 100 and 200 mg/L. The highest C_w value obtained at higher vanadium concentrations indicates that this sorbent may be particularly useful for treating real industrial wastewater with elevated vanadium content, although its applicability should be confirmed using real wastewater matrices. The high working ion-exchange capacity of Lewatit S5528 likely results from the large number of available active sites and the high affinity of the ion-exchange resin functional groups for anionic Vanadium(V) species. Additionally, the macroporous structure of the material promotes ion diffusion into the grains, enabling more efficient use of the exchange capacity, especially at higher solution concentrations.

2.2.8. Real Wastewaters—Application of Lewatit S5528 in Utilization of Spent Catalyst

The spent catalyst from the production of sulfuric acid(VI) was preprepared and leached (5% *w*/*w* HCl; 5% *w*/*w* H_2SO_4; 15% *w*/*w* NaOH, 15% *w*/*w* KOH (*T* = 293K, 6h, S:L =1.5)) according to the procedure shown in Section 3.3. Four solutions, such as S1, S2, S3, and S4, were observed after the vanadium-based catalyst digestion by acids [44,105,106]:

$$V_2O_5 + 2H^+ \rightarrow 2VO_2^+ + H_2O \quad (4)$$

$$10VO_2^+ + 8H_2O \rightarrow H_2V_{10}O_{28}^{4-} + 14H^+ \quad (5)$$

$$H_2V_{10}O_{28}^{4-} \rightarrow HV_{10}O_{28}^{5-} + H^+ \quad (6)$$

$$HV_{10}O_{28}^{5-} \rightarrow V_{10}O_{28}^{6-} + H^+ \quad (7)$$

$$VO_2^+ + SO_4^{2-} \rightarrow VO_2SO_4^- \quad (8)$$

$$VO_2^+ + HSO_4^- \rightarrow VO_2HSO_4 \quad (9)$$

$$3H_2VO_4^- + Fe^0 + 12H^+ \rightarrow 3VO^{2+} + Fe^{3+} + 9H_2O \quad (10)$$

$$3VO^{2+} + Fe^0 + 6H^+ \rightarrow 3V^{3+} + Fe^{3+} + 3H_2O \quad (11)$$

and bases:

$$4NaOH + V_2O_5 \text{ (spent catalyst)} \rightarrow Na_4V_2O_7 + 2H_2O \quad (12)$$

$$Na_4V_2O_7 + H_2O \rightarrow 2HVO_4^{2-} + 4Na^+ \quad (13)$$

$$V_2O_3 + 2NaOH + O_2 \rightarrow 2NaVO_3 + H_2O \quad (14)$$

$$NaVO_3 + H_2O \rightarrow H_2VO_4^- + Na^+ \quad (15)$$

$$VO^{2+} + Fe^{3+} + 5OH^- \rightarrow VO_{2\,(s)} + Fe(OH)_{3\,(s)} + H_2O \quad (16)$$

$$2V^{3+} + Fe^{3+} + 9OH^- \rightarrow V_2O_{3\,(s)} + Fe(OH)_{3\,(s)} + 3H_2O \quad (17)$$

were used in this study for V(V) ion removal, whose composition was described in Table 7 (5% *w*/*w* HCl; density 1.06 g/ml; viscosity 1.07 mm^2/s; pH = 0; 5% *w*/*w* H_2SO_4; density 1.11 g/ml; viscosity 1.14 mm^2/s; pH = 0.52; 15% w/w NaOH; density 1.18 g/ml; viscosity 2.47 mm^2/s; pH = 13.4; 15% *w*/*w* KOH; density 1.11 g/ml; viscosity 1.19 mm^2/s; pH = 14).

Table 7. Physicochemical properties and elemental composition of solutions obtained after vanadium-based catalyst digestion [40].

Digestion Agent	Concentration (mg/L)							
	V	**Fe**	**K**	**Na**	**S**	**Cl**	**Si**	**Cu**
5% *w*/*w* HCl	4774	960	10,910	1853	4895	51,519	-	5.410
5% *w*/*w* H_2SO_4	4886	944	10,910	1921	27,790	-	-	5.170
15% *w*/*w* NaOH	4953	19.2	11,330	93,330	8636	-	937.7	0.600
15% *w*/*w* KOH	4539	16.5	76,240	1824	4301	-	313.4	0.647

The vanadium concentration was comparable across all tested solutions (approximately 4500–5000 mg/L), whereas the iron concentration depended strongly on pH. In alkaline environments, it was significantly lower (16.5 and 19.2 mg/L) due to precipitation

of iron compounds, whereas in solutions after acid digestion, it remained high, at approximately 944 and 960 mg/L. Before V(V) ion adsorption, the S1–S4 solutions were diluted 100-fold and used directly (S1-S4) or after adjustment to pH 5 (S1*–S4*).

Based on the batch and column findings—where Lewatit S5528 consistently exhibited a higher capacity ($q_{e,exp}$ = 226.30 mg/g; C_w = 6.0–28.0 mg/mL) and faster kinetics than S5428—Lewatit S5528 was selected as the representative, top-performing candidate for trials with real spent catalyst leachates. Due to the high initial metal load (4500–5000 mg/L V and 944–960 mg/L Fe in acidic extracts), a 100-fold dilution was applied to avoid overloading the resin bed and to permit evaluation within the analytical and working capacity range of the system. The removal behaviors of V and Fe in Figure 15 clearly highlight the mechanism governing selectivity. In acidic leachates (S1 and S2, pH ~ 2), iron exists as cations (Fe^{3+}), which are excluded by electrostatic repulsion from the positively charged quaternary ammonium groups (pH < pH_{PZC}; Figure S5). Meanwhile, vanadium polyanions (Figure S6) undergo anion exchange, resulting in selective vanadium removal (separation factor $\alpha_{V/Fe} > 10^2$). In contrast, the high iron reduction observed in S1*–S4* (pH 5) is primarily governed by chemical precipitation of $Fe(OH)_3$ rather than direct sorption on the resin, which concurrently enhances vanadium recovery via co-precipitation and optimal polyvanadate exchange.

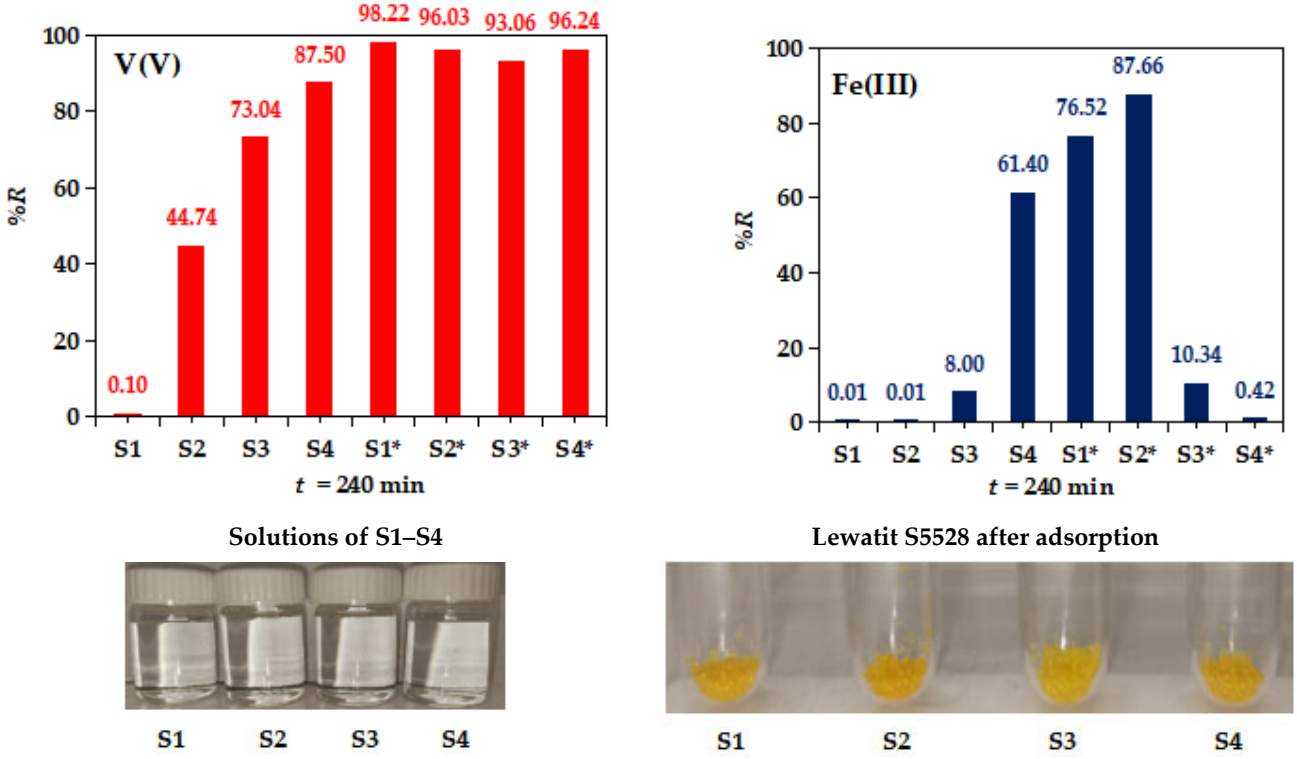


Figure 15. Percentage removal of vanadium and iron ions from leaching solution on Lewatit S5528 and real solutions before adsorption (S1–S4) and Lewatit S5528 after adsorption.

Figure 15 compares the removal efficiency (%*R*) of V(V) and Fe(III) ions in eight systems variants (S1–S4 (own pH) and S1*–S4* (pH adjusted to 5)), allowing for a comparison of process selectivity under different conditions. For V(V), a significant increase in removal efficiency is observed as conditions change from S1 to S4. For S1, the value is negligible (0.10%), while the highest %*R* values were obtained for S2 (acidic solutions, %*R* = 44.74%) and S4 (basic solutions, %*R* = 73.04%), respectively. In the solutions S1*–S4*, the %*R* of vanadium was high and was in the range from 93.06 to 98.22%. The presence of iron in the catalyst affects its catalytic properties and mechanical strength [107]. At the

same time, %*R* for Fe(III) was also the highest in S4 and S2* solutions. In solutions with pH near 5 (S1*–S4*), the Fe(III) concentration was reduced significantly by precipitation as ferric hydroxide, and coprecipitation of vanadium was also observed, resulting in a decrease in its solution concentration [40,107–109]. Precipitation of iron is one of the most frequently used methods. For example, as the literature shows, Dowex® M4195 and Purolite® S957 were applied for vanadium and iron removal from spent catalyst, and the percentage removal value exceeds 95% for Fe(III) and 90% for V(V) by Dowex® M4195 and 96% of Fe(III) and 30% of V(V) by Purolite® S957 [110]. Another examples shows that the highest %*R* for iron ions was obtained from the S2 and S2* solutions for Lewatit MonoPlus TP220 (%*R* = 50.60%-S1, %*R* = 91.86%-S2*), as well as from the S4 and S2* solution for Dowex M4195 (%*R* = 91.23%-S4, %*R* = 45.96%-S2*), whereas the vanadium ions from S2 solutions (%*R* = 88.70% for TP220; %*R* = 78.00% for M4195) and from S4* solution (%*R* = 51.60% for TP220; %*R* = 42.50% for M4195) [40] had a lower %*R*.

2.2.9. Mechanism of V(V) Adsorption

The mechanism of heavy metal adsorption, including V(V), may involve various interactions between metal ions and the adsorbent surface. The most important ones include electrostatic attraction, ion exchange, surface precipitation of compounds, pore filling, and the formation of complexes with the adsorbent's functional groups [18,40,41,111,112]. The mechanism of V(V) ions adsorption onto Lewatit S5428 and Lewatit S5528 could be presented in the simplified scheme (Figure 16). Equations (18)–(20) illustrate stoichiometric exchange between vanadate oxyanions and chloride counterions at quaternary ammonium groups, supported by the loss of chlorine and the appearance of the V–O FT-IR band (~940 cm^{-1}). The decrease in BET surface area and pore constriction reflects steric pore crowding by bulky decavanadate polyanions (~1 nm) rather than an independent non-specific pore-filling mechanism.

$$\text{Resin-Cl} + H_2VO_4^- \leftrightarrow \text{Resin-}H_2VO_4 + Cl^- \quad (18)$$

or for polyanionic species:

$$4\text{Resin-Cl} + H_2V_{10}O_{28}^{4-} \leftrightarrow \text{Resin}_4\text{-}H_2V_{10}O_{28} + 4Cl^- \quad (19)$$

$$5\text{Resin-Cl} + H_2V_{10}O_{25}^{5-} \leftrightarrow \text{Resin}_5\text{-}H_2V_{10}O_{28} + 5Cl^- \quad (20)$$

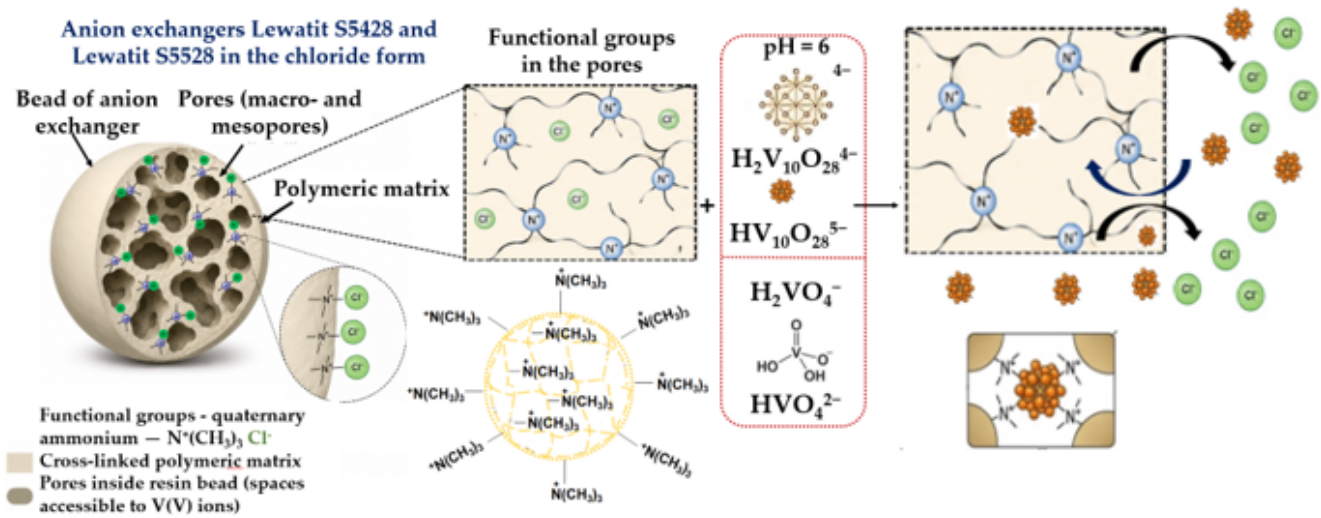


Figure 16. Schematic mechanism of V(V) adsorption on Lewatit resins.

At a pH around 5, V(V) occurs mainly as vanadate anions. In low-concentration solutions, H_2VO^{4-} ions predominate, whereas at higher concentrations, polyvanadates form, primarily $H_2V_{10}O_{28}^{4-}$, $H_2V_{10}O_{28}^{5-}$, and $V_{10}O_{28}^{6-}$, which exhibit a high affinity for anion-exchange resins. The anion exchangers present in the chloride forms and these active anions existing in the resin particles are replaced with the vanadium anions ($H_2V_{10}O_{28}^{4-}$, $H_2V_{10}O_{28}^{5-}$, or eventually at low vanadium concentration $H_2VO_4^-$ HVO_4^{2-}) via an ion exchanger mechanism [40,41,112,113]. During adsorption, the anionic vanadium species were transported from the solution to the resin bead's surface through the liquid boundary layer. They then diffused into the resin pores, where ion exchange occurred with chloride ions bound to the resin functional groups. As a result of this exchange, chloride ions were released from the resin, diffused back through the boundary layer, and entered the solution. The adsorption of V(V) by the strongly basic anion-exchange resins can be attributed, at least in part, to ion-exchange interactions between the anionic vanadate species and the Cl^- counterions associated with the quaternary ammonium functional groups. However, the stoichiometry of this exchange was not determined experimentally in the present study.

The SEM/EDX analysis proved V(V) ion adsorption on ion exchangers. The SEM/EDX analysis of the samples after V(V) the adsorption process (Lewatit S5428 + V(V) and Lewatit S5528 + V(V)) (see Figures 2b,c and S2b,d) showed a practically complete disappearance of the presence of chloride counterions and the appearance of vanadium. The atomic concentrations of vanadium were 6.24% for Lewatit S5428 and 3.78% for Lewatit S5528, respectively. The increase in oxygen content in the EDX analysis of both anion exchangers after V(V) adsorption is due to the introduction of vanadate(V) anions into the resin structure, which contain a significant number of oxygen atoms, which is direct evidence of effective ion exchange of Cl^- with oxygen forms of V(V). SEM images of the pure sample (before contact with vanadium) at 2000× and 5000× magnifications (Figure 2b,c) reveal an extensive, spongy network of open channels for Lewatit S5528. The diverse matrix of both ion exchangers (Lewatis S5428—polyacrylamide matrix, Lewatit S5528—polyacrylic matrix) causes Lewatit S5428 to typically have a slightly stiffer structure, while Lewatit S5528 is characterized by a slightly more flexible structure [114]. Pore channels that were previously empty and dark (deep) become visibly "shallower," smoother, or even completely blocked/flooded for the Lewatit S5528 anion exchanger in the images after V(V) adsorption. This is due to the fact that the more flexible polyacrylic matrix can undergo micro-osmotic shrinkage under the influence of mass loading (introduction of a large number of heavy vanadium atoms) and strong electrostatic interactions. The clusters approach each other so densely that in the SEM image, the porous structure appears more "flooded" and homogeneous. This is direct visual evidence that such large polyoxovanadate clusters are physically packed within the free pore spaces, occupying their volume (pore-filling phenomenon), as evidenced by the pore-size distribution (Figure 5), average pore diameter, and pore volume values (Figure 4), as described in Subchapter 2.1. Slightly less visible morphological changes were observed for the Lewatit S5428 anion exchanger, whose structure is more rigid and less susceptible to shrinkage under the influence of the vanadium cluster charge, suggesting that vanadium anion diffusion into the porous structure is limited to the larger pores (due to the blocking effect of small pores). The adsorption of vanadium onto Lewatit S5428 and Lewatit S5528, and the participation of their functional groups in the adsorption process, was also confirmed by ATR-FT-IR and XPS analyses, as described in detail in Subchapter 2.1.

3. Materials and Methods

3.1. Adsorbent and Adsorbate

Commercial synthetic anion-exchange resins, such as Lewatit S5428 and Lewatit S5528 (Lanxess, Cologne, Germany) were used in the investigations. The specifications of these anion exchangers are as follows:

Lewatit S5428: a white, opaque adsorbent of effective size of 0.5–0.65 mm with a crosslinked polyacrylamide matrix with the quaternary ammonium functional groups. It is classified as type 1, has a strongly basic anion exchanger of macroporous structure, a bead size of 0.4–1.6 mm (> 90%), a uniformity coefficient max. of 1.8, and a total exchange capacity min. of 0.85 val/L. The maximum temperature operation cannot exceed 353 K, it has a pH range of 0–14, a water retention of 63–68%, and a density of approx. 1.06 g/ml [47,50].

Lewatit S5528: a crosslinked polyacrylate matrix (PAc) with the quaternary ammonium functional groups. It is classified as type 1, has a strongly basic anion exchanger of a macroporous structure, a mean bead size of 0.4 –1.6 mm (d50), a uniformity coefficient max. of 1.8, a total exchange capacity of 0.85 val/L, a water content of 66–72%, a maximum temperature of operation 353 K, and a pH range of 0–14 [47,48].

Before use, the anion-exchange resin was pretreated. Prior to the experiments, the resin was placed in a vessel containing distilled water. It was then washed with cold distilled water until the water ran clear, removing impurities such as dust, free monomers, and undergrain. The resin was used in Cl^- form. Wet anion-exchange resins were used in the column experiments, whereas dry resins were used in the batch experiments (dried completely at room temperature).

Before beginning the static tests, the Lewatit S5428 and Lewatit S5528 anion-exchange resins were dried at room temperature (approximately 25 °C) for 24–48 h until a constant mass was achieved. Constant weight was defined as the state in which the difference in mass between three consecutive measurements did not exceed 0.0002 g. The resins prepared in this manner in tightly sealed plastic containers and used in the static tests. In the dynamic tests, the resins were used in their swollen state. The volume of the swollen anion-exchange resin (10 mL) was measured in a graduated cylinder, leaving a layer of distilled water approximately 3 cm thick above the resin bed. The bed was then quantitatively transferred to the column and conditioned with distilled water by passing a volume of water corresponding to 5 bed volumes (5 BV) through the column by gravity. The resins used were from the following batches: Lewatit S5428: material number 03906276, batch number CHS80094. Lewatit S5528: material number 56789719, batch number CHU00536.

The chemicals used in this study, including sodium metavanadate, nitric acid(V), hydrochloric acid, and sodium hydroxide, were of analytical grade and obtained from Chempur (Piekary Ślaskie, Poland). To prepare a V(V) stock solution at 1000 mg/L, an appropriate amount of $NaVO_3$ (Sigma-Aldrich (St. Louis, MO, USA) was dissolved in distilled water containing 5 mL of 25% ammonia. Then, 10 mL of 65% HNO_3 were added, and the solution volume was increased to 1 dm^3 with distilled water. Working V(V) solutions were obtained by appropriately diluting the stock solution. The pH of the solutions was adjusted with 1 mol/L HNO_3 or 1 mol/L NaOH using a pH/EC handheld meter (CPC-411, Elmetron, Poland).

3.2. Analytical Methods

Electrothermal atomic absorption spectrometry (ETAAS) was employed to analyze Vanadium(V) concentrations in solutions after the adsorption process [115,116]. The analysis was conducted using a Varian AA240Z 120 spectrometer (Varian, Mulgrave, Australia) equipped with an electrothermal atomizer (GTA120) operating under an argon

flow with a vanadium hollow cathode lamp (HCL) as the radiation source. Argon was used as the protective gas. The analysis was performed using a four-step time-temperature program that involved sequential stages of drying, pyrolysis to remove the matrix, atomization of vanadium, and cleaning of the graphite furnace. The analysis was conducted under the following conditions: a wavelength of 318.5 nm, a slit width of 0.2 nm and a lamp current of 20 mA. Vanadium quantification was performed using an external linear calibration procedure. Calibration standard of 200 µg/L concentration was used for automatically preparing a series of 50, 100, and 200 µg/L standards by apparatus to establish the calibration curve. The calibration mode was set to linear, with peak height selected as the analytical signal and vanadium concentration as the calibration variable. The calibration curve was used to determine vanadium concentrations in the analysed samples.

For the characterization of anion exchangers before and after V(V) adsorption process, various analytical methods such as CHNS (Carbon, Hydrogen, Nitrogen, Sulfur analysis), AFM (Atomic Force Microscopy), SEM-EDX (Scanning Electron Microscopy with Energy-Dispersive X-ray Spectroscopy), XPS (X-ray Photoelectron Spectroscopy), ATR-FT-IR (Attenuated Total Reflectance Fourier-Transform Infrared Spectroscopy), and N_2 adsorption-desorption isotherms analysis were applied.

Carbon, hydrogen, nitrogen, and sulphur analysis was performed using CHN/CHNS EuroEA3000 elemental analyzers (EuroVector, Pavia, Italy) to determine the percentage abundance of these elements in the adsorbents prior to V(V) adsorption. Two samples of anion-exchange resin (each approx. 2–2.5 mg) were weighed to an accuracy of 0.001 g using a Sartorius M2P analytical microbalance. The samples were then combusted using the Dumas dynamic combustion method, followed by chromatographic separation of the gaseous fractions (N_2, CO_2, H_2O, and SO_2) and subsequent analysis using a catharometer and the Callidus package. The instrument was operated at a carrier pressure of 110 kPa and a purge flow rate of 80 mL/min, with an oxygen volume of 15 mL and ΔP O_2 of 35 kPa. The front oven temperature was set to 980 °C and the oven temperature to 100 °C, while the rear oven was switched off. The sampling delay and total run time were 5 and 400 s, respectively. A linear calibration procedure was applied.

The ASAP 2405 analyzer (Micromeritics Instrument Corporation, Norcross, GA, USA) was applied for both anion exchangers' specific surface area (S_{BET}), the total pore volumes (P_v), and the average pore size (P_s). These parameters were calculated using the adsorption data obtained by means of the Brunauer Emmett–Teller (BET) method. V_{tot} was then determined by integrating the nitrogen adsorbed at $p/p_0 = 0.98$. The micropore volume was calculated by the t-plot method. Prior to the measurements, the samples were degassed at 50 °C. Nitrogen was used as the adsorptive, and the adsorption–desorption measurements were performed at −195.85 °C (approximately 77.3 K).

Analysis of the adsorbents' surface morphology before and after V(V) sorption was performed using an atomic force microscope (AFM) (NanoScope V, Veeco, USA). Furthermore, a Thermo Scientific Phenom ProX G6 Desktop SEM microscope equipped with a high-brightness cerium hexaboride (CeB6) source and EDS (Energy-dispersive spectroscopy)/EBSD (Electron backscatter diffraction) system was employed to identify compositional, topographical, and physical differences between pure anion exchangers and those loaded with V(V).

A Fourier transform infrared spectrometer (Cary 630, Agilent Technologies, Santa Clara, CA, USA) and Agilent MicroLab PC software (version B.04) were used to analyze the functional groups of the ion exchangers and the potential Vanadium(V) binding mechanism. After homogenization, the samples were placed on a diamond attachment, and spectra (absorbance versus wavenumber, 1/cm) were recorded over the frequency range 400–4000 cm^{-1} (spectral resolution 4 cm^{-1}, measurement time 30 s), with baseline correction.

X-ray photoelectron spectroscopy (XPS) was conducted using an ultra-high vacuum multi-chamber analytical system (UHV multi-chamber analytical system, PREVAC, Rogów, Poland) before and after the V(V) ion adsorption process on Lewatit S5428 and S5528 anion exchangers. Samples were degassed at room temperature under a vacuum of ~ 5×10^{-9} mbar. Monochromatic Al Kα radiation (1486.7 eV), generated by a VG Scienta SAX 100 X-ray lamp with an aluminum anode and a VG Scienta XM 780 monochromator, served as the photoelectron source. Measurements were performed under the following conditions: chamber pressure of 2×10^{-8} mbar; accelerating voltage of 12 kV; emission current of 30 mA; pass energy of 50 eV; step size of 0.1 eV; and acquisition time per step of 0.667 s. The binding energy scale was corrected by referencing the main C 1s component (C–C/C–H) to 285.0 eV, following the procedure described by Beamson and Briggs [117]. A uniform energy shift was applied to all spectral regions. Spectral analysis was performed using CasaXPS software (version 2.3.26PR1) with a Tougaard background and Gaussian–Lorentzian peak shapes (GL(30)). Quantitative analysis was performed using standard Scofield relative sensitivity factors implemented in CasaXPS.

The salt addition technique was used to determine the point-of-zero charge of both anion-exchange resins. This method involved adding identical amounts of substrate to a set of solutions with the same ionic concentration but different pH values [118]. In 100 mL Erlenmeyer flasks, 0.5 g of anion exchanger were placed, followed by the addition of 50 mL of 0.1 mol/L KNO_3. The pH of each solution was adjusted using 1 mol/L HCl and 1 mol/L NaOH to obtain the following pH values: 2, 3, 4, 5, 6, 7, 8, 9, 10, and 11 (±0.1 pH unit). The initial pH value of each sample was designated pH_i. The samples were shaken for 24 h using a mechanical shaker at 170 rpm. After removing the samples from the shaker, the pH of each tube was measured again and designated pH_f. The PZC was obtained from the intersection point of the curve plotted as ΔpH versus pH_i.

3.3. Batch and Column Experiments

Batch adsorption experiments were conducted in 100 mL Erlenmeyer flasks, with the following parameters: anion exchanger mass, solution pH, initial V(V) solution concentration, temperature, and stirring time. To evaluate the effect of the anion exchanger mass, 0.01–0.1 g of sorbent were added to each flask, followed by the addition of 20 mL of a 50 mg/L V(V) solution. The ratio of anion exchanger dosage to the solution volume was 1:25. The solutions were then agitated at 170 cycles/min. and amplitude 8 at room temperature for 240 min using the mechanical shaker (Elpin +357, Lubawa, Poland). After the specified time interval, the samples were separated by filtration through filter paper, and the Vanadium(V) concentration was determined by electrothermal atomic absorption spectrometry (ETAAS). Having determined the optimal adsorbent mass (0.1 g), the effects of pH (2–10), initial metal ion concentration (5–1000 mg/L), phase contact time (1–1440 min), and temperature (295–333 K) were investigated. Kinetic studies were performed with V(V) solutions at initial concentrations ranging from 50 to 200 mg/L at 295 K, whereas isotherm studies were conducted at concentrations ranging from 5 to 1000 mg/L at different temperatures (295, 313, and 333 K). The possibility of vanadium desorption from anion exchangers loaded with V(V) ions was evaluated using HCl and NaOH at 0.1–1 mol/L (one cycle of adsorption–desorption). The adsorption experiments were performed independently in triplicate ($n = 3$), and the average values were calculated. The standard deviation did not exceed 5%. The experimental procedure was presented in Figure 17.

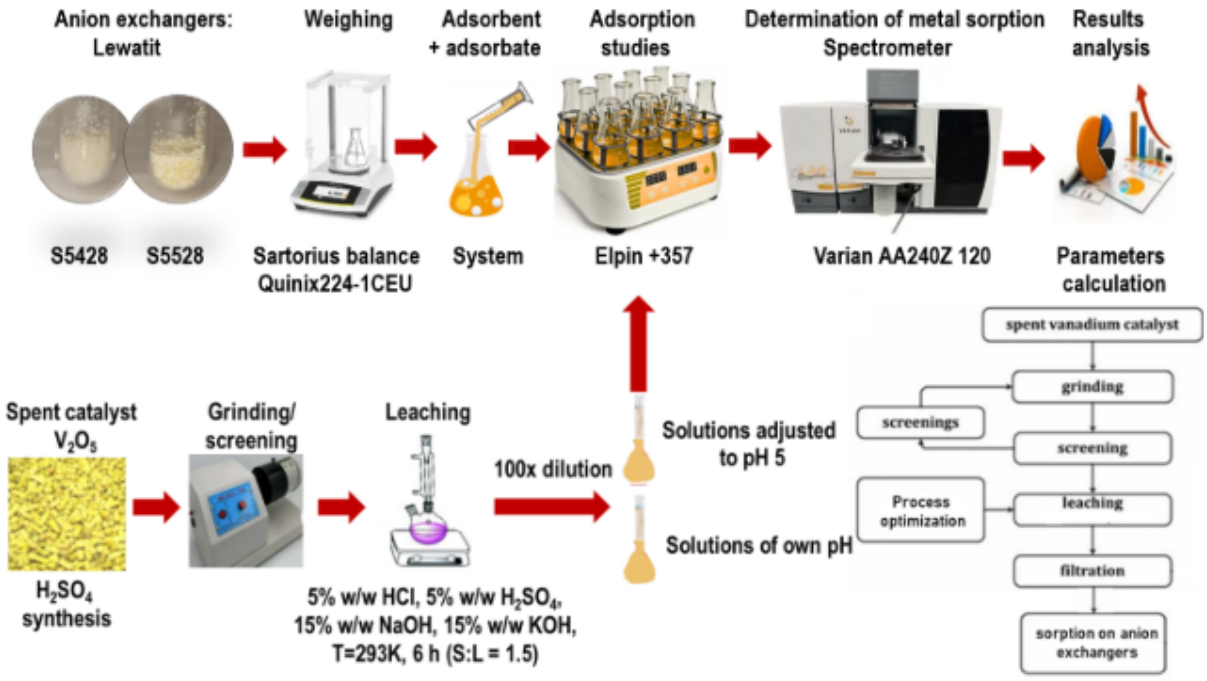


Figure 17. Experimental procedure applied in the batch studies of V(V) adsorption on anion exchangers from the model and real solutions.

To prove the applicability of the anion-exchange resins, experiments were also performed to remove vanadium and iron ions from real leachates obtained after digesting spent V_2O_5 catalysts from sulfuric acid production. The digestion process employed 5% *w*/*w* hydrochloric acid, 5% w/w sulfuric acid, 15% *w*/*w* sodium hydroxide, or 15% *w*/*w* potassium hydroxide at ambient temperature for 6 h (S:L = 1.5). The leachates were diluted 100-fold and applied as the adsorbate. Their pH values were 2.02, 2.21, 13.56, and 13.37, respectively. In the studies, diluted leachates adjusted to pH 5 were also applied. After shaking the samples and separating the phases, the Vanadium(V) concentration was obtained similarly to that mentioned previously, whereas the iron(III) concentration was obtained using flame atomic absorption spectroscopy (FAAS, Varian AA240Z 120) at 248.3 nm, with a slit width of 0.2 nm and a lamp current of 10 mA.

The column (dynamic studies) experiments were carried out using glass columns with an internal diameter of Ø = 10 mm and a height of 25 cm connected to glass balloons via rubber hoses. The column was packed with 10 mL of swollen anion-exchange resin, which had a bed height of approximately 12.7 cm.

V(V) solutions with an initial concentration of 50, 100, or 200 mg/L, and at a pH of 6, were passed through the column at a constant flow rate of 0.4 mL/min at room temperature (295 K). The eluate was collected in fractions with appropriate volumes until the metal concentrations in the effluent equaled the initial concentrations. The concentration of vanadium in the collected solutions was then analyzed using the ETAAS analytical method. The next step was to plot C/C_0 versus V (mL) curves, i.e., the breakthrough curves for the tested systems, where C/C_0 represents the ratio of the V(V) concentration in the effluent to that in the influent solution. Subsequently, the column parameters were calculated.

3.4. Calculation of the Basic Parameters of the Experiments

Based on the batch method, the amount of V(V) ions adsorbed on the S5428 or S5528 anion exchanger at a defined time (q_t) (mg/g) and at equilibrium (q_e) (mg/g), as well as the

adsorption percentage (%S) (%) and the desorption percentage (%D) (%), were determined. Using the column method, the distribution coefficients for weight (D_w) and volume (D_b), as well as the working ion-exchange capacity (C_w), were determined. The formulas used to calculate adsorption parameters are presented in Table 8.

Table 8. Adsorption efficiency determination by the static and dynamic studies [18,40,41].

Abbrev.	Parameters.	Equation	No.
	Batch method		
q_t (mg/g)	amount of V(V) adsorbed after time t	$q_t = \frac{(C_0 - C_t) \times V}{m}$	(22)
q_e (mg/g)	amount of V(V) adsorbed at equilibrium	$q_e = \frac{(C_o - C_e) \times V}{m}$	(23)
%S (%)	adsorption percentage	$\%S = \frac{C_0 - C_t}{C_0} \times 100\%$	(24)
%D (%)	desorption percentage	$\%D = \frac{C_{\mathrm{des}}}{C_0} \times 100\%$	(25)
	Dynamic method		
D_w (mL/g)	weight distribution coefficient	$D_w = \frac{U'' - U_0 - V_f}{m_j}$	(26)
D_b	bed distribution coefficient	$D_b = D_w \times d$	(27)
C_w (mg/mL)	working ion-exchange capacity	$C_w = \frac{U_p \times C_0}{V_j}$	(28)

where: C_0, C_e, C_t—the initial, equilibrium, after time t concentration of V(V) in the water phase (mg/L), V—the volume of solution (L), m—the mass of dry anion exchanger (g), U''—the eluate volume for C/C$_0$ = 0.5 (mL), U_0—the dead column volume (2 mL), V_f—the free volume of the sorbent bed (4 mL), m_j—the mass of dry anion exchanger in the column (g), d—the anion-exchange density (g/mL), U_p—the volume of eluate to the break through the column (L), Vj—the volume of the anion exchanger in the column.

3.5. Kinetic, Isotherm, and Thermodynamic Parameters

In order to investigate the kinetics of adsorption of V(V) ions on Lewatit S5428 and Lewatit S5528, the adsorption kinetic models such as the Lagergren pseudo-first order (PFO) [88], the Ho-McKay pseudo-second order (PSO) [89], and the intraparticle Weber-Morris diffusion (IPD) [90] were used. The experimental kinetic parameters for the studied V(V) ions were calculated using the equations presented in Table 9.

Table 9. Kinetic, Isotherm, and Thermodynamic parameters description.

Abbrev.	Parameters	Equation	No.
	Kinetic parameters		
PFO	k_1 (1/min) is the PFO rate constant, k_1 = −2.303 × slope, q_e and q_t (mg/g) are the amounts of V(V) ions sorbed at the equilibrium, and at any time t, q_e =10$^{\mathrm{intercept}}$, t is the contact time	non-linear: $\frac{dq_t}{dt} = k_1(q_e - q_t)$	(29)
		linear: $\log(q_e - q_t) = \log q_e - \frac{k_1}{2.303} t$	(30)
PSO	k_2 (g/mg min) is the PSO rate constant, k_2 = slope^2/intercept, q_e and q_t (mg/g) are the amounts of V(V) ions sorbed at the equilibrium and at any time t, q_e = 1/slope	non-linear: $\frac{dq_t}{dt} = k_2(q_e - q_t)^2$	(31)
		linear:	(32)

		$\frac{t}{q_t} = \frac{1}{k_2 q_e^2} + \frac{1}{q_e} t$	
	h is the initial adsorption rate	$h = k_2 q_e^2$	(33)
IPD	k_i (mg/g min$^{0.5}$) is the IPD rate constant, k_i = slope, C is the Weber–Morris diffusion constant, C = intercept	linear: $q_t = k_i t^{1/2} + C$	(34)
Isotherm parameters			
Langmuir	q_e (mg/g) is the amount of V(V) ions sorbed at the equilibrium, C_e (mg/L) is the equilibrium concentration of the solution, Q_0 (mg/g) is the maximum adsorption capacity, k_L (L/mg) is the Langmuir constant (related to the free energy of adsorption)	non-linear: $q_e = \frac{k_L Q_0 C_e}{1 + C_e k_L}$	(35)
		linear: $\frac{C_e}{q_e} = \frac{1}{Q_0 k_L} + \frac{C_e}{Q_0}$	(36)
Freundlich	k_F (mg$^{1-1/n}$ L$^{1/n}$/g) and $1/n$ are the Freundlich constants connected with the adsorption capacity of the adsorbent and the surface heterogeneity, $1/n$ indicates the adsorption favourability	non-linear: $q_e = k_F C_e^{\frac{1}{n}}$	(37)
		linear: $log\ q_e = log\ k_F + \frac{1}{n} log\ C_e$	(38)
Temkin	R (8.314 J/mol K) is the gas constant, T (K) is the temperature, C_e (mg/L) is the equilibrium concentration of solution, A (L/g) and b_T (J/mol) are the Temkin constants	non-linear: $q_e = \frac{RT}{b_T} lnAC_e$	(39)
		linear: $q_e = (\frac{RT}{b_T}) lnA + (\frac{RT}{b_T}) lnC_e$	(40)
Dubinin-Radushkevich	q_m (mg/g) is the maximum adsorption capacity, k_{DR} (mol^2 J^2) is the constant related to the adsorption energy, ε (J/mol) is the adsorption potential	non-linear: $q_e = q_m e^{k_{DR}\varepsilon^2}$	(41)
		linear: $lnq_e = lnq_m - k_{DR}\varepsilon^2$	(42)
	E (J/mol) is the mean free energy for the V(V) ions removal from the adsorption site to infinity	$\varepsilon = RTln[1 + \frac{1}{C_e}]$	(43)
		$E = \frac{1}{\sqrt{2k_{DR}}}$	(44)
Thermodynamic parameters			
ΔG^o ΔS^o ΔH^o	ΔG^o (J/mol) is the Gibbs free energy, R (8.314 J/mol K) is the gas constant, T (K) is the temperature, Kc (L/g) is the distribution constant at equilibrium, q_e (mol/g) is the amount of V(V) ions sorbed at the equilibrium, and C_e (mol/L) is the equilibrium concentration of V(V) in solution, ΔS^o (J/mol K) is the entropy, ΔH^o (J/mol) is the enthalpy	$\Delta G^o = -RTlnK_C$	(45)
		$K_C = \frac{q_e}{C_e}$	(46)
		$lnK_C = \frac{\Delta S^o}{R} - \frac{\Delta H^o}{RT}$	(47)

The Langmuir [90–93], Freundlich [91,92,94], Temkin [32,91,95,96], and Dubinin-Radushkevich [91,92] isotherm models were employed to fit the equilibrium adsorption data [91]. Although the Langmuir adsorption model was originally developed to describe adsorption in gas–solid systems, it is also commonly used to evaluate and compare the adsorption capacity of different materials [92,93]. This isotherm describes how molecules interact with a surface, assuming a balance between adsorption and desorption rates. The adsorption rate depends on the fraction of the surface that remains unoccupied, whereas the desorption rate depends on the area already covered by adsorbed molecules [92]. Key features of the Langmuir Isotherm include the following: (1) Homogeneous adsorption:

adsorption occurs uniformly on the surface; all adsorption sites are equivalent. (2) Constant heat of adsorption: the energy released during adsorption is the same for all sites and does not depend on how many molecules are already adsorbed. (3) Chemisorption mechanism: adsorbate molecules bind to the surface via chemical interactions. (4) Negligible adsorbate–adsorbate interactions: molecules already adsorbed do not influence the adsorption of other molecules. (5) Monolayer adsorption: each adsorption site holds only one molecule; no multilayer formation. If a solute molecule approaches an occupied site, it is rejected back into the solution. (6) Low-concentration behavior: at low solute concentrations, the isotherm reduces to Henry's Law (linear behavior). (7) High-concentration behavior: at higher concentrations, the model predicts saturation corresponding to monolayer adsorption capacity [95].

One important parameter in the Langmuir isotherm is the separation factor, R_L, which is a dimensionless value used to assess the favorability of the adsorption process. It is calculated using the formula:

$$R_L = \frac{1}{1 + K_L C_0} \quad (48)$$

where K_L is the Langmuir constant (mg/g), and C_0 is the initial concentration of V(V) ions being adsorbed (mg/g). The value of R_L helps determine the nature of the adsorption: if $R_L = 0$, the adsorption is irreversible, if $R_L > 0$ and $R_L < 1$, the adsorption is favorable, and if $R_L = 1$, the adsorption is linear; if $R_L > 1$, the adsorption is unfavorable [93].

The Freundlich isotherm is also frequently used for isotherm modelling, and its key features are presented below. (1) Empirical model: it is an empirical equation that assumes the adsorption site energies are exponentially distributed. (2) Surface heterogeneity: the value of n reflects the heterogeneity of the adsorbent surface (typically, $0 < n < 1$). This model describes adsorption occurring on a heterogeneous surface, characterized by adsorption sites with different energy levels. (3) Convex relationship: the q_e vs. C_e curve is always convex upward, indicating that always $n < 1$. (4) Low-concentration behavior: at low solute concentrations, when $n = 1$, the isotherm simplifies to Henry's Law. (5) Non-ideal, multilayer adsorption: accounts for non-ideal adsorption behavior and the possibility of multilayer formation on the surface. (6) No saturation limit: the model does not predict a maximum adsorption capacity (i.e., plateau is not reached at high C_e) [91,92,94,95].

The Temkin isotherm model considers the influence of interactions between adsorbed molecules during adsorption. It makes an assumption: (1) Exponential dependence on surface coverage: the rates of adsorption and desorption increase exponentially as the surface becomes more covered. (2) Variable adsorption energy: the heat of adsorption and the activation energy change exponentially with increasing surface coverage. (3) Limited applicability range: this isotherm is not valid at very low or very high equilibrium concentrations; it is only applicable within a moderate range of equilibrium concentrations. (4) Heterogeneous adsorption: the model assumes that adsorption occurs on a non-uniform surface with energetically diverse sites. (5) Intermediate coverage is best suited: the model provides the most accurate predictions for adsorption behavior within the coverage range of $0.2 < q/q_m < 0.8$. (6) Linear energy variation: the activation energies of adsorption and desorption, as well as the heat of adsorption, change linearly between their minimum and maximum values [91,92,95,96].

The Dubinin-Radushkevich model is also known as the theory of volume filling of micropores. This model views adsorption as the process of filling up the tiny pores (micropores) of an adsorbent, rather than forming a surface layer. The model is generally used to describe adsorption on heterogeneous surfaces with a Gaussian energy distribution (E (J/mol) reflects the characteristic energy of the system, which depends on the adsorbent and adsorbate). This model is only suitable for an intermediate range of adsorbate

concentrations [91,92,95]. The description of the isotherm model and parameters is presented in Table 9.

Thermodynamic analysis is essential in adsorption studies, as it helps determine whether adsorption occurs through physical or chemical interactions. As adsorption is a temperature-dependent process, it is suitable for thermodynamic evaluation. Key thermodynamic parameters such as Gibbs free energy change ($\Delta G°$), enthalpy change ($\Delta H°$), and entropy change ($\Delta S°$) can be determined by analyzing experimental adsorption data (Table 9). In liquid-phase adsorption, important thermodynamic quantities such as $\Delta G°$, $\Delta H°$, and $\Delta S°$ are obtained from the equilibrium constants of certain isotherm models, which are used either directly or indirectly for these calculations [119,120]. The Gibbs free energy change ($\Delta G°$) indicates the spontaneity of the adsorption process: a negative value suggests that the process is spontaneous. The enthalpy change ($\Delta H°$) provides information about the heat involved, indicating whether the process is endothermic or exothermic. In contrast, the entropy change ($\Delta S°$) reflects the degree of disorder or randomness at the solid–liquid interface. Together, these parameters help to assess the feasibility and nature of the adsorption mechanism [119].

4. Conclusions

The paper presents the comparison of the adsorption ability of two strongly basic anion exchangers, Lewatit S5428 and Lewatit S5528, for V(V) ions. Its removal was carried out from the model, and real solutions were obtained after the spent catalyst was leached using batch and column modes. The obtained data revealed the anionite mass, the solution pH, the initial V(V) concentration, the phase contact time, and the effect of temperature on the adsorption ability of V(V) ions. The quantitative V(V) ions adsorption for Lewatit S5528 was obtained at the optimal experimental conditions, such as the anionite mass of 0.1 g, volume of the solution of 20 mL, the initial V(V) ion concentration of 50 mg V(V)/L, pH = 6, phase contact time of 15 min, amplitude of 8, and agitation speed of 170 rpm and 298 K. Lewatit S5528 shows better adsorption performance in both batch and column modes compared to Lewatit S5428. The experimental adsorption capacity (the batch mode) and the working ion-exchange capacity (the column mode) were 226.30 mg/g and 6 mg/mL for Lewatit S5528, respectively, and were about 20% and 17% higher than for Lewatit S5428 (181.20 mg/g and 5 mg/mL), respectively. The adsorption of V(V) ions onto Lewatit resins was well described by the Freundlich isotherm and the pseudo-second-order kinetic model. Moreover, both the film diffusion and the intraparticle diffusion play significant roles in the adsorption process. Based on the calculated thermodynamic parameters, the V(V) ion adsorption on Lewatit resins was exothermic, spontaneous, and favorable. The loaded V(V) ion resins could be regenerated with sodium hydroxide solutions, and the best desorption efficiency, 81% for Lewatit S5428 and 100% for Lewatit S5528, was obtained using a 1 mol/L NaOH solution. The physicochemical characteristics of anion-exchange resin before and after V(V) ion adsorption (CHNS, ATR-FT-IR, XPS, and ASAP) proved the type of polymeric matrix declared by the producer and the presence of quaternary amine functional groups, which are involved in the V(V) ion adsorption process and the main mechanism of V(V) ion binding, with ion exchange identified as the main mechanism responsible for V(V) ion binding.

Supplementary Materials: The following supporting information can be downloaded at: https://www.mdpi.com/article/10.3390/molecules31234308/s1, Figure S1: Comparison of vanadium treatment methods; Table S1: CHNS analysis of the anion exchangers Lewatit S5428 and Lewatit S5528; Figure S2: SEM images and EDX elemental maps before and after V(V) sorption; Figure S3: 2D and 3D AFM images of the anion exchangers before and after V(V) sorption; Figure S4: XPS

spectra of C 1s, O 1s, N 1s, and V 2p; Figure S5: Point-of-zero charge (pH_{PZC}) of Lewatit anion exchangers; Figure S6: Vanadium species distribution depending on solution pH; Figures S7–S8: Kinetic model fitting for V(V) sorption on Lewatit S5428 and Lewatit S5528; Table S2: Comparison of adsorption isotherm parameters; Figure S9: Van't Hoff plots for Lewatit anion exchangers.

Author Contributions: Conceptualization, A.W., E.Z.-S.; methodology, A.W., E.Z.-S.; software, A.W., E.Z.-S.; validation, A.W.; formal analysis, A.W.; investigation, A.W., E.Z.-S.; data curation, A.W.; writing—original draft preparation, A.W., E.Z.-S.; writing—review and editing, A.W., E.Z.-S.; supervision: A.W. All authors have read and agreed to the published version of the manuscript.

Funding: This research received no external funding.

Data Availability Statement: The original contributions presented in this study are included in the article/Supplementary Material.

Acknowledgments: The authors would like to thank Agnieszka Lipke for help in laboratory work.

Conflicts of Interest: The authors declare no conflict of interest.

References

1. Rehder, D. Implications of Vanadium in Technical Applications and Pharmaceutical Issues. *Inorg. Chim. Acta* **2017**, *455*, 378–389. https://doi.org/10.1016/j.ica.2016.06.021.
2. Bobba, S.; Carrara, S.; Huisman, J.; Mathieux, F.; Pavel, C. *Critical Raw Materials for Strategic Technologies and Sectors in the EU: A Foresight Study*; Publications Office of the European Union: Luxembourg, 2020. https://doi.org/10.2873/58081.
3. Grohol, M.; Veeh, C. *Study on the Critical Raw Materials for the EU 2023—Final Report*; Publications Office of the European Union: Luxembourg, 2023. https://doi.org/10.2873/725585.
4. European Parliament; Council of the European Union. Regulation (EU) 2024/1252 of the European Parliament and of the Council of 11 April 2024. Available online: https://eur-lex.europa.eu/eli/reg/2024/1252/oj (accessed on 1 September 2026).
5. Gustafsson, J.P. Vanadium geochemistry in the biogeosphere—Speciation, solid-solution interactions, and ecotoxicity. *Appl. Geochem.* **2019**, *102*, 1–25. https://doi.org/10.1016/j.apgeochem.2018.12.027.
6. Petranikova, M.; Tkaczyk, A.H.; Bartl, A.; Amato, A.; Lapkovskis, V.; Tunsu, C. Vanadium sustainability in the context of innovative recycling and sourcing development. *Waste Manag.* **2020**, *113*, 521–544. https://doi.org/10.1016/j.wasman.2020.04.007.
7. Pyrzyńska, K.; Wierzbicki, T. Determination of vanadium species in environmental samples. *Talanta* **2004**, *64*, 823–829. https://doi.org/10.1016/j.talanta.2004.05.007.
8. Wnuk, E. Mobility, bioavailability, and toxicity of vanadium regulated by physicochemical and biological properties of the soil. *J. Soil Sci. Plant Nutr.* **2023**, *23*, 1386–1396. https://doi.org/10.1007/s42729-023-01130-9.
9. Zhang, B.; Zhang, H.; He, J.; Zhou, S.; Dong, H.; Rinklebe, J.; Ok, Y.S. Vanadium in the environment: Biogeochemistry and bioremediation. *Environ. Sci. Technol.* **2023**, *57*, 14770–14786. https://doi.org/10.1021/acs.est.3c04508.
10. Das, S.; Sultana, K.W.; Ndhlala, A.R.; Mondal, M.; Chandra, I. Heavy metal pollution in the environment and its impact on health: Exploring green technology for remediation. *Environ. Health Insights* **2023**, *17*, 11786302231201259. https://doi.org/10.1177/11786302231201259.
11. Briffa, J.; Sinagra, E.; Blundell, R. Heavy metal pollution in the environment and their toxicological effects on humans. *Heliyon* **2020**, *6*, e04691. https://doi.org/10.1016/j.heliyon.2020.e04691.
12. Huang, J.H.; Huang, F.; Evans, L.; Glasauer, S. Vanadium: Global (bio)geochemistry. *Chem. Geol.* **2015**, *417*, 68–89. https://doi.org/10.1016/j.chemgeo.2015.09.019.
13. Imtiaz, M.; Rizwan, M.S.; Xiong, S.; Li, H.; Ashraf, M.; Shahzad, S.M.; Shahzad, M.; Rizwan, M.; Tu, S. Vanadium, Recent Advancements and Research Prospects: A Review. *Environ. Int.* **2015**, *80*, 79–88. https://doi.org/10.1016/j.envint.2015.03.018.
14. Liu, Y.; Huang, Y.; Li, H.; Duan, H. Recent advances in removal techniques of vanadium from water: A comprehensive review. *Chemosphere* **2022**, *287*, 132021. https://doi.org/10.1016/j.chemosphere.2021.132021.
15. Supe Tulcan, R.X.; Ouyang, W.; Lin, C.; He, M.; Wang, B. Vanadium pollution and health risks in marine ecosystems: Anthropogenic sources over natural contributions. *Water Res.* **2021**, *207*, 117838. https://doi.org/10.1016/j.watres.2021.117838.
16. Fadaei, A. Vanadium Removal from Water and Wastewater by Different Technologies: A Review Study. *Proc. Int. Acad. Ecol. Environ. Sci.* **2025**, *15*, 19–39.

17. Peng, H.; Tang, D.; Liao, M.; Wu, Y.; Fan, X.; Li, B.; Huang, H.; Shi, W. A Clean Method for Vanadium(V) Reduction with Oxalic Acid. *Metals* **2022**, *12*, 557. https://doi.org/10.3390/met12040557.
18. Kończyk, J.; Kluziak, K.; Kołodyńska, D. Adsorption of Vanadium(V) Ions from Aqueous Solutions on Different Biomass-Derived Biochars. *J. Environ. Manag.* **2022**, *313*, 114958. https://doi.org/10.1016/j.jenvman.2022.114958.
19. He, Q.; Si, S.; Zhao, J.; Yan, H.; Sun, B.; Cai, Q.; Yu, Y. Removal of Vanadium from Vanadium-Containing Wastewater by Amino-Modified Municipal Sludge-Derived Ceramic. *Saudi J. Biol. Sci.* **2018**, *25*, 1664–1669. https://doi.org/10.1016/j.sjbs.2016.08.016.
20. Liu, Z.; Zhang, Y.; Dai, Z.; Huang, J.; Liu, C. Coextraction of Vanadium and Manganese from High-Manganese Containing Vanadium Wastewater by a Solvent Extraction–Precipitation Process. *Front. Chem. Sci. Eng.* **2020**, *14*, 789–798. https://doi.org/10.1007/s11705-019-1887-z.
21. Ghanim, B.M.; Courtney, R.; Pembroke, J.T.; Leahy, J.J.; O'Dwyer, T.F.; Murnane, J.G. Vanadium Removal and Recovery from Aqueous Solution with Repeated Use of a KOH-Modified Seaweed Biochar Adsorbent: Characterisation and Removal Mechanisms. *J. Chem. Technol. Biotechnol.* **2025**, *100*, 2039–2052. https://doi.org/10.1002/jctb.70015.
22. Rehder, D. Vanadium: Its Role for Humans. In *Interrelations Between Essential Metal Ions and Human Diseases*; Metal Ions in Life Sciences; Sigel, A., Sigel, H., Sigel, R.K.O., Eds.; Springer: Dordrecht, The Netherlands, 2013; Volume 13, pp. 139–169. https://doi.org/10.1007/978-94-007-7500-8_5.
23. French, R.J.; Jones, P.J.H. Role of Vanadium in Nutrition: Metabolism, Essentiality and Dietary Considerations. *Life Sci.* **1993**, *52*, 339–346. https://doi.org/10.1016/0024-3205(93)90146-T.
24. Hanus-Fajerska, E.; Wiszniewska, A.; Kamińska, I. A Dual Role of Vanadium in Environmental Systems—Beneficial and Detrimental Effects on Terrestrial Plants and Humans. *Plants* **2021**, *10*, 1110. https://doi.org/10.3390/plants10061110.
25. Grant, A.; Middleton, R. An assessment of metal contamination of sediments in the Humber Estuary, U.K. *Estuar. Coast. Shelf Sci.* **1990**, *31*, 71–85. https://doi.org/10.1016/0272-7714(90)90029-Q.
26. Caeiro, S.; Costa, M.H.; Ramos, T.B.; Fernandes, F.; Silveira, N.; Coimbra, A.; Medeiros, G.; Painho, M. Assessing heavy metal contamination in Sado Estuary sediment: An index analysis approach. *Ecol. Indic.* **2005**, *5*, 151–169. https://doi.org/10.1016/j.ecolind.2005.02.001.
27. Peng, H.; Guo, J.; Li, B.; Huisheng, H.; Wenbing, S.; Zuohua, L. Removal and recovery of vanadium from waste by chemical precipitation, adsorption, solvent extraction, remediation, photo-catalyst reduction and membrane filtration. A review. *Environ. Chem. Lett.* **2022**, *20*, 1763–1776. https://doi.org/10.1007/s10311-022-01395-z.
28. Qasem, N.A.A.; Mohammed, R.H.; Lawal, D.U. Removal of heavy metal ions from wastewater: A comprehensive and critical review. *npj Clean Water* **2021**, *4*, 36. https://doi.org/10.1038/s41545-021-00127-0.
29. Gomes, H.I.; Jones, A.; Rogerson, M.; Burke, I.T.; Mayes, W.M. Vanadium removal and recovery from bauxite residue leachates by ion exchange. *Environ. Sci. Pollut. Res.* **2016**, *23*, 23034–23042. https://doi.org/10.1007/s11356-016-7514-3.
30. Kuchekar, S.R.; Aher, H.R.; Dhage, P.M. Removal of vanadium from industrial effluents by natural ion exchanger. *Int. J. Civ. Mech. Eng.* **2019**, *13*, 564–570.
31. Li, M.; Zhang, B.; Zou, S.; Liu, Q.; Yang, M. Highly Selective Adsorption of Vanadium(V) by Nano-Hydrous Zirconium Oxide-Modified Anion Exchange Resin. *J. Hazard. Mater.* **2020**, *384*, 121386. https://doi.org/10.1016/j.jhazmat.2019.121386.
32. Polowczyk, H.; Bastrzyk, M.; Kozłowska, A.; Kociołek-Balawejder, A. Amberlite IRA 400 and IRA 743 Chelating Resins for the Sorption and Recovery of Vanadium from Aqueous Solutions. *Hydrometallurgy* **2011**, *110*, 67–73. https://doi.org/10.101/j.hydromet.2017.02.017.
33. Drużyński, S.; Mazurek, K.; Białowicz, K. The Use of Ion Exchange in the Recovery of Vanadium from the Mass of a Spent Catalyst Used in the Oxidation of SO_2 to SO_3. *Pol. J. Chem. Technol.* **2014**, *16*, 69–73. https://doi.org/10.2478/pjct-2014-0032.
34. Gurjar, V.R.; Koujalagi, P.S.; Revankar, H.N.; Kulkarni, R.M. Adsorptive Removal of Vanadium from Aqueous Media by Ion Exchange Resin. *Emerg. Mater.* **2022**, *5*, 1543–1551. https://doi.org/10.1007/s42247-021-00251-0.
35. Huang, J.; Su, P.; Wu, W.; Liao, S.; Qin, H.; Wu, X.; He, X.; Fan, Y. Concentration and Separation of Vanadium from Alkaline Media by Strong Alkaline Anion-Exchange Resin 717. *Rare Met.* **2010**, *29*, 439–443. https://doi.org/10.1007/s12598-010-0146-8.
36. Keränen, A.; Leiviskä, T.; Salakka, A.; Tanskanen, J. Removal of Nickel and Vanadium from Ammoniacal Industrial Wastewater by Ion Exchange and Adsorption on Activated Carbon. *Desalin. Water Treat.* **2013**, *53*, 2645–2654. https://doi.org/10.1080/19443994.2013.868832.
37. Li, Q.G.; Zeng, L.; Mao, L.S.; Yang, Y.N.; Zhang, Q.X. Completely Removing Vanadium from Ammonium Molybdate Solution Using Chelating Ion Exchange Resins. *Hydrometallurgy* **2009**, *98*, 287–290. https://doi.org/10.1016/j.hydromet.2009.05.014.
38. Li, W.; Zhang, Y.; Liu, T.; Huang, J.; Wang, Y. Comparison of Ion Exchange and Solvent Extraction in Recovering Vanadium from Sulfuric Acid Leach Solutions of Stone Coal. *Hydrometallurgy* **2013**, *131–132*, 1–7. https://doi.org/10.1016/j.hydromet.2012.09.009.

39. Pyrzyńska, K.; Wierzbicki, T. Pre-Concentration and Separation of Vanadium on Amberlite IRA-904 Resin Functionalized with Porphyrin Ligands. *Anal. Chim. Acta* **2005**, *540*, 91–94. https://doi.org/10.1016/j.aca.2004.09.015.
40. Wołowicz, A.; Hubicki, Z. Removal of Vanadium by Ion Exchange Resins from Model and Real Solutions from Spent V_2O_5 Catalyst. *Hydrometallurgy* **2022**, *211*, 105871. https://doi.org/10.1016/j.hydromet.2022.105871.
41. Wołowicz, A.; Hubicki, Z. Vanadium(V) Removal from Aqueous Solutions and Real Wastewaters onto Anion Exchangers and Lewatit AF5. *Molecules* **2022**, *27*, 5432. https://doi.org/10.3390/molecules27175432.
42. Zhu, X.; Li, W.; Zhang, C. Extraction and Removal of Vanadium by Adsorption with Resin 201*7 from Vanadium Waste Liquid. *Environ. Res.* **2020**, *180*, 108865. https://doi.org/10.1016/j.envres.2019.108865.
43. Zhu, X.; Yang, X.; Li, W.; Liu, Y. Efficient Removal and Recovery of Vanadium (IV and V) from High Acidic Waste Water with Resins D851 and D201: A Comparative Study. *J. Water Process Eng.* **2022**, *49*, 103153. https://doi.org/10.1016/j.jwpe.2022.103153.
44. Fan, Y.; Wang, X.; Wang, M. Separation and Recovery of Chromium and Vanadium from Vanadium-Containing Chromate Solution by Ion Exchange. *Hydrometallurgy* **2013**, *136*, 31–35. https://doi.org/10.1016/j.hydromet.2013.03.008.
45. Mazurek, K.; Grzesiak, P.; Drużyński, S.; Kiełkowska, U.; Wróbel, A.; Szalla, A. Method of Utilization of the Spent Vanadium Catalyst. *Pol. J. Chem. Technol.* **2018**, *20*, 1–7. https://doi.org/10.2478/pjct-2018-0031.
46. Lee, J.-C.; Kim, E.K.; Chung, K.W.; Kim, R.; Jeon, H.-S. A Review on the Metallurgical Recycling of Vanadium from Slags: Towards a Sustainable Vanadium Production. *J. Mater. Res. Technol.* **2021**, *12*, 343–364. https://doi.org/10.1016/j.jmrt.2021.02.065.
47. Wawrzkiewicz, M.; Wołowicz, A.; Hubicki, Z. Strongly basic anion exchange resin based on a cross-linked polyacrylate for simultaneous C.I. Acid Green 16, Zn(II), Cu(II), Ni(II) and phenol removal. *Molecules* **2022**, *27*, 2096. https://doi.org/10.3390/molecules27072096.
48. LANXESS. Product Data Sheet. Available online: https://www.lenntech.com (accessed on 1 January 2025).
49. Helfferich, F.G. *Ion Exchange*; Dover Publications: New York, NY, USA, 1995.
50. Wiercik, P.; Domańska, M.; Łomotowski, J.; Kuśnierz, M.; Konieczny, T. A new approach to assessing the ageing process of strongly basic anion-exchange resins: Preliminary research, *Desalin. Water Treat.* **2019**, *143*, 148–157. https://doi.org/10.5004/dwt.2019.23497.
51. Gengenbach, T.R.; Major, G.H.; Linford, M.R.; Easton, C.D. Practical guides for X-ray photoelectron spectroscopy (XPS): Interpreting the carbon 1s spectrum. *J. Vac. Sci. Technol. A* **2021**, *39*, 013204. https://doi.org/10.1116/6.0000682.
52. Michałek, T.; Wojtaszek, K.; Youssif, M.M.; Żabiński, P.; Kołczyk-Siedlecka, K.; Kowalik, R.; Socha, R.P.; Hessel, V.; Wojnicki, M. Adsorption of Au(III), Pt(IV), Pd(II), and Rh(III) ions on activated carbon in a batch reactor supported by microwave radiation. *Sci. Rep.* **2025**, *15*, 5852. https://doi.org/10.1038/s41598-025-89990-2.
53. Zabielska-Konopka, M.; Zambrzycka-Szelewa, E.; Bobrowska, D.M.; Godlewska-Żyłkiewicz, B. Selective separation of platinum, palladium, and rhodium from spent automotive catalysts using a polymeric sorbent. *Hydrometallurgy* **2026**, *244*, 106769. https://doi.org/10.1016/j.hydromet.2026.106769.
54. Ahmer, M.F.; Uddin, M.K. Structure, properties and industrial applications of anion exchange resins for the removal of electroactive nitrate ions from contaminated water. *RSC Adv.* **2024**, *14*, 33629–33648. https://doi.org/10.1039/D4RA03871A.
55. Thommes, M.; Kaneko, K.; Neimark, A.V.; Olivier, J.P.; Rodriguez-Reinoso, F.; Rouquerol, J.; Sing, K.S.W. Physisorption of gases, with special reference to the evaluation of surface area and pore size distribution (IUPAC Technical Report). *Pure Appl. Chem.* **2015**, *87*, 1051–1069. https://doi.org/10.1515/pac-2014-1117.
56. Thommes, M.; Schlumberger C. Characterization of Nanoporous Materials. *Annu. Rev. Chem. Biomol. Eng.* **2021**, *12*, 137–162. https://doi.org/10.1146/annurev-chembioeng-061720-081242.
57. Wiercik, P.; Frączek, B.; Chrobot, P. Fouling of anion exchanger by image and FTIR analyses. *J. Environ. Chem. Eng.* **2020**, *8*, 103761. https://doi.org/10.1016/j.jece.2020.103761.
58. Mikolaszek, B.; Jamrógiewicz, M.; Mojsiewicz-Pieńkowska, K.; Sznitowska, M. Microscopic and spectroscopic imaging and thermal analysis of acrylates, silicones and active pharmaceutical ingredients in adhesive transdermal patches. *Polymers* **2022**, *14*, 2888. https://doi.org/10.3390/polym14142888.
59. Socrates, G. *Infrared and Raman Characteristic Group Frequencies: Tables and Charts*, 3rd ed.; John Wiley & Sons: Chichester, UK, 2001.
60. Kołodyńska, D.; Fila, D.; Hubicki, Z. Recovery of lanthanum(III) and nickel(II) ions from acidic solutions by the highly effective ion exchanger. *Molecules* **2020**, *25*, 3718. https://doi.org/10.3390/molecules25163718.
61. Beamson, G.; Briggs, D. *High Resolution XPS of Organic Polymers—The Scienta ESCA300 Database*; Wiley-Interscience: Chichester, UK, 1992.
62. Biesinger, M.C. Accessing the robustness of adventitious carbon for charge referencing (correction) purposes in XPS analysis: Insights from a multi-user facility data review. *Appl. Surf. Sci.* **2022**, *597*, 153681. https://doi.org/10.1016/j.apsusc.2022.153681.

63. Grey, L.H.; Nie, H.-Y.; Biesinger, M.C. Defining the nature of adventitious carbon and improving its merit as a charge correction reference for XPS. *Appl. Surf. Sci.* **2024**, *653*, 159319. https://doi.org/10.1016/j.apsusc.2024.159319.
64. Rueda, F.; Mendialdua, J.; Rodríguez, A.; Casanova, R.; Barbaux, Y.; Gengembre, L.; Jalowiecki, L.; Bouqueniaux, D. Quantitative XPS studies of a natural catalyst. *J. Electron Spectrosc. Relat. Phenom.* **1995**, *70*, 225–231. https://doi.org/10.1016/0368-2048(94)02229-1.
65. Whiteley, J.M.; Woo, J.H.; Hu, E.; Nam, K.-W.; Lee, S.-H. Empowering the lithium metal battery through a silicon-based superionic conductor. *J. Electrochem. Soc.* **2014**, *161*, A1812. https://doi.org/10.1149/2.0501412jes.
66. Biesinger, M.C.; Lau, L.W.M.; Gerson, A.R.; Smart, R.S.C. Resolving surface chemical states in XPS analysis of first row transition metals, oxides and hydroxides: Sc, Ti, V, Cu and Zn. *Appl. Surf. Sci.* **2010**, *257*, 887–898. https://doi.org/10.1016/j.apsusc.2010.07.086.
67. Chenakin, S.P.; Prada Silvy, R.; Kruse, N. Effect of X-rays on the surface chemical state of Al_2O_3, V_2O_5, and aluminovanadate oxide. *J. Phys. Chem. B* **2005**, *109*, 14611–14618. https://doi.org/10.1021/jp051944j.
68. Hävecker, M.; Düngen, P.; Buller, S.; Knop-Gericke, A.; Trunschke, A.; Schlögl, R. Restructuring of silica supported vanadia during propane oxidative dehydrogenation studied by combined synchrotron radiation based in situ soft X-ray absorption and photoemission. *Catal. Struct. React.* **2017**, *3*, 104–111. https://doi.org/10.1080/2055074X.2017.1287535.
69. Fiol, N.; Villaescusa, I. Determination of sorbent point zero charge: Usefulness in sorption studies. *Environ. Chem. Lett.* **2009**, *7*, 79–84. https://doi.org/10.1007/s10311-008-0139-0.
70. Kosmulski, M. The pH dependent surface charging and points of zero charge. VIII. Update. *Adv. Colloid Interface Sci.* **2020**, *275*, 102064. https://doi.org/10.1016/j.cis.2019.102064.
71. Kosmulski, M. The pH dependent surface charging and points of zero charge. X. Update. *Adv. Colloid Interface Sci.* **2023**, *319*, 102973. https://doi.org/10.1016/j.cis.2023.102973.
72. Li, P.; Newsome, L.; Graf, A.; Hudson-Edwards, K.A.; Morgan, D.; Crane, R. Removal of Vanadium(V) Ions from Acidic Water Using Reusable Manganese Oxide Sorbents. *J. Hazard. Mater.* **2025**, *490*, 137765. https://doi.org/10.1016/j.jhazmat.2025.137765.
73. Wiercik, P.; Garbowski, T.; Chrobot, P. The Study of Humic Substances' Impact on Anion Exchangers. *Materials* **2024**, *17*, 1237. https://doi.org/10.3390/ma17061237.
74. Gao, F.; Olayiwola, A.U.; Liu, B.; Wang, S.; Du, H.; Li, J.; Wang, X.; Chen, D.; Zhang, Y. Review of Vanadium Production Part I: Primary Resources. *Miner. Process. Extr. Metall. Rev.* **2022**, *43*, 466–488. https://doi.org/10.1080/08827508.2021.1883013.
75. Peacock, C.L.; Sherman, D.M. Vanadium(V) Adsorption onto Goethite (α-FeOOH) at pH 1.5–12: A Surface Complexation Model Based on Ab Initio Molecular Geometries and EXAFS Spectroscopy. *Geochim. Cosmochim. Acta* **2004**, *68*, 1723–1733. https://doi.org/10.1016/j.gca.2003.10.018.
76. Zhou, J.; Bao, S.; Zhang, Y.; Chen, B.; Liang, Y.; Hou, X.; Yang, S.; Ping, Y.; Zhou, Z. Adsorption Property and Mechanism of Vanadium(V) by Supported Bifunctionalized Ionic Liquid. *Colloids Surf. A Physicochem. Eng. Asp.* **2024**, *681*, 132753. https://doi.org/10.1016/j.colsurfa.2023.132753.
77. Luo, D.; Huang, J.; Zhang, Y.; Liu, H.; Hu, P. Efficient and Environment-Friendly Vanadium(V) Extraction from Vanadium Shale Leachate Using Tri-n-Octylmethylammonium Chloride. *Sep. Purif. Technol.* **2020**, *237*, 116482. https://doi.org/10.1016/j.seppur.2019.116482.
78. Namasivayam, C.; Sangeetha, D. Removal and recovery of vanadium(V) by adsorption onto $ZnCl_2$ activated carbon: Kinetics and isotherms. *Adsorption* **2006**, *12*, 103–117. https://doi.org/10.1007/s10450-006-0373-3.
79. Marin, N.M.; Nita Lazar, M.; Popa, M.; Galaon, T.; Pascu, L.F. Current Trends in Development and Use of Polymeric Ion-Exchange Resins in Wastewater Treatment. *Materials* **2024**, *17*, 5994.
80. Harland, C.E. *Ion Exchange: Theory and Practice*; Royal Society of Chemistry: Cambridge, UK, 1994.
81. Yeom, B.-Y.; Lee, C.-S.; Hwang, T.-S. A new hybrid ion exchanger: Effect of system parameters on the adsorption of vanadium(V). *J. Hazard Mater.* **2009**, *166*, 415–420. https://doi.org/10.1016/j.jhazmat.2008.11.032.
82. Zulu B., Oyewo O.A., Sithole B., Leswifi T.Y., Onyango M.S., Functionalized Sawdust-Derived Cellulose Nanocrystalline Adsorbent for Efficient Removal of Vanadium From Aqueous Solution, *Front. Environ. Sci.* **2020**, *8*, 56. https://doi.org/10.3389/fenvs.2020.00056.
83. Burdzy, K.; Chen, Y.-G.; Lv, G.-Y.; Chen, S.-H.; Kołodyńska, D. Application of Ion Exchangers with the N-Methyl-D-Glucamine Groups in the V(V) Ions Adsorption Process. *Materials* **2022**, *15*, 1026. https://doi.org/10.3390/ma15031026.
84. Chen, B.; Bao, S.X.; Zhang, Y.M.; Zheng, R.W. A High-Efficiency Approach for the Synthesis of N235-Impregnated Resins and the Application in Enhanced Adsorption and Separation of Vanadium(V). *Minerals* **2018**, *8*, 358. https://doi.org/10.3390/min8080358.

85. Gomes, H.I.; Jones, A.; Rogerson, M.; Greenway, G.M.; Lisbona, D.F.; Burke, I.T.; Mayes, W.M. Removal and Recovery of Vanadium from Alkaline Steel Slag Leachates with Anion Exchange Resins. *J. Environ. Manag.* **2017**, *187*, 384–392. https://doi.org/10.1016/j.jenvman.2016.10.063.
86. Hu, X.; Wang, X.; Xiao, L.; Song, S.; Zhang, B. Removal of Vanadium from Molybdate Solution by Ion Exchange. *Hydrometallurgy* **2009**, *95*, 203–206. https://doi.org/10.1016/j.hydromet.2008.05.051.
87. Zheng, R.W.; Bao, S.X.; Zhang, Y.M. Synthesis of Di-(2-Ethylhexyl) Phosphoric Acid (D2EHPA)-Tributyl Phosphate (TBP) Impregnated Resin and Application in Adsorption of Vanadium(IV). *Minerals* **2018**, *8*, 206. https://doi.org/10.3390/min8050206.
88. Lagergren, S. About the Theory of So-Called Adsorption of Soluble Substances. *K. Sven. Vetenskapsakad. Handl.* **1898**, *24*, 1–39.
89. Ho, Y.S.; McKay, G. Pseudo-Second-Order Model for Sorption Processes. *Process Biochem.* **1999**, *34*, 451–465. https://doi.org/10.1016/S0032-9592(98)00112-5.
90. Weber, W.J.; Morris, J.C. Kinetics of Adsorption on Carbon from Solution. *J. Sanit. Eng. Div.* **1963**, *89*, 31–60. https://doi.org/10.1061/JSEDAI.0000430.
91. Al-Ghouti, M.A.; Da'ana, D.A. Guidelines for the Use and Interpretation of Adsorption Isotherm Models: A Review. *J. Hazard. Mater.* **2020**, *393*, 122383. https://doi.org/10.1016/j.jhazmat.2020.122383.
92. Ayawei, N.; Ebelegi, A.N.; Wankasi, D. Modelling and Interpretation of Adsorption Isotherms. *J. Chem.* **2017**, *2017*, 3039817. https://doi.org/10.1155/2017/3039817.
93. Langmuir, I. The Adsorption of Gases on Plane Surfaces of Glass, Mica and Platinum. *J. Am. Chem. Soc.* **1918**, *40*, 1361–1403.
94. Freundlich, H.M.F. Over the Adsorption in Solution. *J. Phys. Chem.* **1906**, *57*, 385–471.
95. Murphy, O.P.; Vashishtha, M.; Palanisamy, P.; Kumar, K.V. A Review on the Adsorption Isotherms and Design Calculations for the Optimization of Adsorbent Mass and Contact Time. *ACS Omega* **2023**, *8*, 17407–17430. https://doi.org/10.1021/acsomega.2c08155.
96. Temkin, M.I.; Pyzhev, V. Kinetics of Ammonia Synthesis on Promoted Iron Catalysts. *Acta Physicochim. URSS* **1940**, *12*, 327–356.
97. Sivarajasekar, N.; Baskar, R. Adsorption of Basic Magenta II onto H_2SO_4-Activated Immature Gossypium hirsutum Seeds: Kinetics, Isotherms, Mass Transfer, Thermodynamics and Process Design. *Arab. J. Chem.* **2019**, *12*, 1322–1337. https://doi.org/10.1016/j.arabjc.2014.10.040.
98. Mudhoo, A.; Pittman, C.U. The Dubinin-Radushkevich models: Dissecting the p_s/p to c_s/c_e replacement in solid-aqueous interfacial adsorption and tracking the validity of $E = 8$ kJ mol^{-1} for assigning sorption type. *Chem. Eng. Res. Des.* **2023**, *198*, 370–402. https://doi.org/10.1016/j.cherd.2023.09.020.
99. Peng, H.; Qiu, H.; Wang, C.; Yuan, B.; Huang, H.; Li, B. Thermodynamic and Kinetic Studies on Adsorption of Vanadium with Glutamic Acid. *ACS Omega* **2021**, *6*, 21563–21570. https://doi.org/10.1021/acsomega.1c02590.
100. Tarley, C.R.T.; Corazza, M.Z.; Somera, B.F.; Segatelli, M.G. Preparation of New Ion-Selective Cross-Linked Poly(Vinylimidazole-co-Ethylene Glycol Dimethacrylate) Using a Double-Imprinting Process for the Preconcentration of Pb^{2+} Ions. *J. Colloid Interface Sci.* **2015**, *450*, 254–263. https://doi.org/10.1016/j.jcis.2015.02.074.
101. Mătușoiu, F.; Negrea, A.; Ciopec, M.; Duțeanu, N.; Negrea, P.; Ianăși, P.; Ianăși, C. Vanadium(V) Adsorption from Aqueous Solutions Using Xerogel on the Basis of Silica and Iron Oxide Matrix. *Materials* **2022**, *15*, 8970. https://doi.org/10.3390/ma15248970.
102. Jeon, J.H.; Cueva Sola, A.B.; Lee, J.-Y.; Koduru, J.R.; Jyothi, R.K. Separation of Vanadium and Tungsten from Synthetic and Spent Catalyst Leach Solutions Using an Ion-Exchange Resin. *RSC Adv.* **2022**, *12*, 3635–3645. https://doi.org/10.1039/D1RA05253E.
103. Zeng, X.; Zhao, K.; Si, S.; Liang, F.; He, Q. Adsorption of Vanadium with 312 Resin. *Chin. J. Rare Met.* **2009**, *33*, 446–449.
104. Zhao, Z.; Li, X.; Zhao, Q. Recovery of V_2O_5 from Bayer Liquor by Ion Exchange. *Rare Met.* **2010**, *29*, 117–120. https://doi.org/10.1007/s12598-010-0020-8.
105. Ognyanova, A.; Ozturk, A.T.; De Michelis, I.; Ferella, F.; Taglieri, G.; Akcil, A.; Vegliò, F. Metal Extraction from Spent Sulfuric Acid Catalyst through Alkaline and Acidic Leaching. *Hydrometallurgy* **2010**, *100*, 20–28. https://doi.org/10.1016/j.hydromet.2009.09.009.
106. Romanovskaia, E.; Romanovski, V.; Kwapinski, W.; Kurilo, I. Selective Recovery of Vanadium Pentoxide from Spent Catalysts of Sulfuric Acid Production: Sustainable Approach. *Hydrometallurgy* **2021**, *200*, 105568. https://doi.org/10.1016/j.hydromet.2021.105568.
107. Mazurek, K. Recovery of vanadium, potassium and iron from a spent vanadium catalyst by oxalic acid solution leaching, precipitation and ion exchange processes. *Hydrometallurgy* **2013**, *134–135*, 26–31. https://doi.org/10.1016/j.hydromet.2013.01.011.

108. Chen, L.; Liu, F.; Li, D. Precipitation of Crystallized Hydrated Iron(III) Vanadate from Industrial Vanadium Leaching Solution. *Hydrometallurgy* **2011**, *105*, 229–233. https://doi.org/10.1016/j.hydromet.2010.10.002.
109. Kong, X.; Chen, J.; Tang, Y.; Lv, Y.; Chen, T.; Wang, H. Enhanced Removal of Vanadium(V) from Groundwater by Layered Double Hydroxide-Supported Nanoscale Zerovalent Iron. *J. Hazard. Mater.* **2020**, *392*, 122392. https://doi.org/10.1016/j.jhazmat.2020.122392.
110. Mazurek, K.; Trypuć, M. Selective Separation of Vanadium and Iron from Vanadium Catalyst Leachate. *Przem. Chem.* **2014**, *93*, 258–263. https://doi.org/10.12916/przemchem.2014.258.
111. Zhang, Y.; Zhang, W.; Li, Y.; Cao, X.; Jiang, X.; Nie, Z. Selective Adsorption–Desorption Behavior and Mechanism of Vanadium(V) from the Bayer System by D301 Resin. *JOM* **2026**, *78*, 4451–4462. https://doi.org/10.1007/s11837-026-08165-0.
112. Yang, Y.; Li, H.Y.; Lin, M.M.; Xie, B. Batch Studies for Removing Vanadium(V) and Chromium(VI) from Aqueous Solution Using Anion Exchange Resin. In *Rare Metal Technology 2018*; The Minerals, Metals & Materials Series; Kim, H., Wesstrom, B., Alam, S., Ouchi, T., Azimi, G., Neelameggham, N.R., Wang, S., Guan, X., Eds.; Springer: Cham, Switzerland, 2018. https://doi.org/10.1007/978-3-319-72350-1_28.
113. Li, H.Y.; Li, C.; Zhang, M.; Wang, K.; Xie, B. Removal of V(V) from Aqueous Cr(VI)-Bearing Solution Using Anion Exchange Resin: Equilibrium and Kinetics in Batch Studies. *Hydrometallurgy* **2016**, *165*, 381–389. https://doi.org/10.1016/j.hydromet.2015.10.018.
114. Kausar, A. Polyacrylamide Matrix Nanocomposite: Perspectives in Design, Properties and Application. In *Polymer Nanocomposites*; Mishra, M.K., Ed.; CRC Press: Boca Raton, FL, USA, 2025. https://doi.org/10.1201/9780367694265-EPPMPT7-1.
115. Zhao, L.; Zhu, X.; Feng, K.; Wang, B. Speciation Analysis of Inorganic Vanadium (V(IV)/V(V)) by Graphite Furnace Atomic Absorption Spectrometry Following Ion-Exchange Separation. *Int. J. Environ. Anal. Chem.* **2006**, *86*, 931–939. https://doi.org/10.1080/03067310600687633.
116. Butcher, D.J. Recent Developments in Graphite Furnace Atomic Absorption and Molecular Absorption Spectrometries (GFAAS and GFMAS): Direct Analysis, Speciation, Preconcentration, and Solid and Slurry Sampling. *Appl. Spectrosc. Rev.* **2025**, *60*, 431–449. https://doi.org/10.1080/05704928.2024.2447585.
117. Beamson, G.; Briggs, D. *The XPS of Polymers Database*; SurfaceSpectra Ltd.: Manchester, UK, 2000.
118. Bello, A.; Leiviskä, T.; Zhang, R.; Tanskanen, J.; Maziarz, P.; Matusik, J.; Bhatnagar, A. Synthesis of Zerovalent Iron from Water Treatment Residue as a Conjugate with Kaolin and Its Application for Vanadium Removal. *J. Hazard. Mater.* **2019**, *374*, 372–381. https://doi.org/10.1016/j.jhazmat.2019.04.056.
119. Ebelegi, A.N.; Ayawei, N.; Wankasi, D. Interpretation of Adsorption Thermodynamics and Kinetics. *Open J. Phys. Chem.* **2020**, *10*, 166–182. https://doi.org/10.4236/ojpc.2020.103010.
120. Nguyen Tran, H.; Lima, E.C.; Juang, R.-S.; Bollinger, J.-C.; Chao, H.-P. Thermodynamic Parameters of Liquid-Phase Adsorption Process Calculated from Different Equilibrium Constants Related to Adsorption Isotherms: A Comparison Study. *J. Environ. Chem. Eng.* **2021**, *9*, 106674. https://doi.org/10.1016/j.jece.2021.106674.

Disclaimer/Publisher's Note: The statements, opinions and data contained in all publications are solely those of the individual author(s) and contributor(s) and not of MDPI and/or the editor(s). MDPI and/or the editor(s) disclaim responsibility for any injury to people or property resulting from any ideas, methods, instructions or products referred to in the content.